Electronic Supplementary Material (ESI) for Dalton Transactions.

New ruthenium(II) complexes with quinone diimine and substituted bipyridine as inert ligands: Synthesis, characterization, mechanism of action, DNA/HSA binding affinity and cytotoxic activity

Milica Međedović,[a] Ana Rilak Simović,*[b] Dušan Ćoćić,[a] Laura Senft,[c] Sanja Matic[d], Danijela Todorovic[e], Suzana Popovic[f], Dejan Baskic[f] and Biljana Petrović*[a]

[a]*University of Kragujevac, Faculty of Science, Department of Chemistry, Radoja Domanovića 12, 34000 Kragujevac, Serbia.*

[b]*University of Kragujevac, Institute for Information Technologies Kragujevac, Department of Natural Sciences, Jovana Cvijića bb, 34000 Kragujevac, Serbia.*

[c]*Department Chemie, Ludwig-Maximilians Universität (LMU) München, 81377 München, Germany.*

[d]*Department of Pharmacy, Faculty of Medical Sciences, University of Kragujevac, Svetozara Markovica 69, 34000 Kragujevac, Serbia*.

[e]*University of Kragujevac, Faculty of Medical Sciences, Department of Genetics, Svetozara Markovića 69, 34000 Kragujevac, Serbia*.

[f]*University of Kragujevac, Faculty of Medical Sciences, Centre for Molecular Medicine and Stem Cell Research, Svetozara Markovića 69, 34000 Kragujevac, Serbia.*

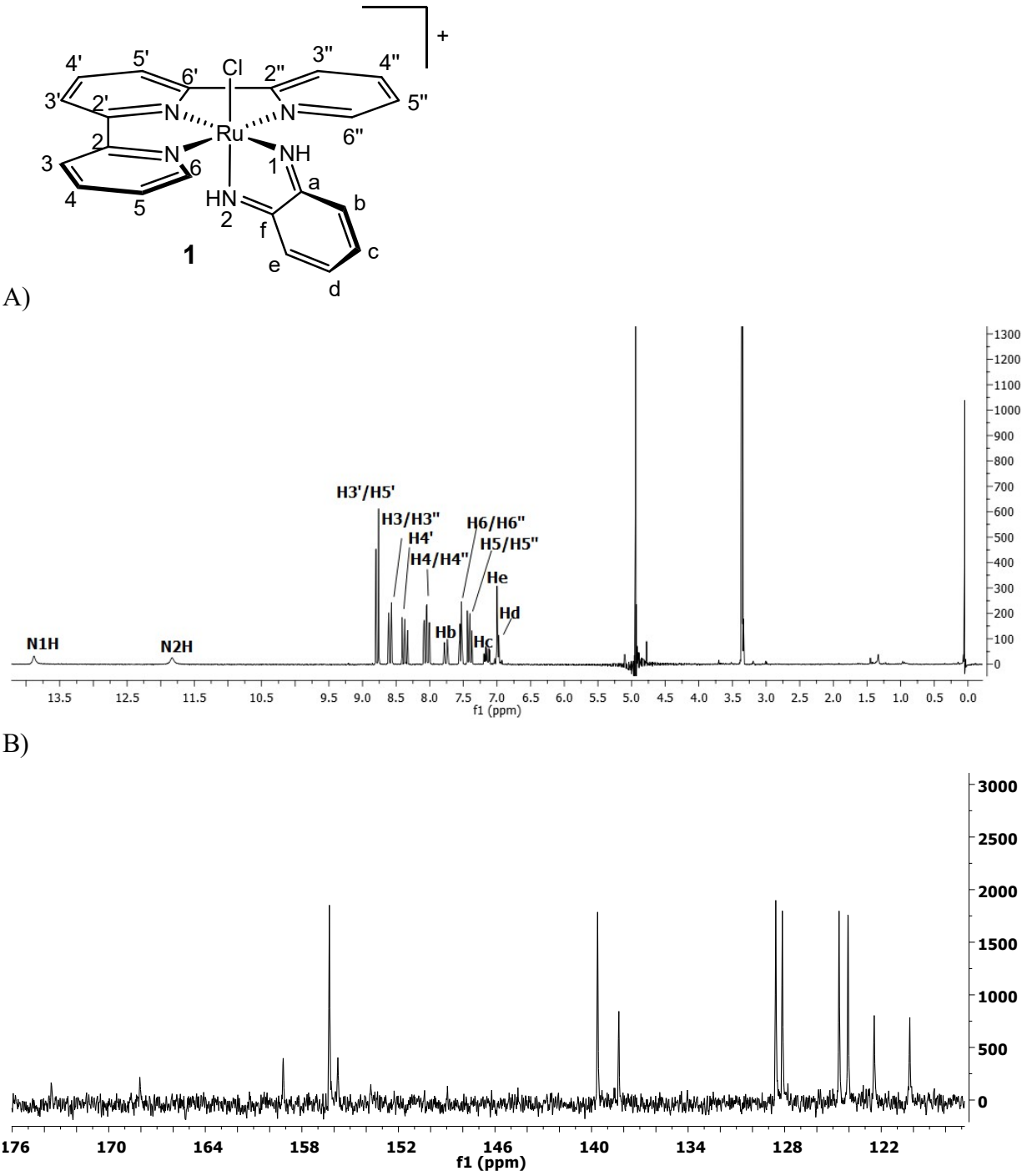

Fig. S1. A) ^{1}H and B) ^{13}C NMR spectrum of [Ru(tpy)(*o*-bqdi)Cl]Cl (**1**) in CD_3OD at 298 K.

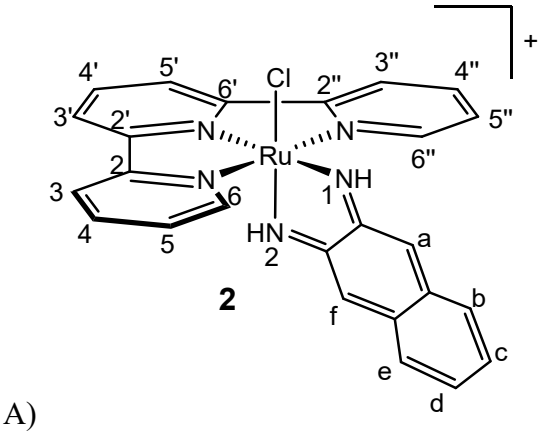

A)

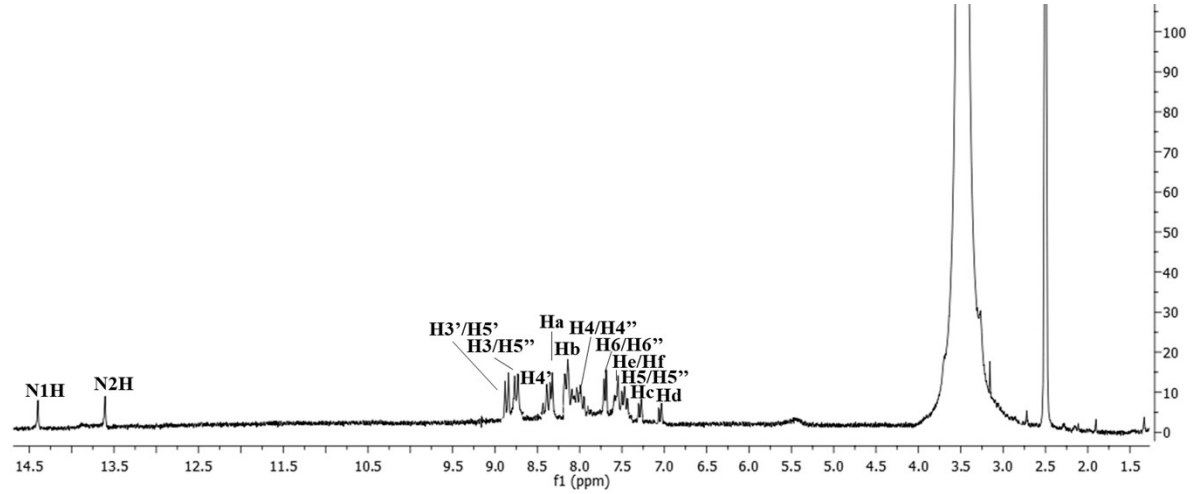

B)

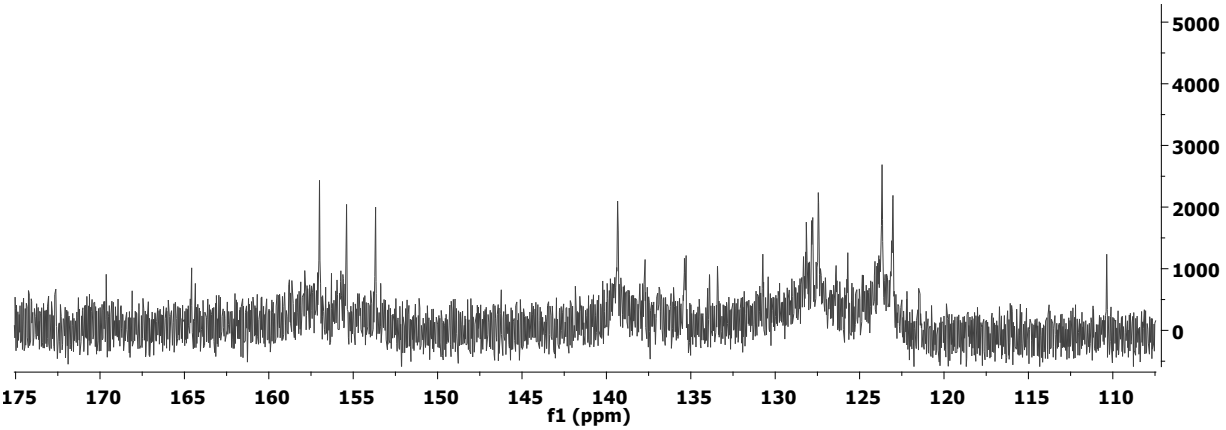

Fig. S2. A) ^{1}H and B) ^{13}C NMR spectrum of [Ru(tpy)(nqdi)Cl]Cl (**2**) in DMSO-d_6 at 298 K.

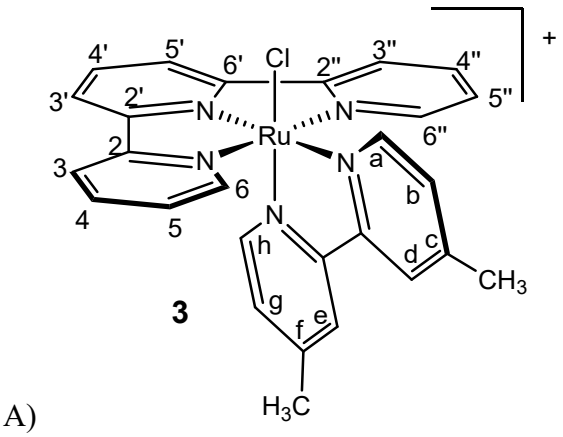

A)

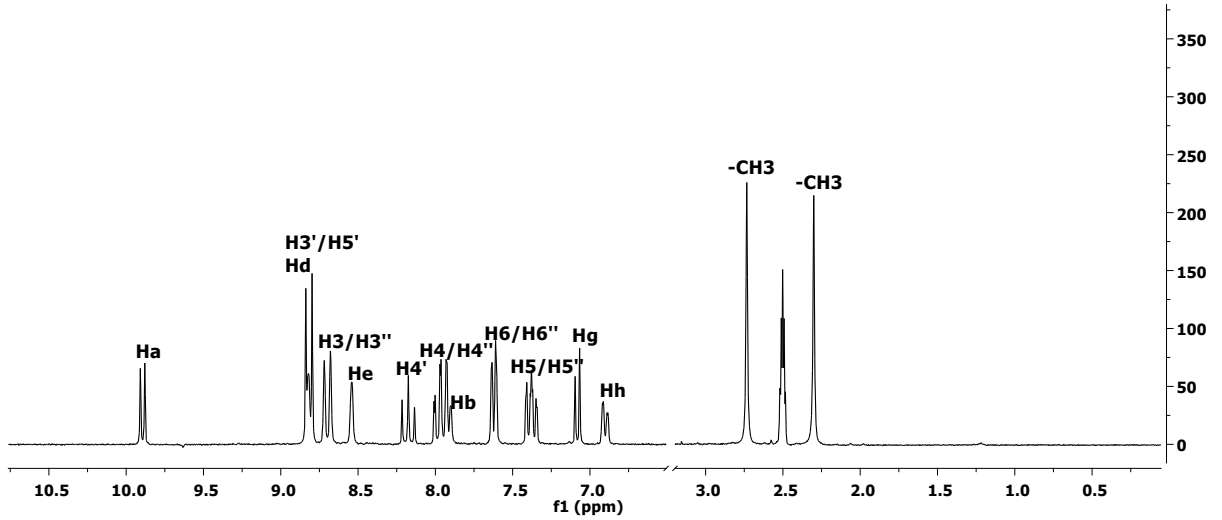

B)

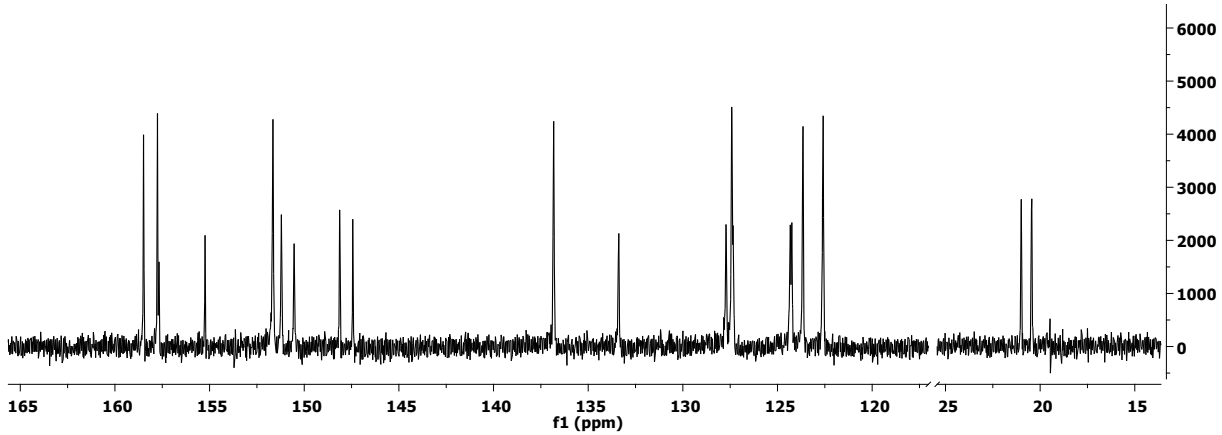

Fig. S3. A) ^{1}H and B) ^{13}C NMR spectrum of [Ru(tpy)(dmbpy)Cl]Cl (**3**) in DMSO-d_6 at 298 K.

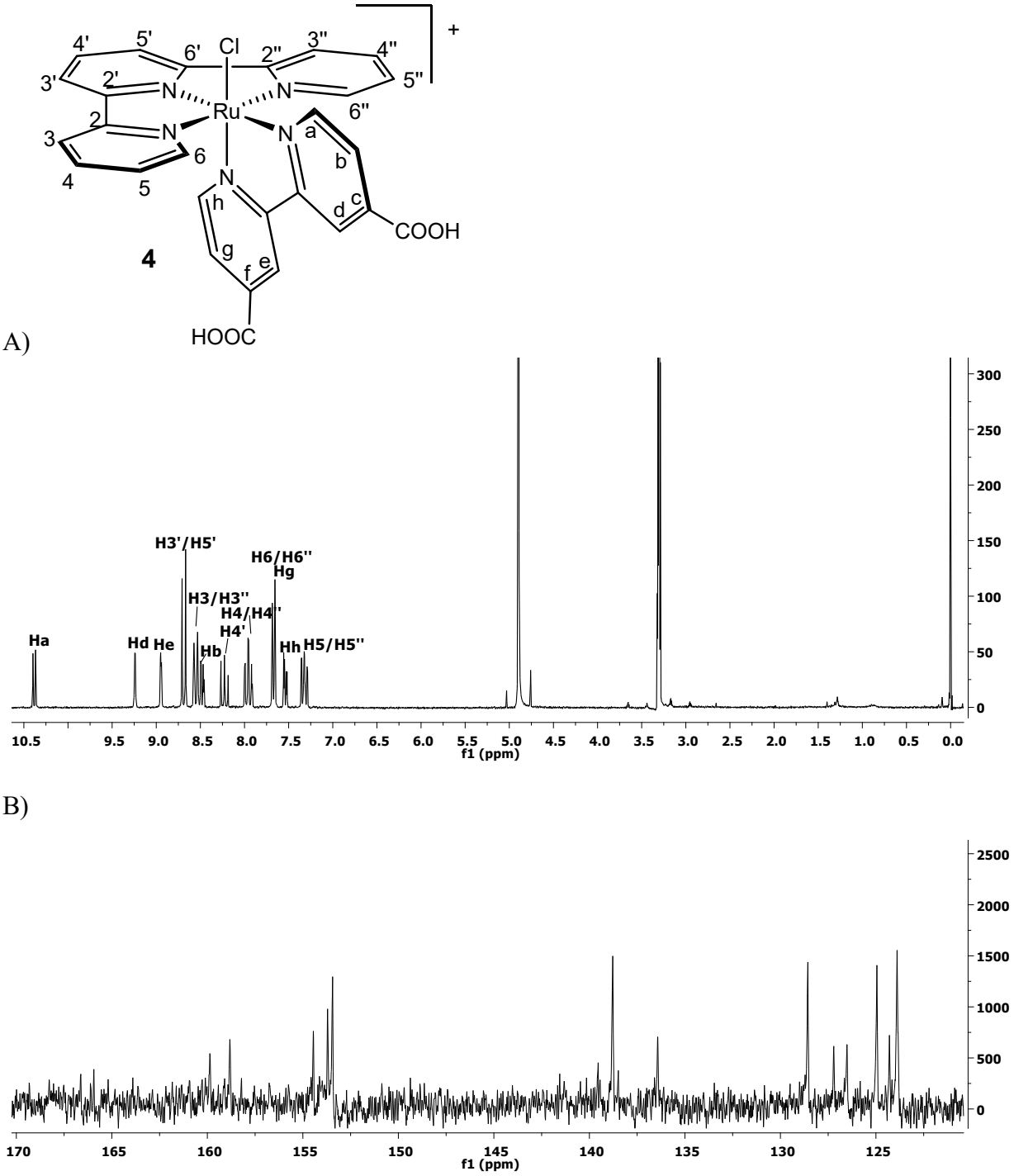

Fig. S4. A) ^{1}H and B) ^{13}C NMR spectrum of [Ru(tpy)(dcbpy)Cl]Cl (**4**) in CD_3OD at 298 K.

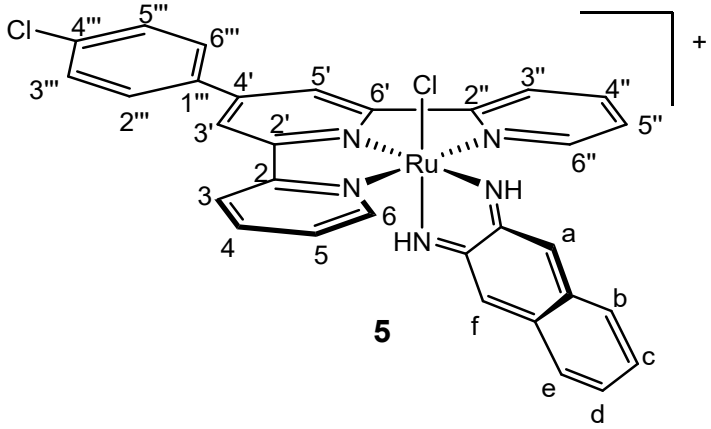

A)

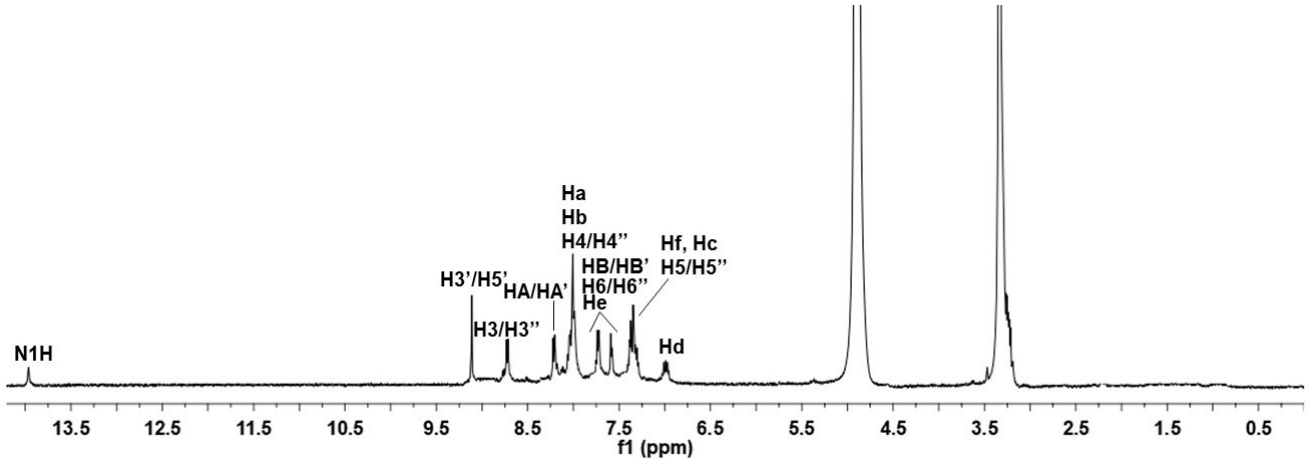

B)

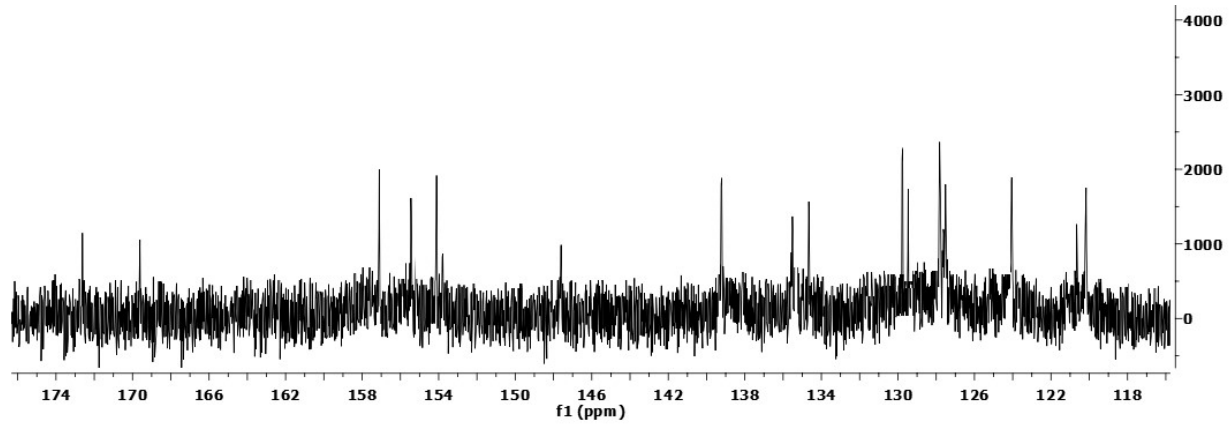

Fig. S5. A) ^{1}H NMR spectrum in CD_3OD and B) ^{13}C NMR spectrum in DMSO-d^6 of [Ru(Cl-Ph-tpy)(nqdi)Cl]Cl (**5**) at 298 K.

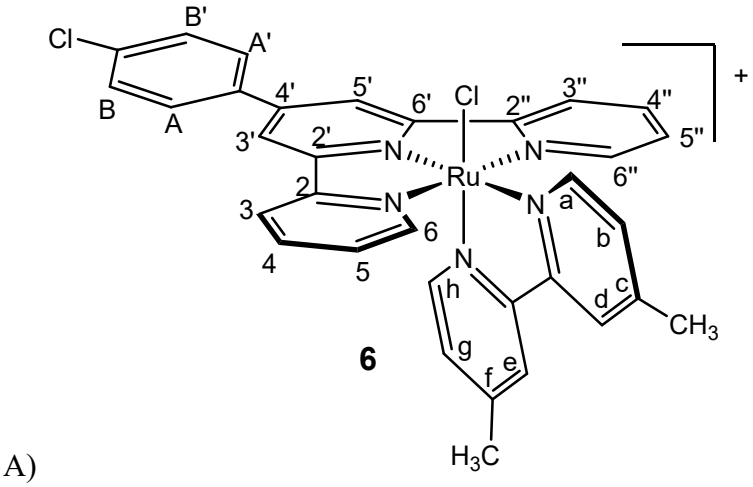

A)

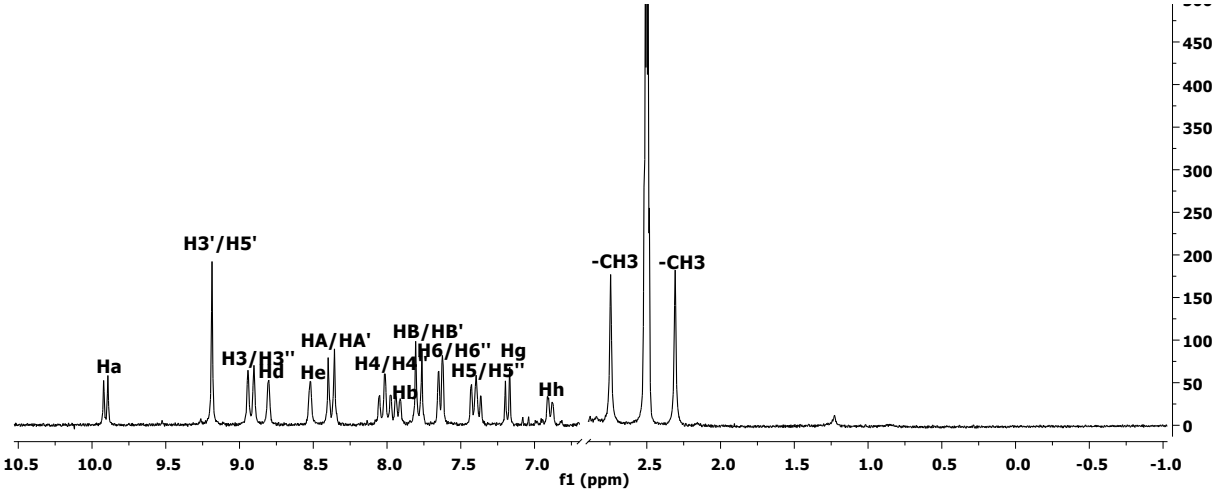

B)

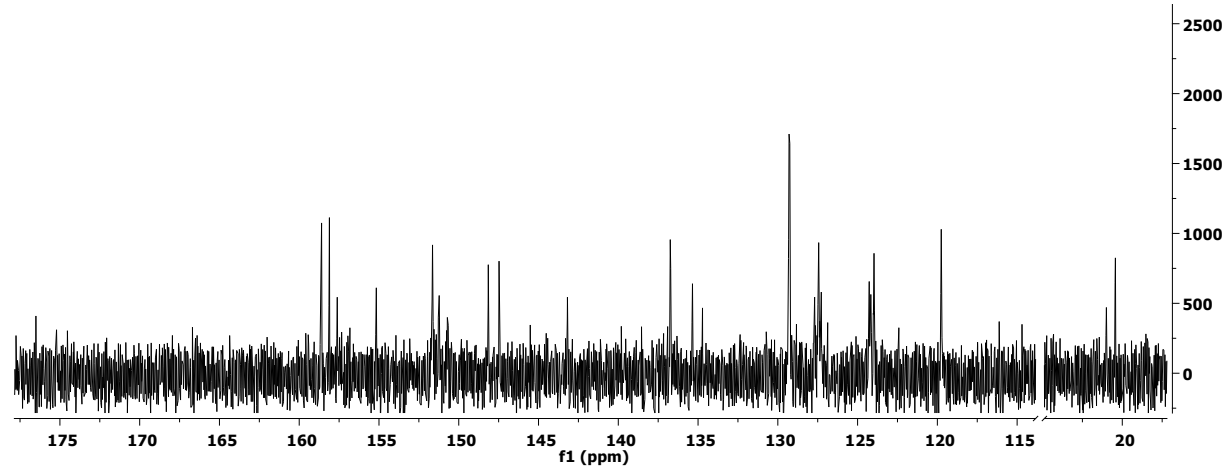

Fig. S6. A) ^{1}H and B) ^{13}C NMR spectrum of [Ru(Cl-Ph-tpy)(dmbpy)Cl]Cl (**6**) in DMSO-d_6 at 298 K.

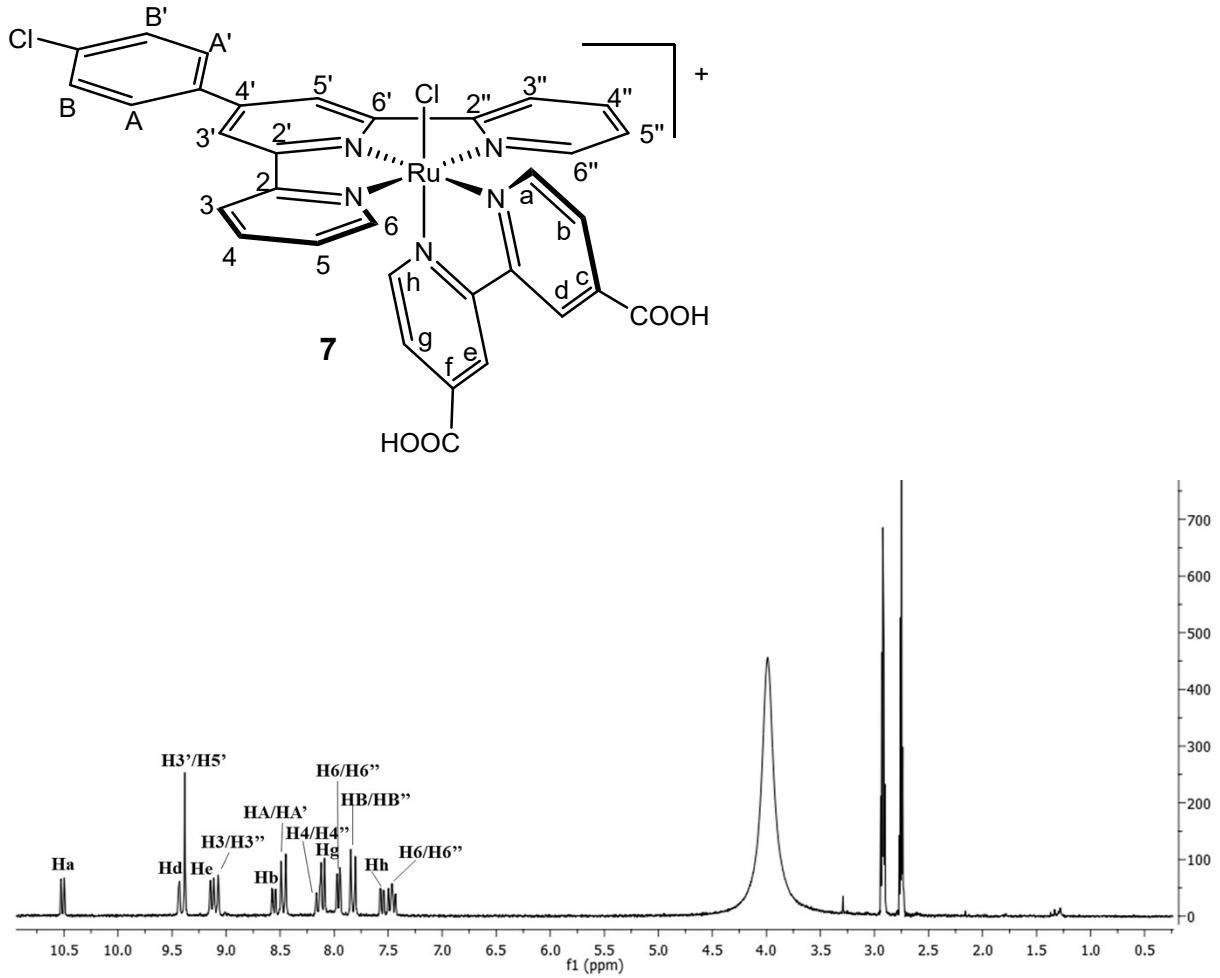

Fig. S7. ^{1}H NMR spectrum of [Ru(Cl-Ph-tpy)(dcbpy)Cl]Cl (**7**) in CD_3OD at 298 K.

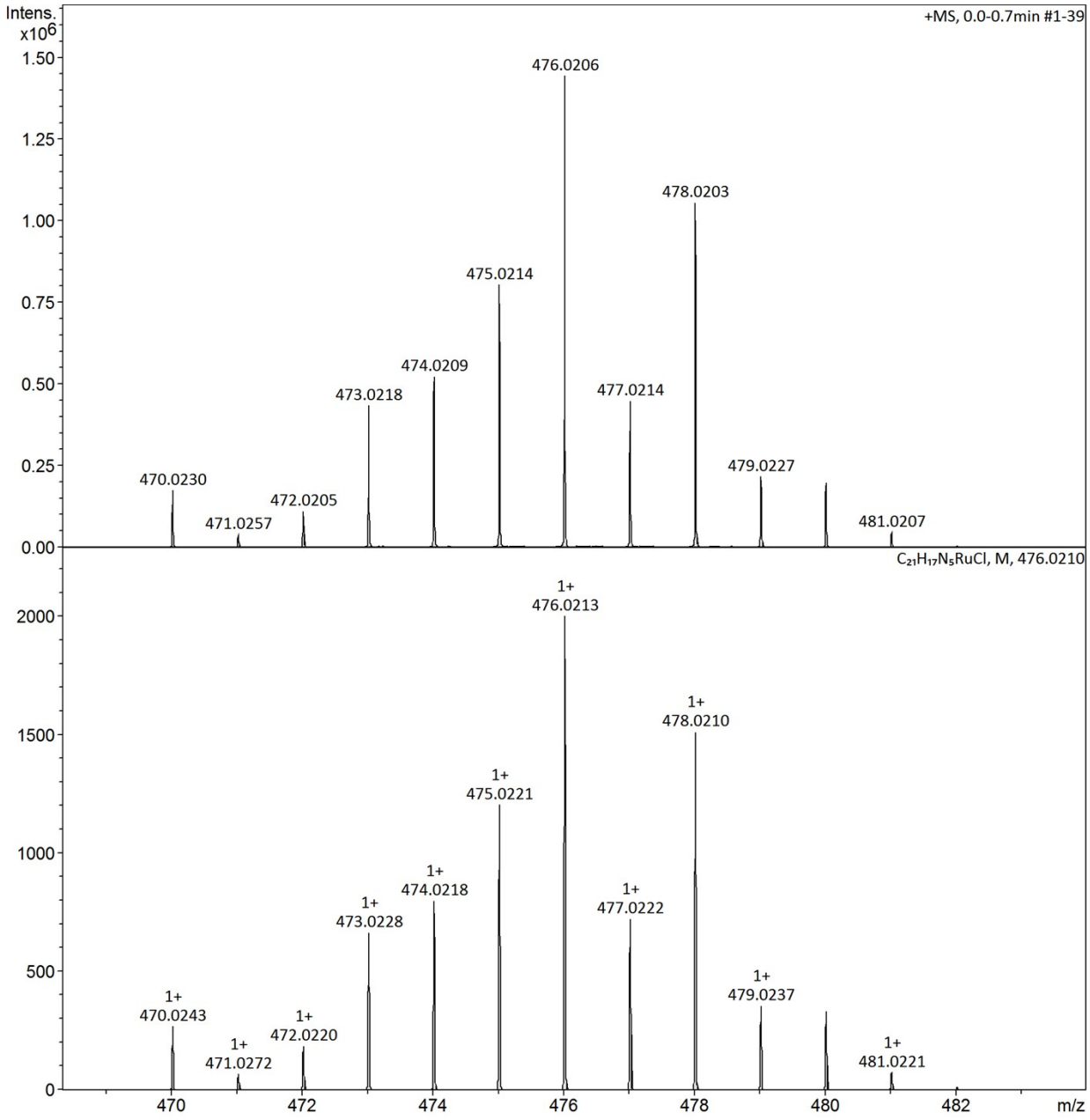

Fig. S8. ESI mass spectrum of complex **1** dissolved in acetonitrile. The spectrum was acquired in positive mode. Instrumental settings were: the source voltage was 3.5 kV, the flow rates were 180 µL/hour, the drying gas (N_2), to aid solvent removal, was held at 180 °C and the spray gas was held at 20 °C. The theoretical and experimentally obtained isotopic distributions are shown in parallel.

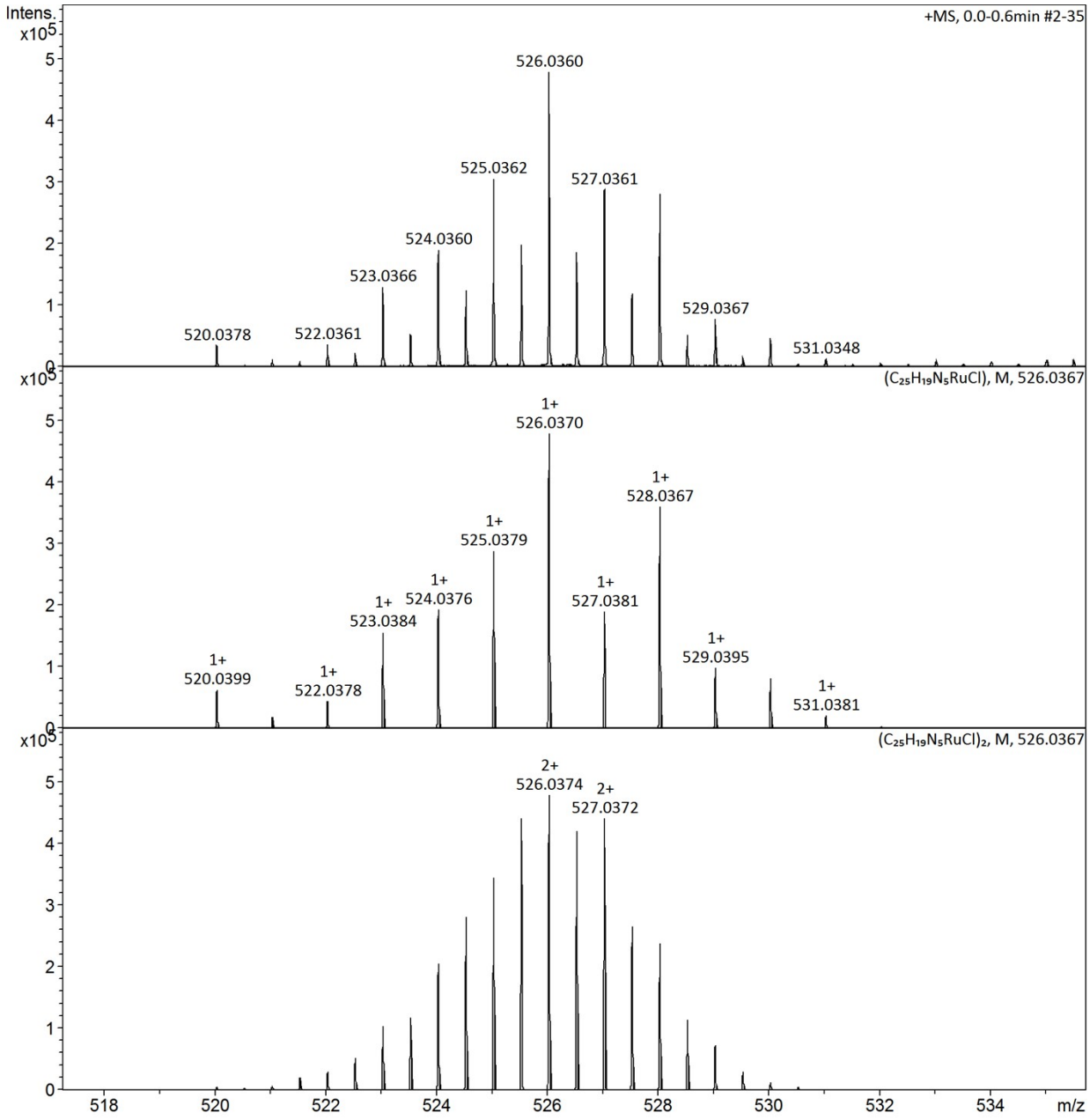

Fig. S9. ESI mass spectrum of complex **2** dissolved in acetonitrile. The spectrum was acquired in positive mode. Instrumental settings were: the source voltage was 3.5 kV, the flow rates were 180 µL/hour, the drying gas (N_2), to aid solvent removal, was held at 180 °C and the spray gas was held at 20 °C. The theoretical and experimentally obtained isotopic distributions are shown in parallel.

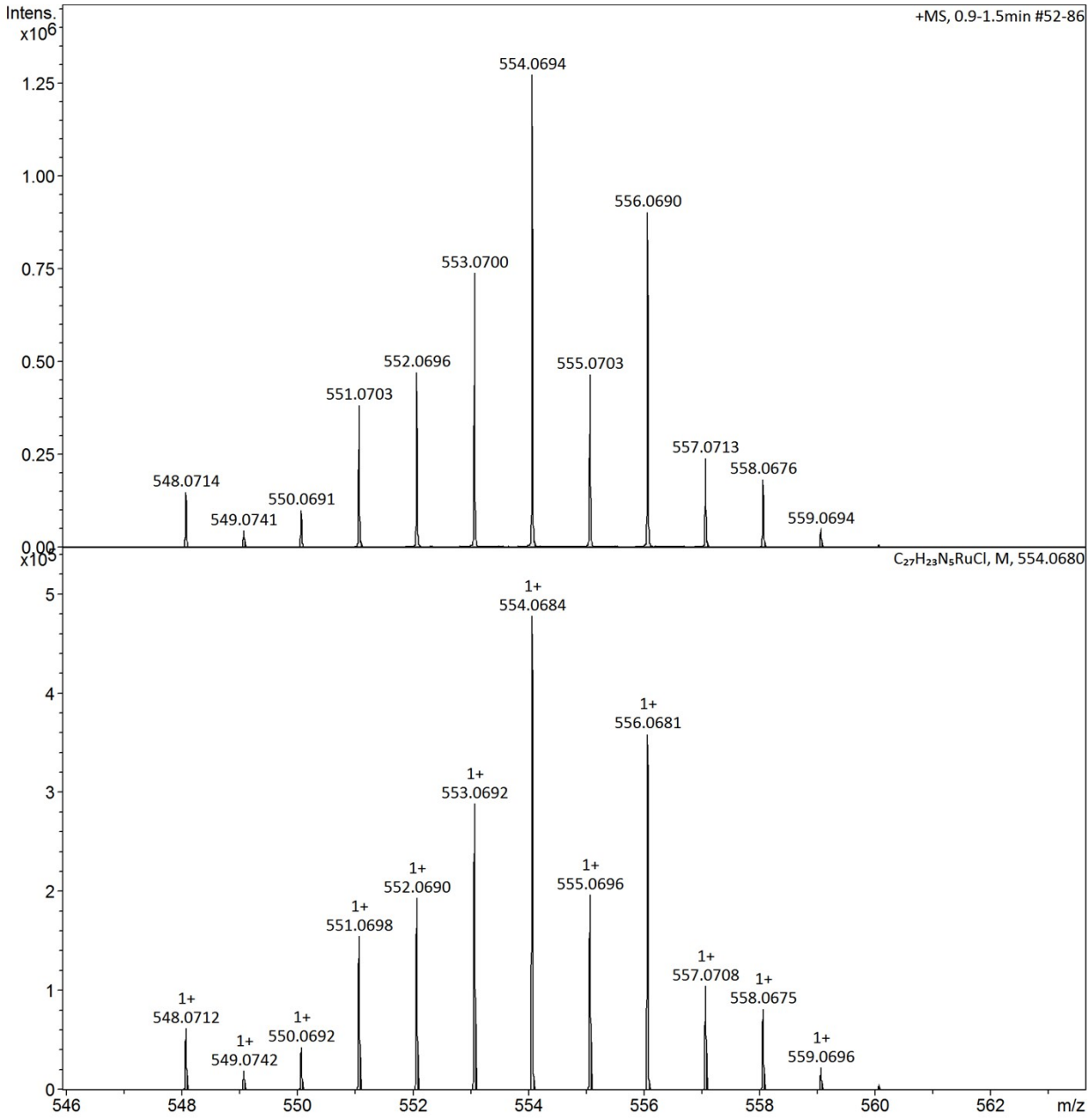

Fig. S10. ESI mass spectrum of complex **3** dissolved in acetonitrile. The spectrum was acquired in positive mode. Instrumental settings were: the source voltage was 3.5 kV, the flow rates were 180 µL/hour, the drying gas (N_2), to aid solvent removal, was held at 180 °C and the spray gas was held at 20 °C. The theoretical and experimentally obtained isotopic distributions are shown in parallel.

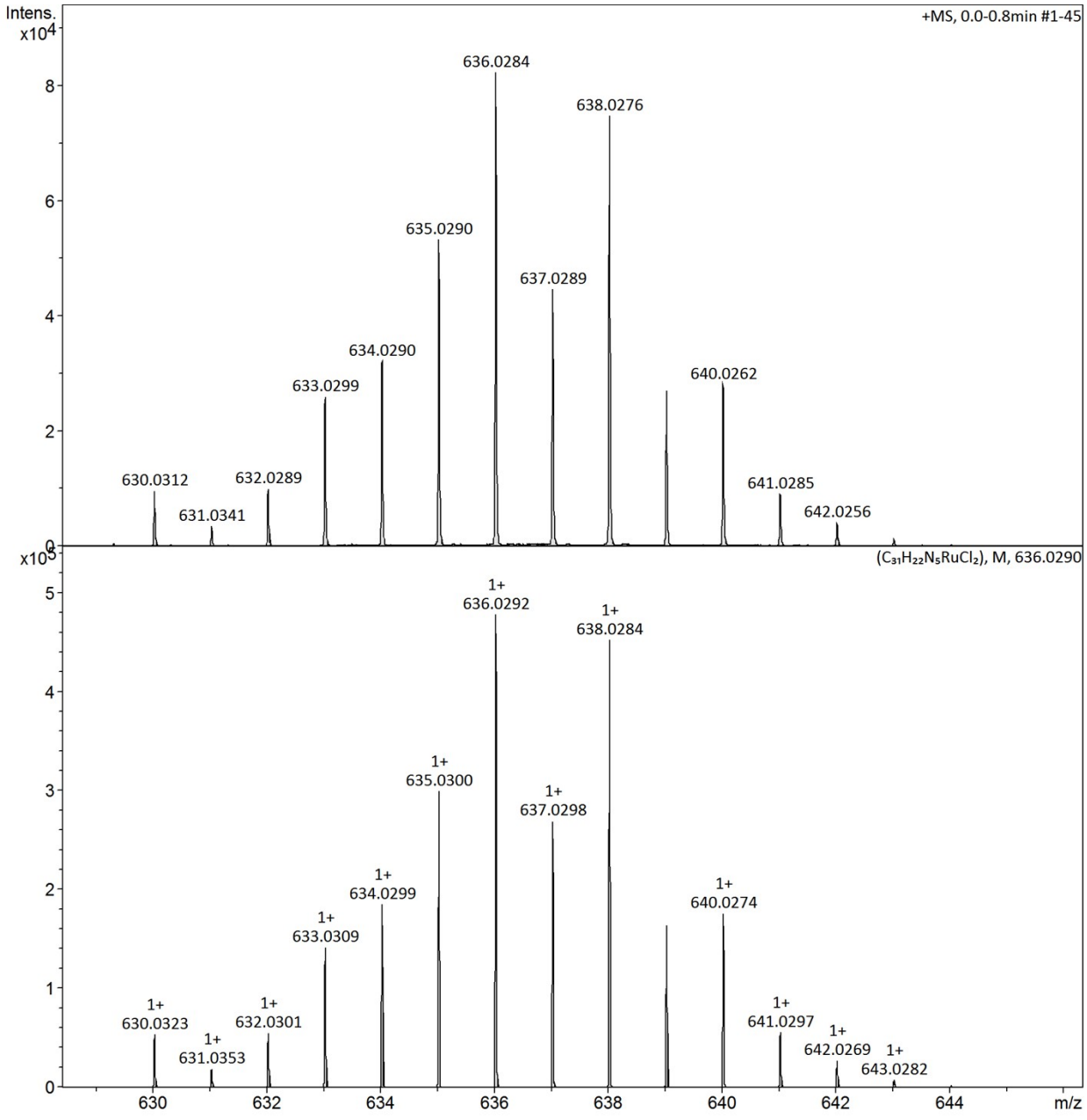

Fig. S11. ESI mass spectrum of complex **5** dissolved in acetonitrile. The spectrum was acquired in positive mode. Instrumental settings were: the source voltage was 3.5 kV, the flow rates were 180 µL/hour, the drying gas (N_2), to aid solvent removal, was held at 180 °C and the spray gas was held at 20 °C. The theoretical and experimentally obtained isotopic distributions are shown in parallel.

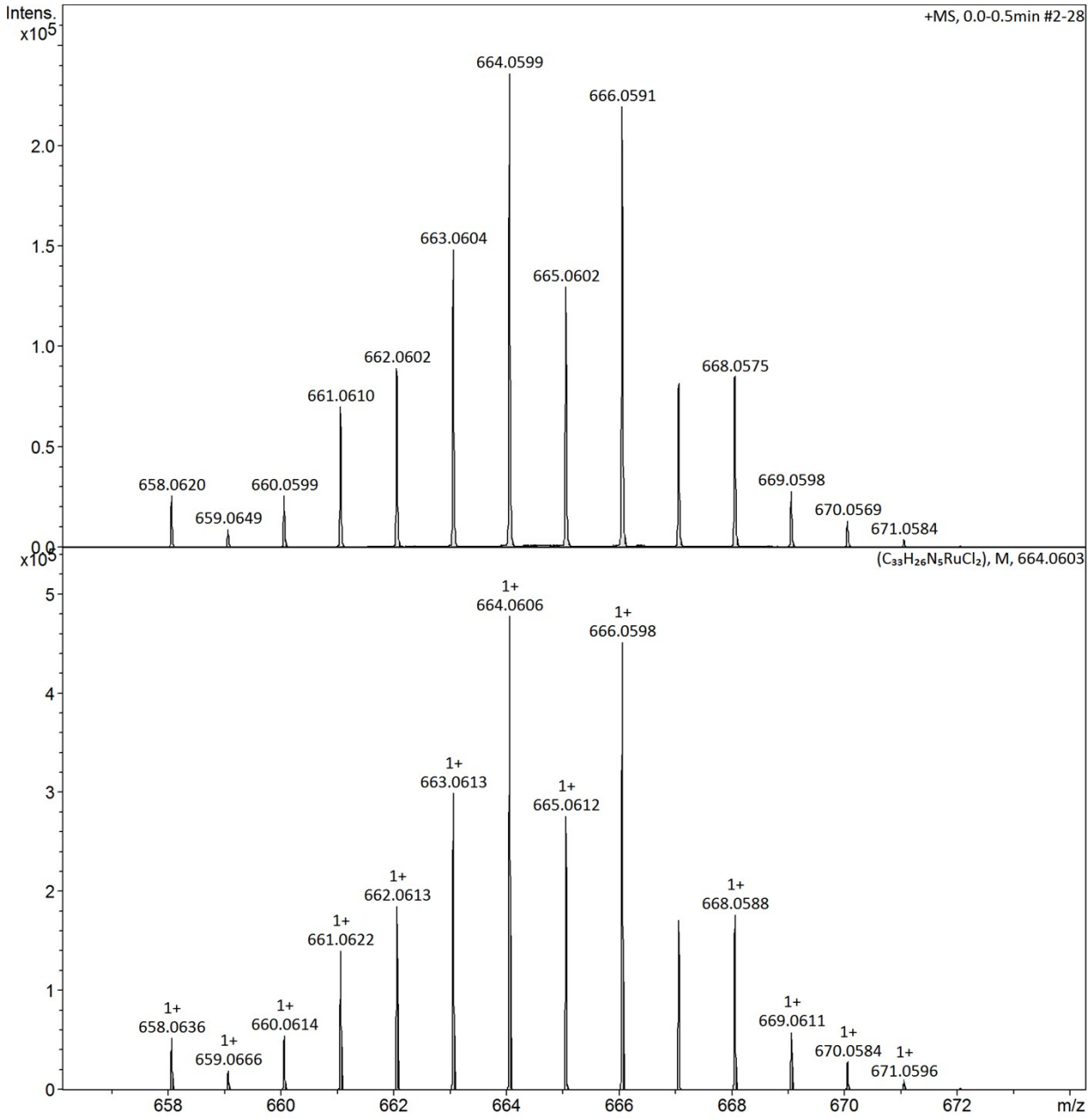

Fig. S12. ESI mass spectrum of complex **6** dissolved in acetonitrile. The spectrum was acquired in positive mode. Instrumental settings were: the source voltage was 3.5 kV, the flow rates were 180 µL/hour, the drying gas (N_2), to aid solvent removal, was held at 180 °C and the spray gas was held at 20 °C. The theoretical and experimentally obtained isotopic distributions are shown in parallel.

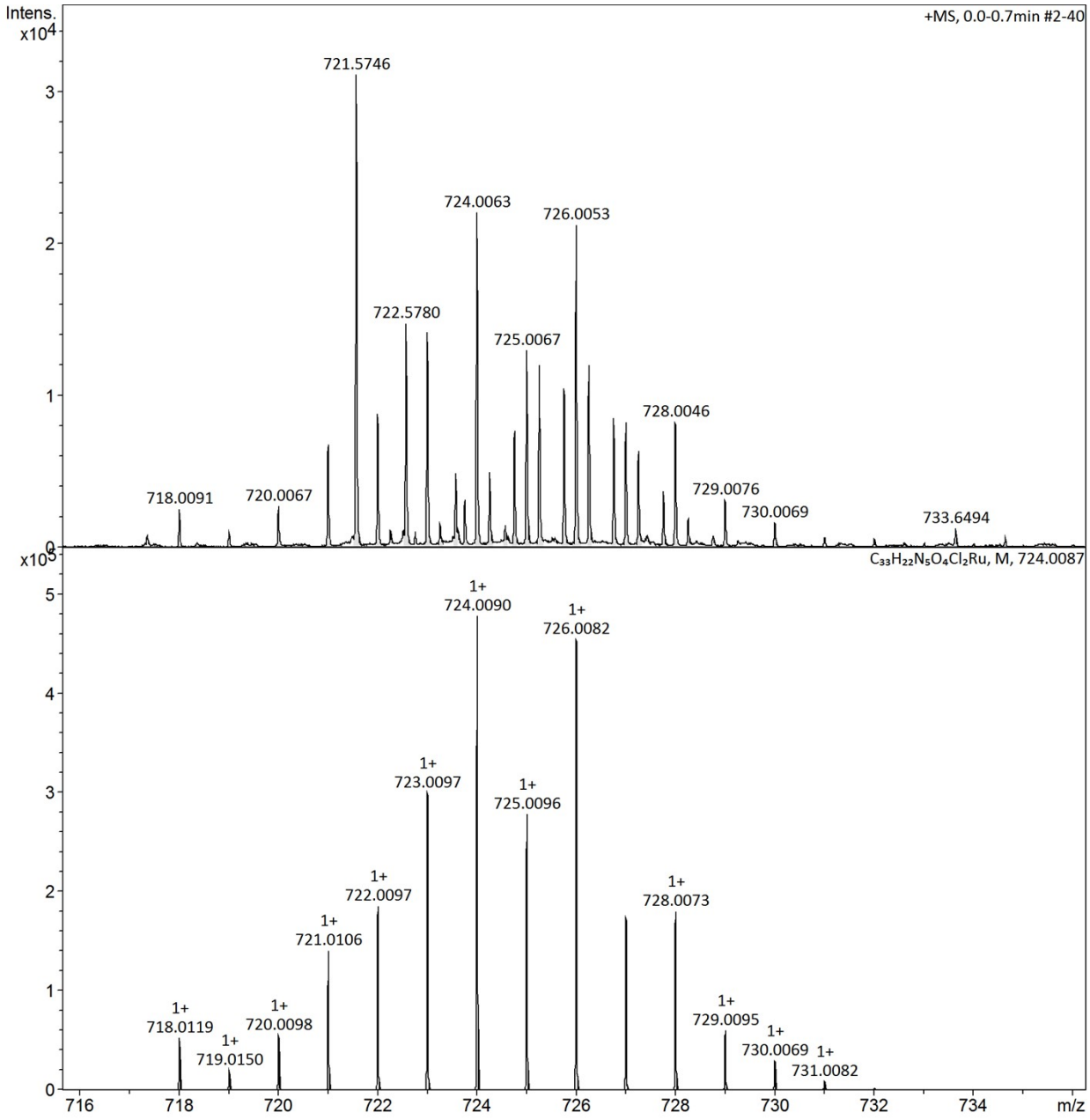

Fig. S13. ESI mass spectrum of complex **7** dissolved in acetonitrile. The spectrum was acquired in positive mode. Instrumental settings were: the source voltage was 3.5 kV, the flow rates were 180 µL/hour, the drying gas (N_2), to aid solvent removal, was held at 180 °C and the spray gas was held at 20 °C. The theoretical and experimentally obtained isotopic distributions are shown in parallel.

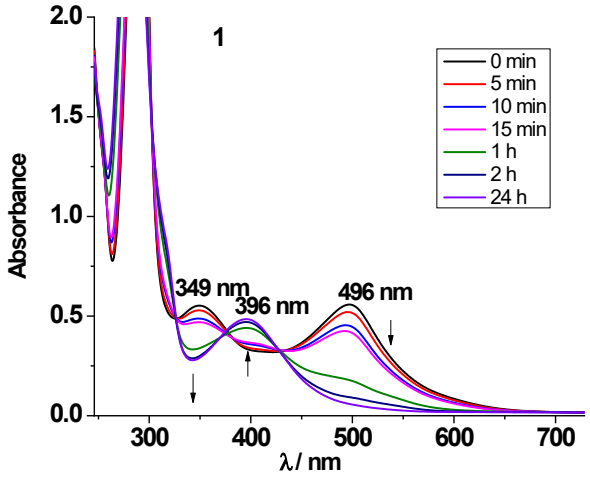
1
Absorbance
λ / nm
0 min
5 min
10 min
15 min
1 h
2 h
24 h
349 nm
396 nm
496 nm

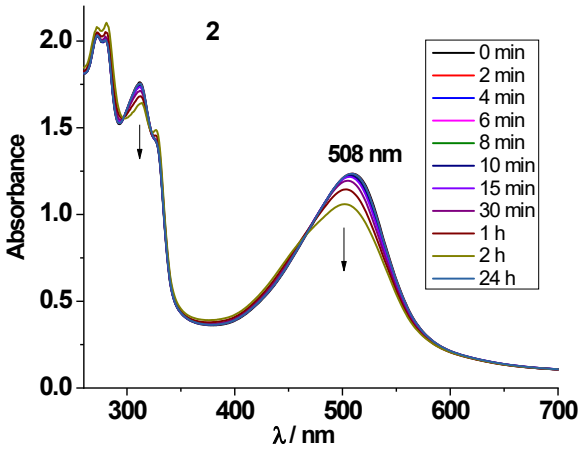
2
Absorbance
λ / nm
0 min
2 min
4 min
6 min
8 min
10 min
15 min
30 min
1 h
2 h
24 h
508 nm

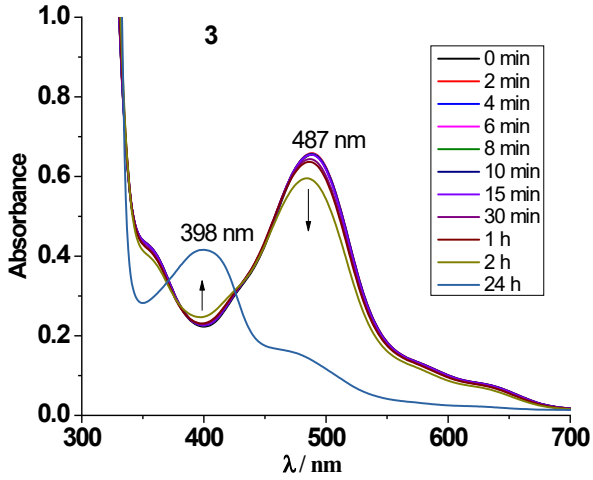
3
Absorbance
λ / nm
0 min
2 min
4 min
6 min
8 min
10 min
15 min
30 min
1 h
2 h
24 h
398 nm
487 nm

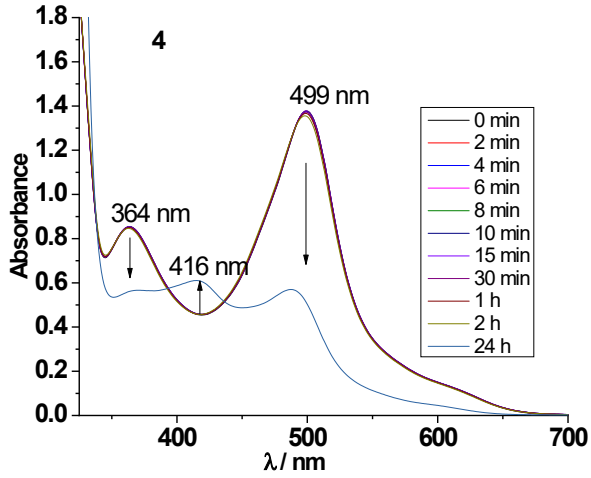
4
Absorbance
λ / nm
0 min
2 min
4 min
6 min
8 min
10 min
15 min
30 min
1 h
2 h
24 h
364 nm
416 nm
499 nm

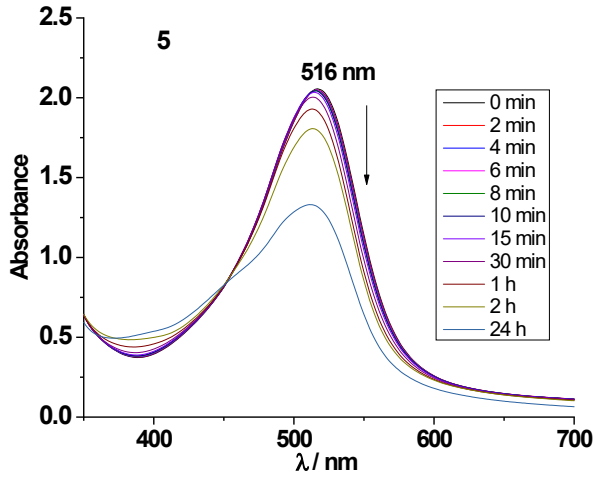
5
Absorbance
λ / nm
0 min
2 min
4 min
6 min
8 min
10 min
15 min
30 min
1 h
2 h
24 h
516 nm

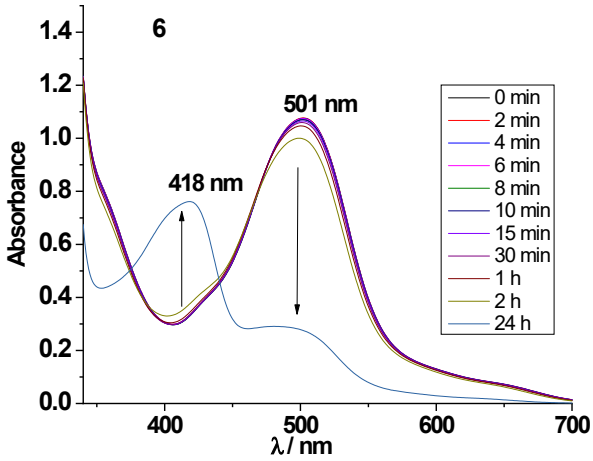
6
Absorbance
λ / nm
0 min
2 min
4 min
6 min
8 min
10 min
15 min
30 min
1 h
2 h
24 h
418 nm
501 nm

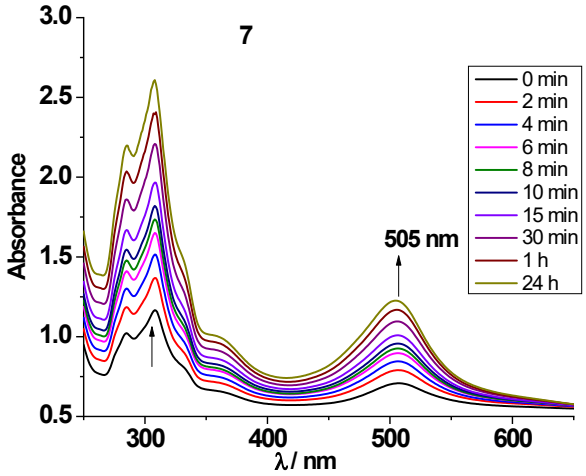

Fig. S14. UV-Vis spectra of complexes **1 – 7** in water over a 24 h period. [Ru(II)] = 1×10^{-4} M, T = 298 K.

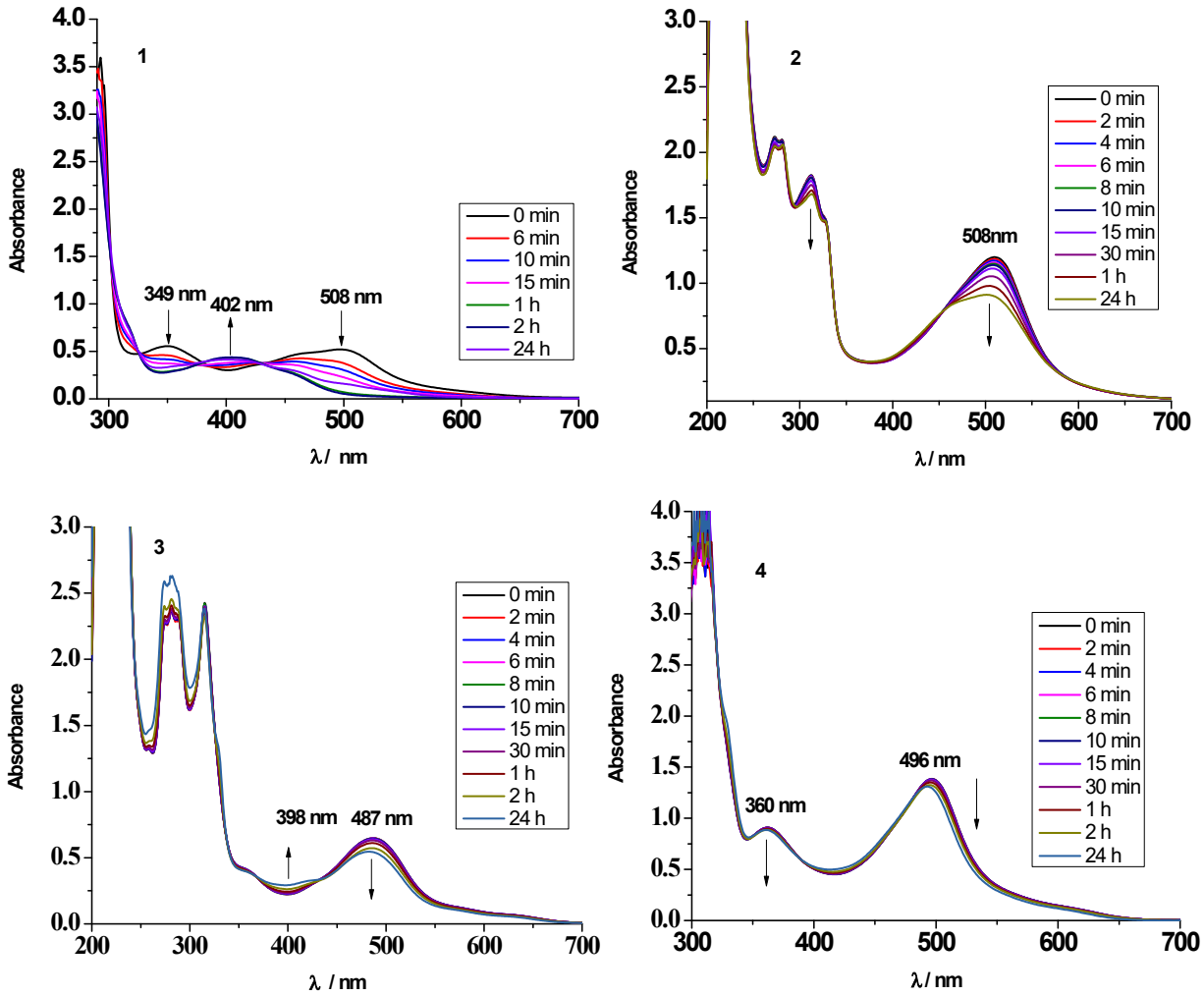

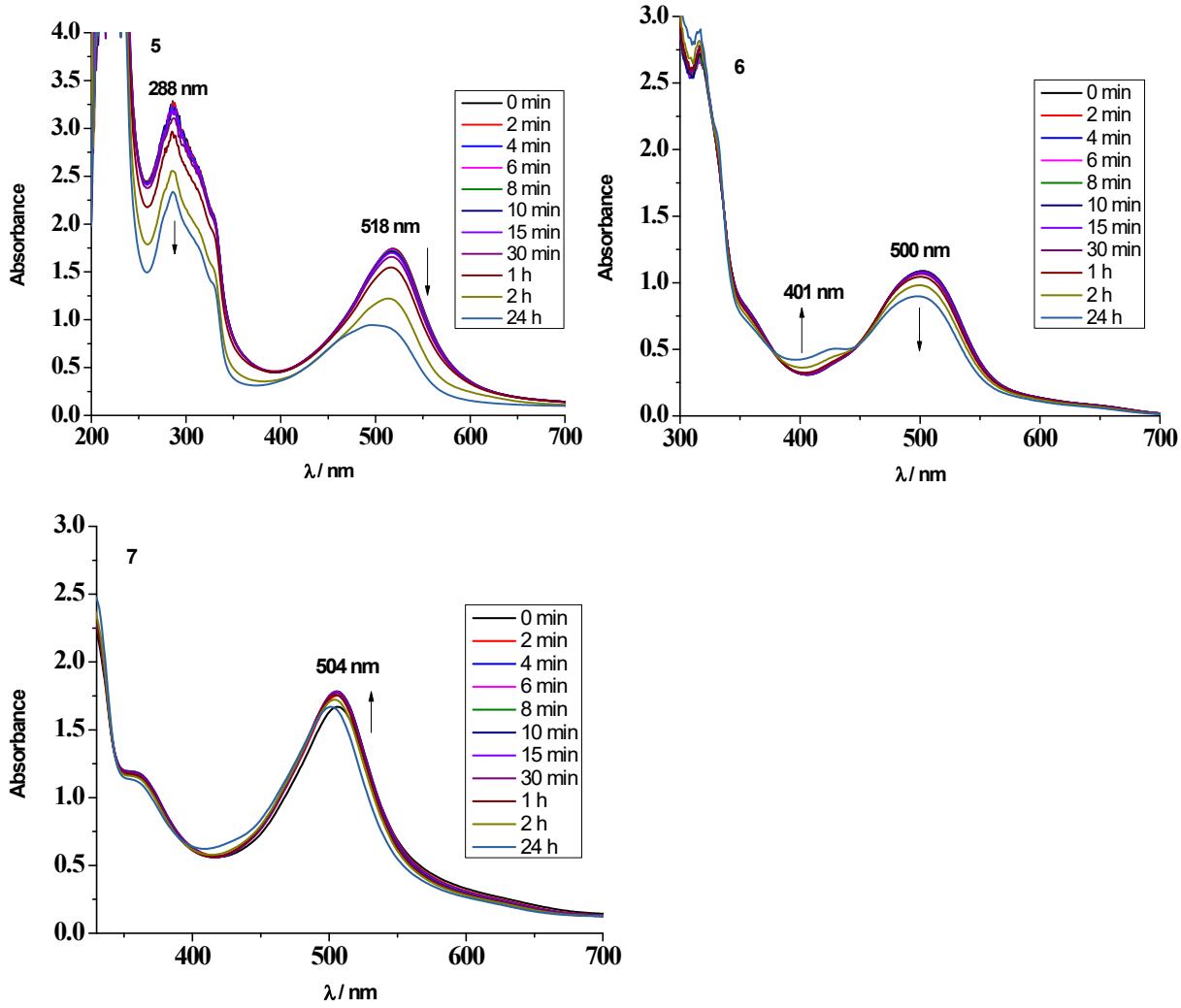

Fig. S15. UV-Vis spectra of complexes **1** – **7** in 10 mM PBS over a 24 h period. [Ru(II)] = 1×10^{-4} M, T = 298 K.

a) b)

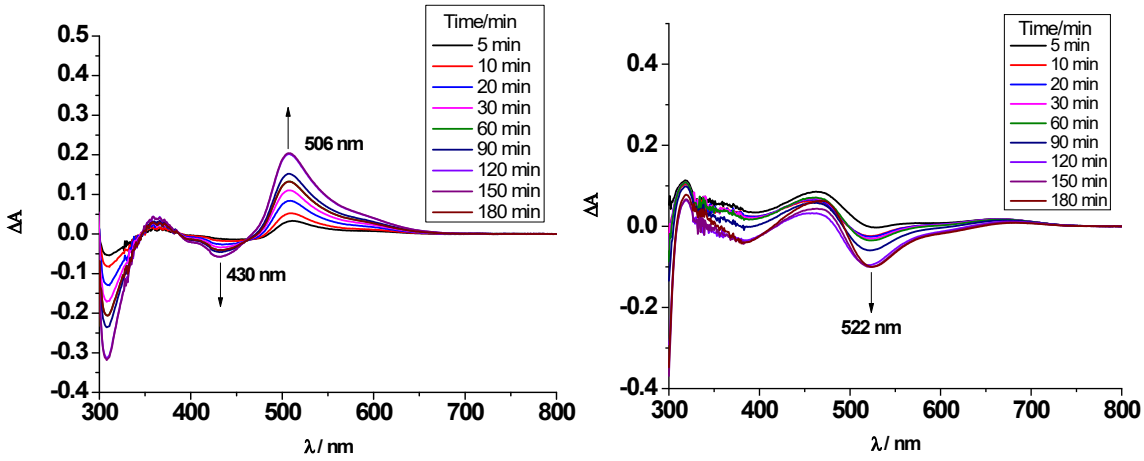

c)

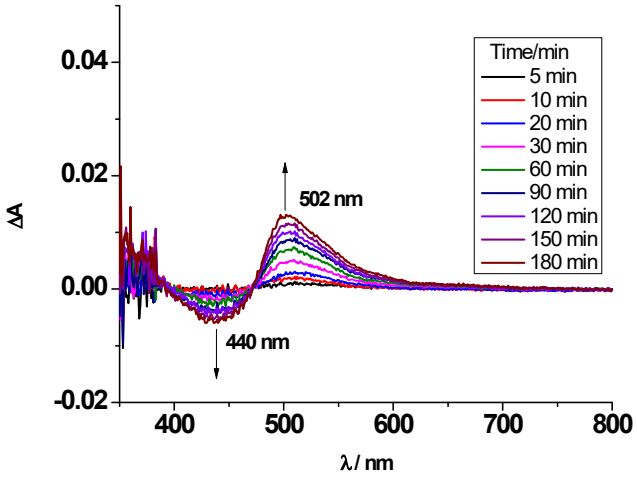

Fig. S16. Time evolution of UV-Vis difference spectra during the interaction of complex **1** with 5'-GMP (a), L-Cys (b) and L-Met (c).

a) b)

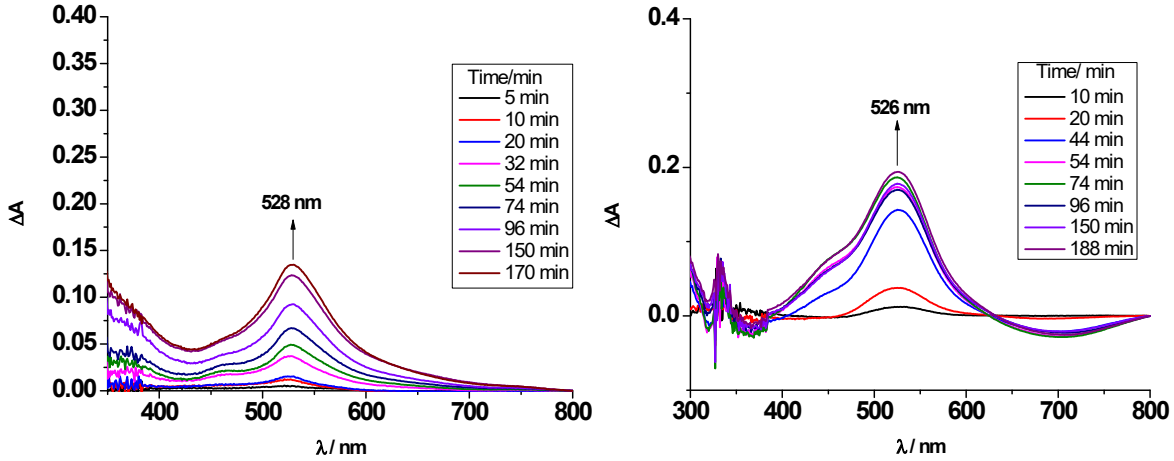

c)

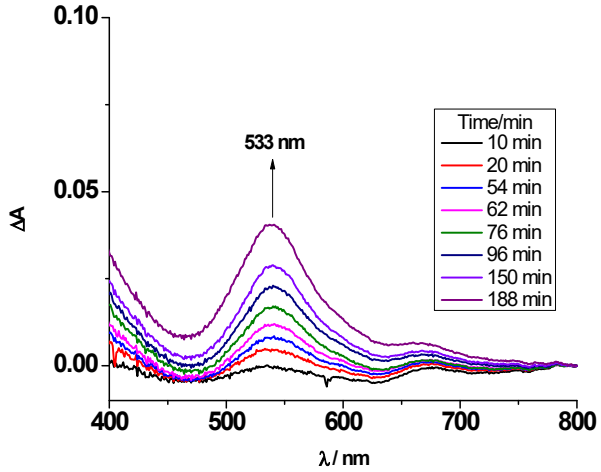

Fig. S17. Time evolution of UV-Vis difference spectra during the interaction of complex **2** with 5'-GMP (a), L-Cys (b) and L-Met (c).

a) b)

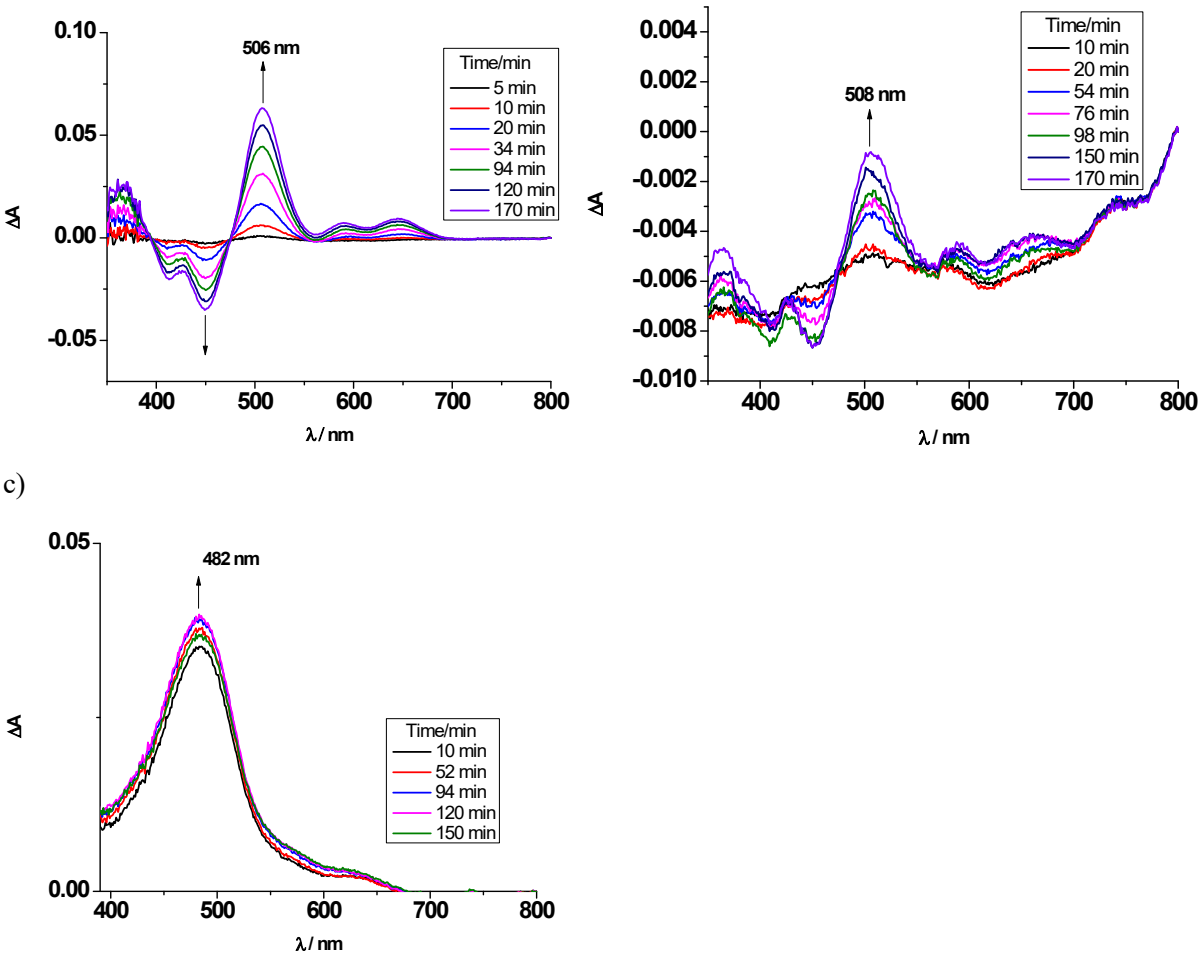

Fig. S18. Time evolution of UV-Vis difference spectra during the interaction of complex **3** with 5'-GMP (a), L-Cys (b) and L-Met (c).

a) b)

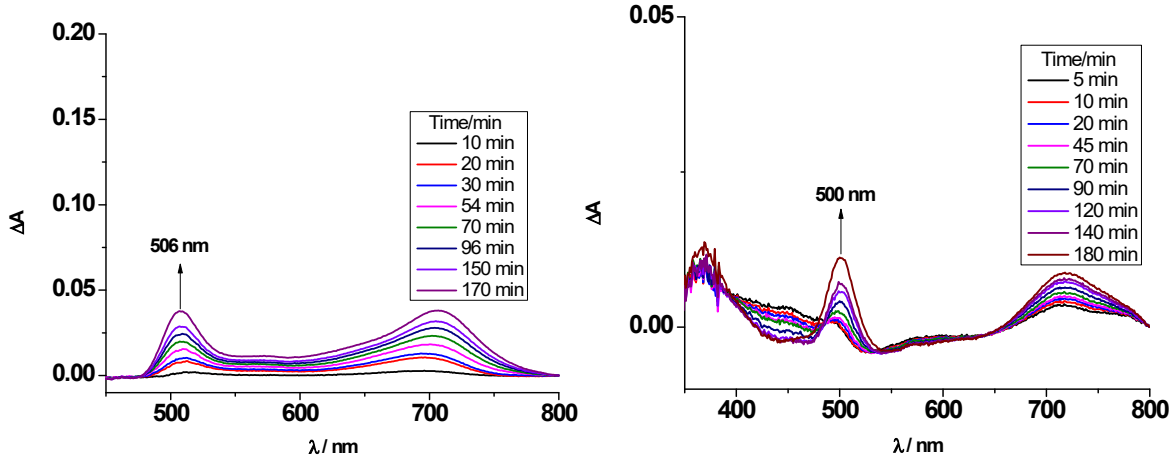

c)

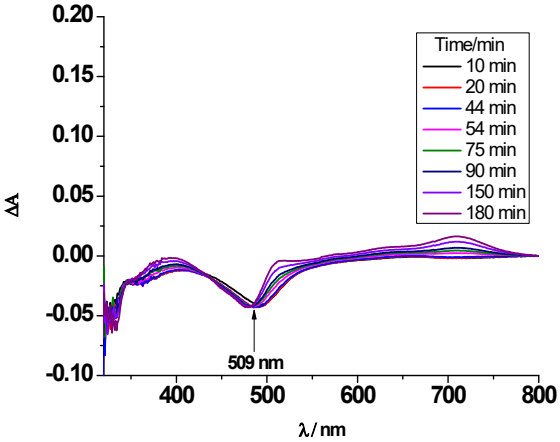

Fig. S19. Time evolution of UV-Vis difference spectra during the interaction of complex **4** with 5'-GMP (a), L-Cys (b) and L-Met (c).

a) b)

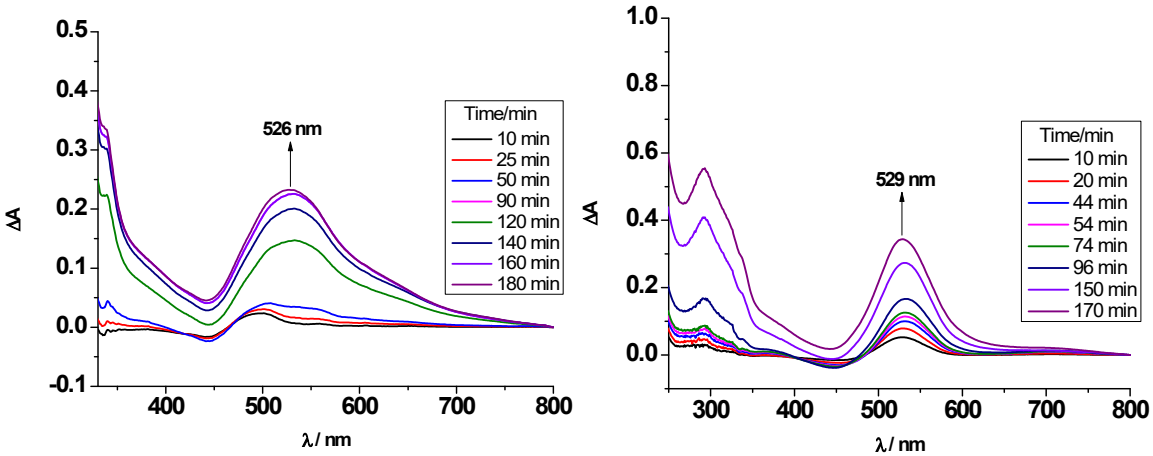

c)

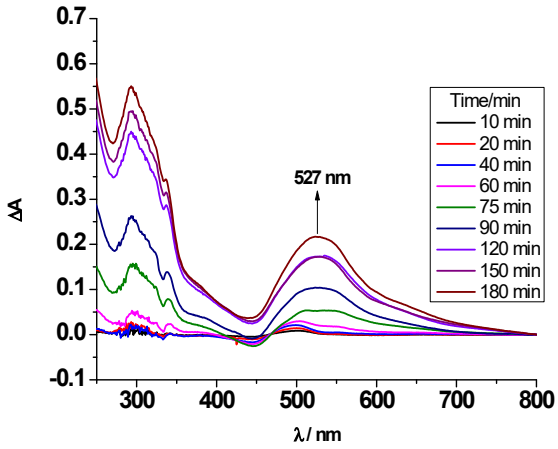

Fig. S20. Time evolution of UV-Vis difference spectra during the interaction of complex **5** with 5'-GMP (a), L-Cys (b) and L-Met (c).

a) b)

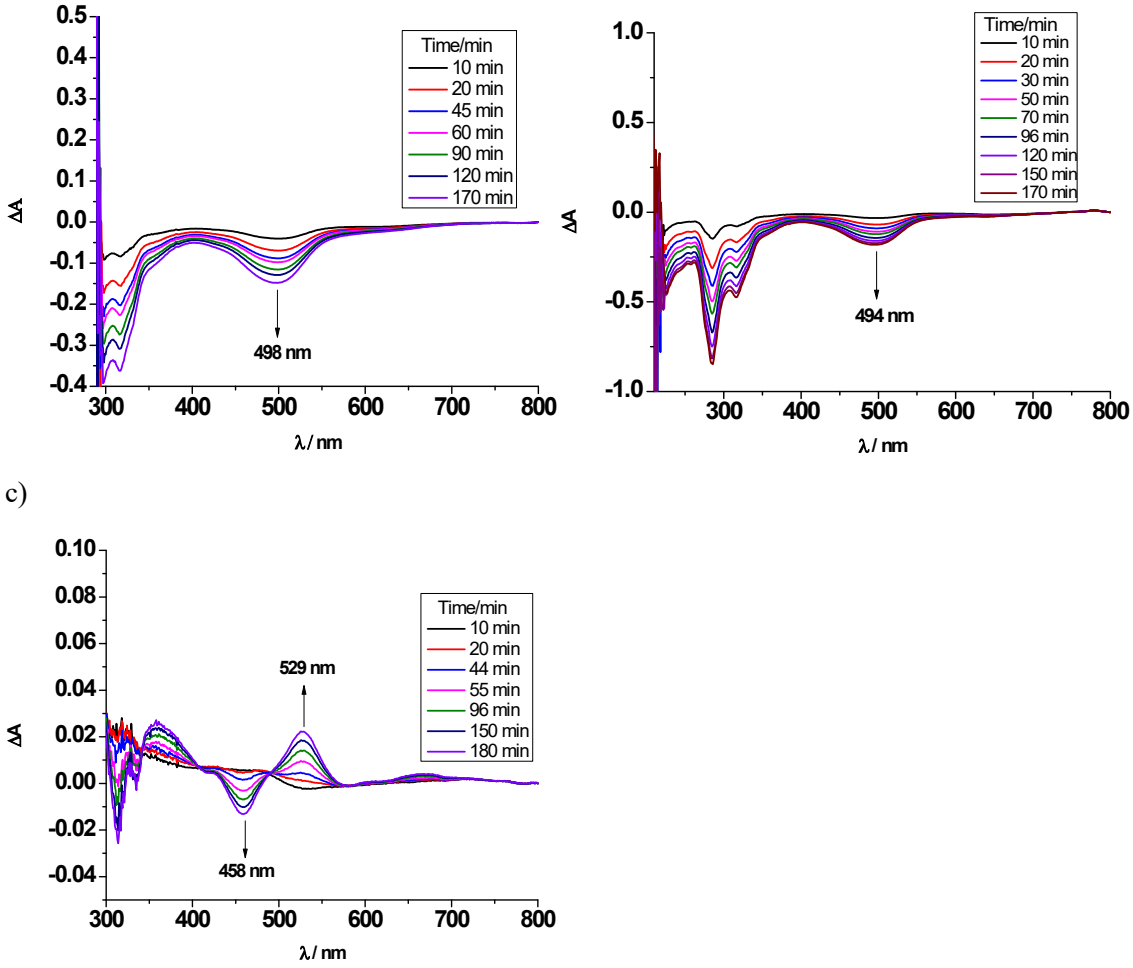

Fig. S21. Time evolution of UV-Vis difference spectra during the interaction of complex **6** with 5'-GMP (a), L-Cys (b) and L-Met (c).

a) b)

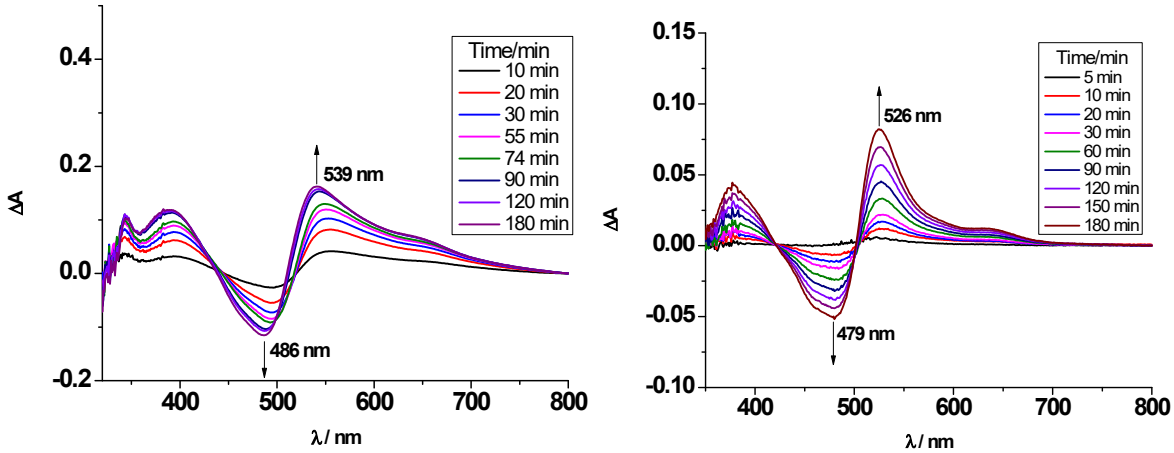

c)

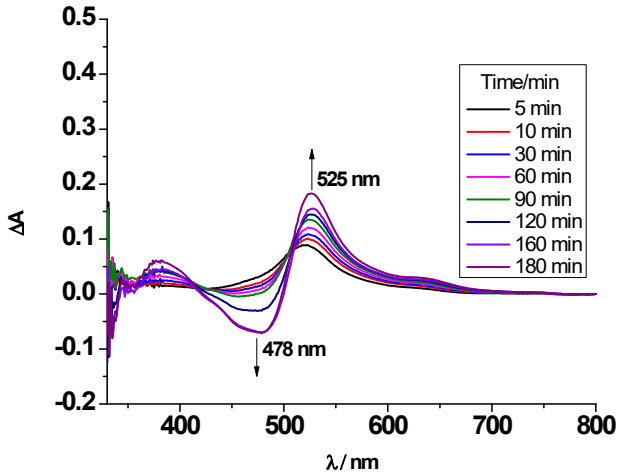

Fig. S22. Time evolution of UV-Vis difference spectra during the interaction of complex **7** with 5'-GMP (a), L-Cys (b) and L-Met (c).

(a) **b)**

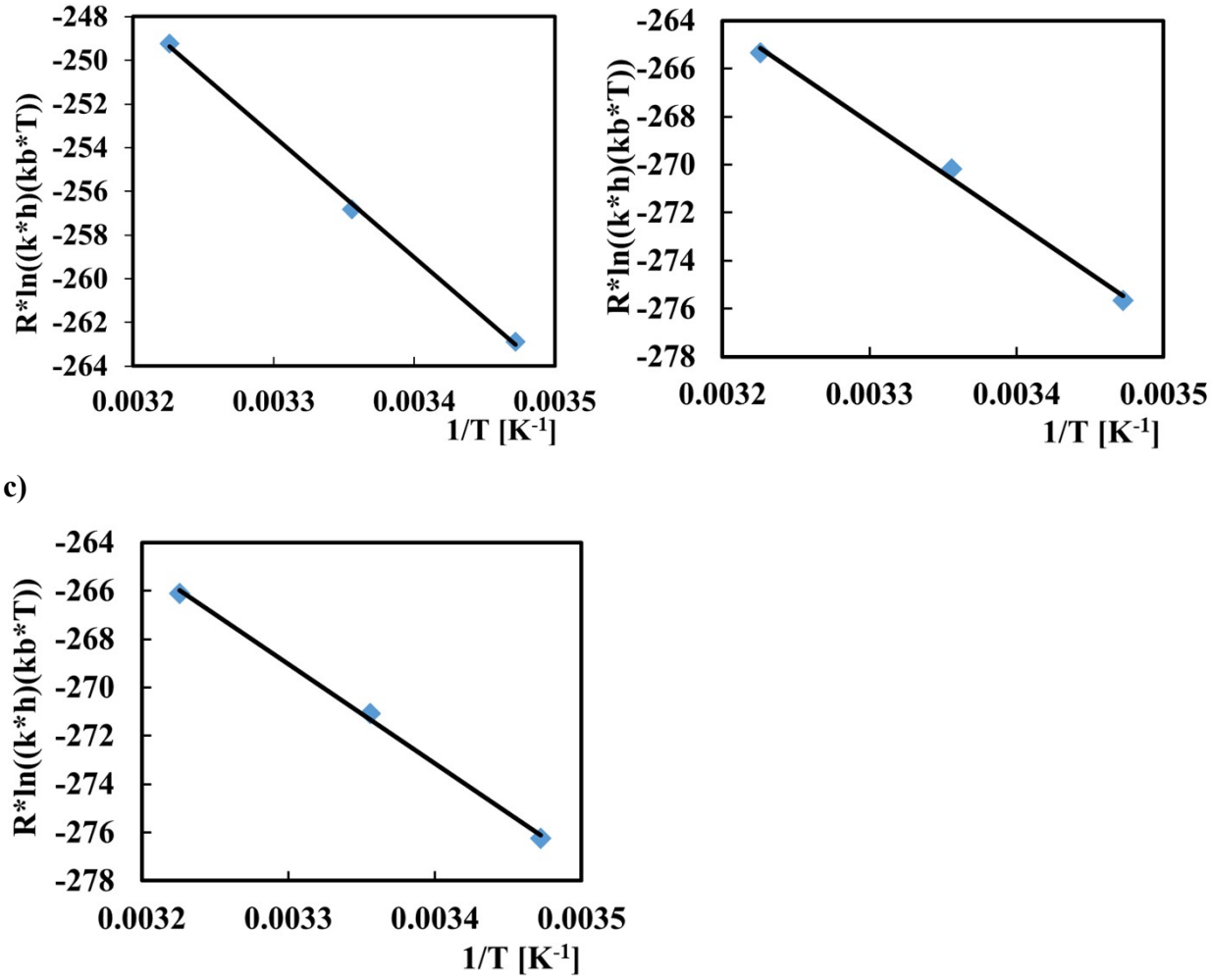

c)

Fig. S23. Eyring plots for the reactions of complex **1** with 5'-GMP (a), L-Cys (b) and L-Met (c).

DNA-binding studies

Calculation of the DNA-binding constants

In order to compare quantitatively the binding strength of complexes, the intrinsic binding constants K_b were determined by monitoring the changes in absorption at the MLCT band with increasing concentration of CT DNA using the following equation (S1)[S1]

$$[DNA]/(\varepsilon_A - \varepsilon_f) = [DNA]/(\varepsilon_b - \varepsilon_f) + 1/[K_b(\varepsilon_b - \varepsilon_f)] \quad (S1)$$

K_b is given by the ratio of the slope to the *y* intercept in plots $[DNA]/(\varepsilon_A - \varepsilon_f)$ *vs.* [DNA] (Fig. S39), where [DNA] is the concentration of DNA in base pairs, $\varepsilon_A = A_{obsd}/[complex]$, ε_f is the extinction coefficient for the unbound complex and ε_b is the extinction coefficient for the complex in the fully bound form.

Stern-Volmer equation for EB and Hoechst competitive studies

The relative binding of complexes to CT-DNA is described by Stern-Volmer equation (S2)[S2]:

$$I_0/I = 1 + K_{sv}[Q] \quad (S2)$$

where I_0 and I are the emission intensities in the absence and in the presence of the quencher (complexes **1, 2** or **3**), respectively, [Q] is the total concentration of quencher, K_{sv} is the Stern-Volmer quenching constant, which can be obtained from the slope of the plot of I_0/I *vs.* [Q] (Fig. S41).

Stern-Volmer equation for HSA quenching studies

Fluorescence quenching is described by Stern–Volmer equation:

$$I_0/I = 1 + k_q \tau_0 [Q] = 1 + K_{sv}[Q] \quad (S3)$$

where I_0 = the initial tryptophan fluorescence intensity of HSA, I = the tryptophan fluorescence intensity of HSA after the addition of the quencher, k_q = the quenching rate constants of HSA, K_{sv} = Stern-Volmer quenching constant, τ_0 = the average lifetime of HSA without the quencher, [Q] = the concentration of the quencher respectively.

$$K_{sv} = k_q \tau_0 \quad (S4)$$

and, taking as fluorescence lifetime (τ_0) of tryptophan in HSA at around 10^{-8} s, K_{sv} (M^{-1}) can be obtained by the slope of the diagram I_0/I *vs.* [Q] (Stern-Volmer plots, Fig. S44), and subsequently the approximate k_q (M^{-1} s^{-1}) may be calculated.[S2]

Scatchard equation for HSA quenching studies

From Scatchard equation:

$$\log (I_0 - I/I) = \log K_b + n \log [Q] \quad \text{(S5)}$$

where, K_b and n are the binding constant and the number of the binding sites, respectively. The number of the binding sites and the binding constant have been obtained from the slope and intercept of the linear plot of $\log[(I_0 - I)/I]$ *vs.* $\log [Q]$.

References

S1. A. M. Pyle, J. P. Rehmann, R. Meshoyrer, C. V. Kumar, N. J. Turro and J. K. Barton, *J. Am. Chem. Soc*., 1989, **111**, 3051-3058.

S2. R. Lakowicz and G. Weber, *Biochemistry*, 1973, **12**, 4161-4170.

S3. S. Wu, W. Yuan, H. Wang, Q. Zhang, M. Liu, K. Yu, *J. Inorg. Biochem*., 2008, **102**, 2026-2034.\

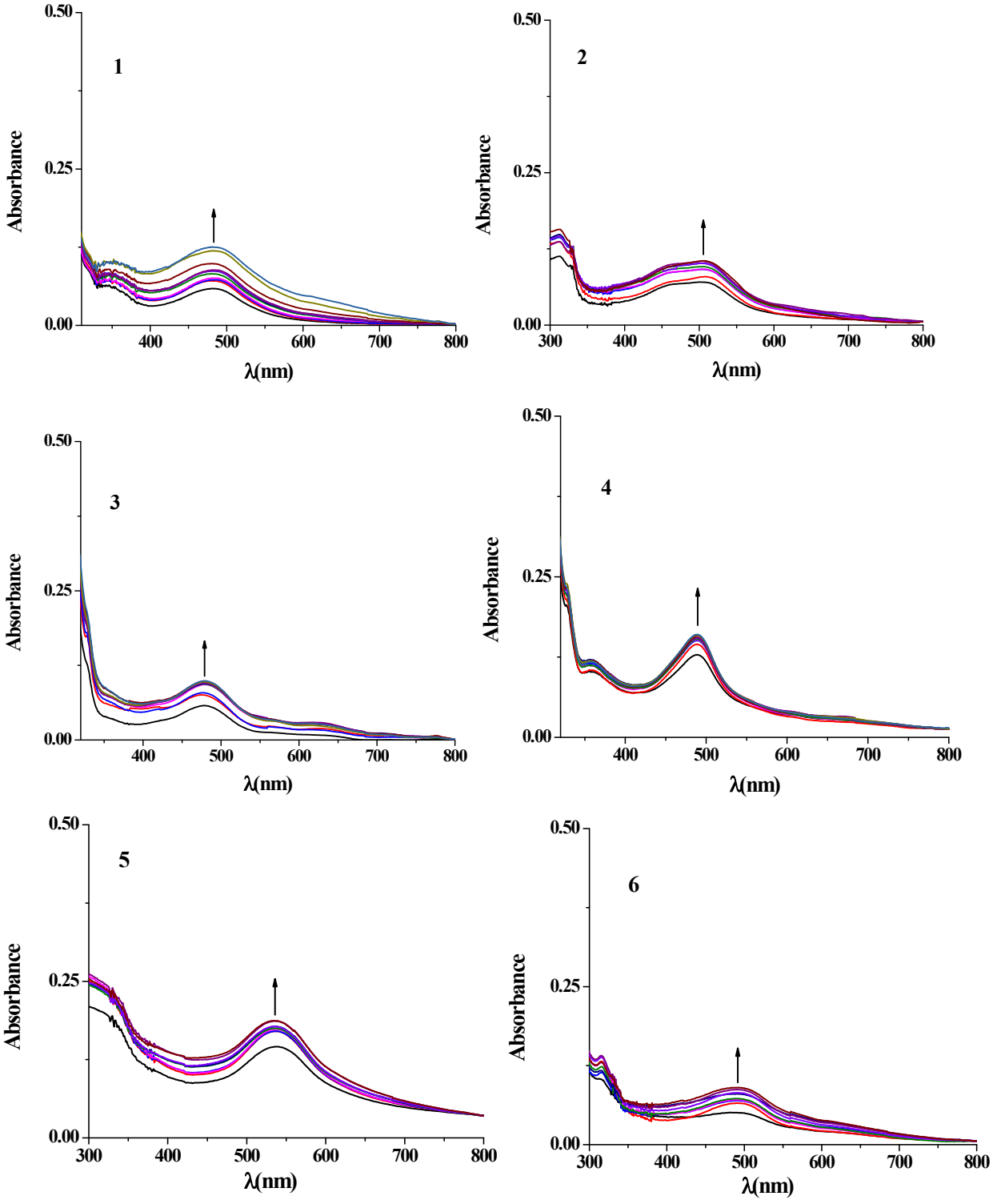
1
2
3
4
5
6
Absorbance
λ(nm)
0.00
0.25
0.50
300
400
500
600
700
800

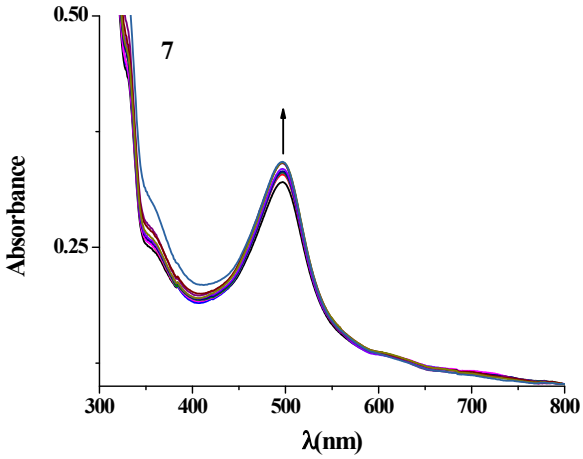

Fig. S24. Absorption spectra of complexes **1**–**7** in 10 mM PBS upon addition of CT DNA. [Ru] = 1.00 x 10^{-5}, [DNA] = (0-2) x 10^{-5} M. Arrows show the absorbance changing upon increasing CT DNA concentrations.

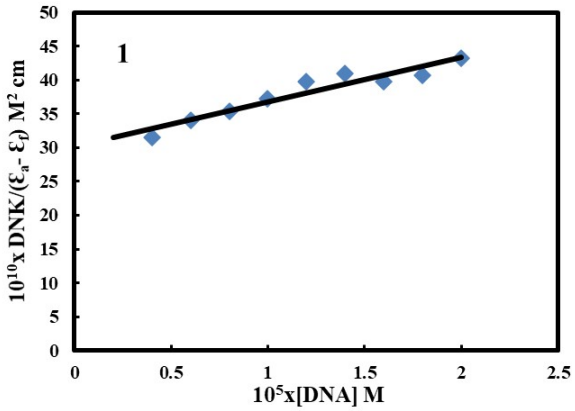
1
10^{10}x DNK/(ε_a- ε_f) M^2 cm
10^5x[DNA] M

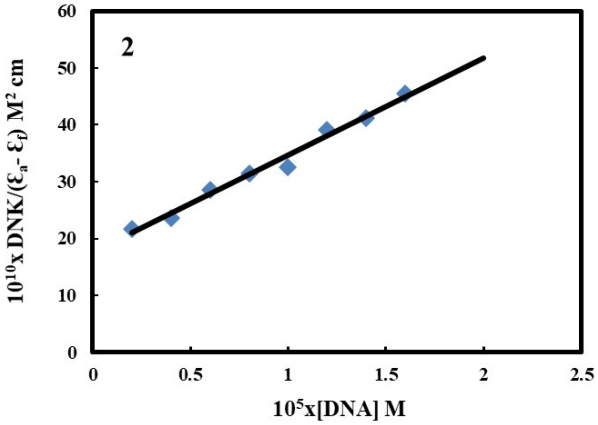
2
10^{10}x DNK/(ε_a- ε_f) M^2 cm
10^5x[DNA] M

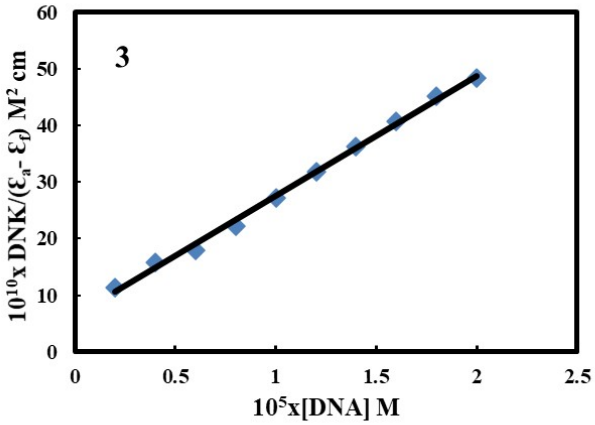
3
10^{10}x DNK/(ε_a- ε_f) M^2 cm
10^5x[DNA] M

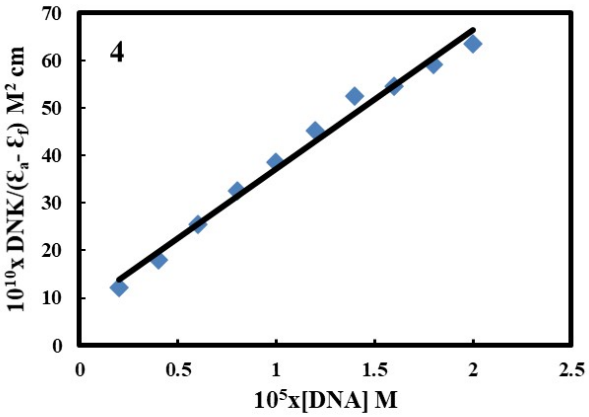
4
10^{10}x DNK/(ε_a- ε_f) M^2 cm
10^5x[DNA] M

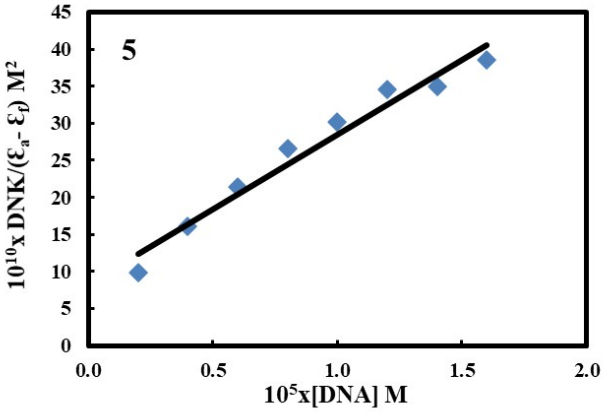
5
10^{10}x DNK/(ε_a- ε_f) M^2
10^5x[DNA] M

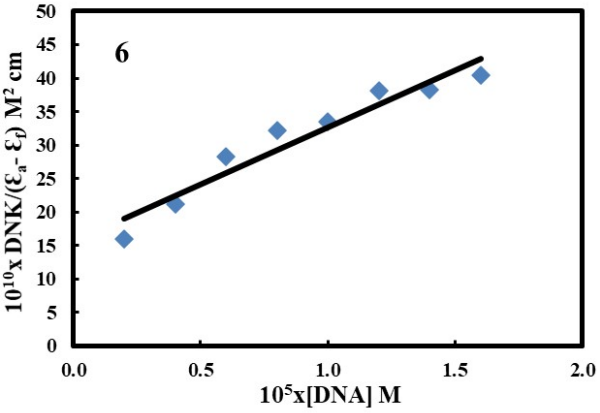
6
10^{10}x DNK/(ε_a- ε_f) M^2 cm
10^5x[DNA] M

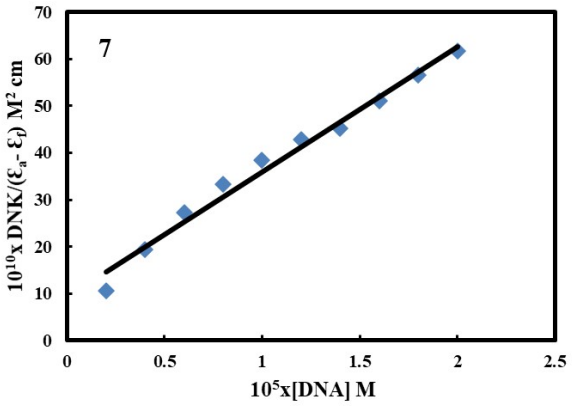

Fig. S25. Plots of [DNA]/($\varepsilon_A - \varepsilon_f$) *vs.* [DNA] for complexes **1–7**.

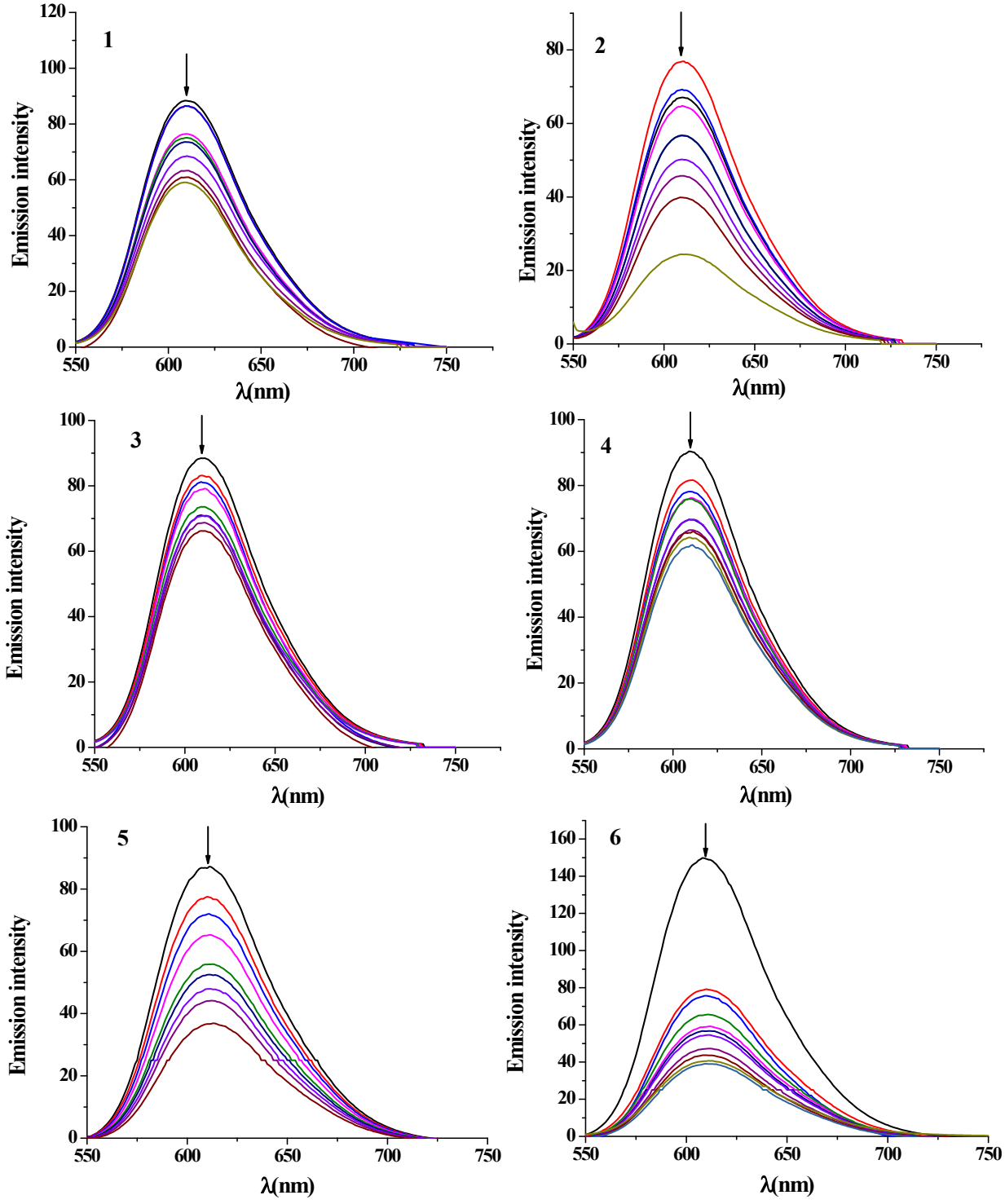
1
Emission intensity
λ(nm)
2
Emission intensity
λ(nm)
3
Emission intensity
λ(nm)
4
Emission intensity
λ(nm)
5
Emission intensity
λ(nm)
6
Emission intensity
λ(nm)

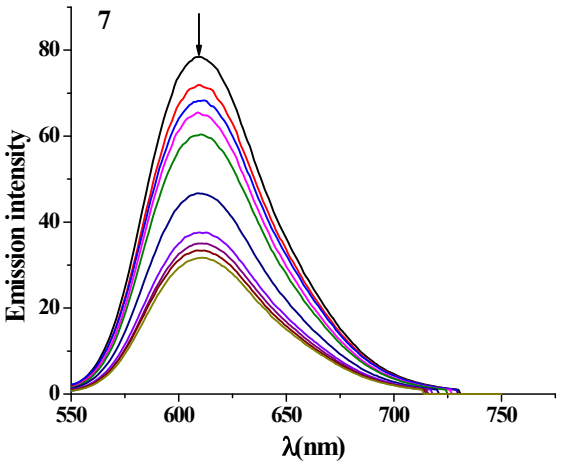

Fig. S26. Emission spectra of EB bound to DNA in the presence of complexes **1–7**. [EB] = 28,6 μM, [DNA] = 28,6 μM; [Ru] = 0–57,2 μM; λ_{ex} = 527 nm. The arrows show the change of the intensity upon increasing the concentration of complexes.

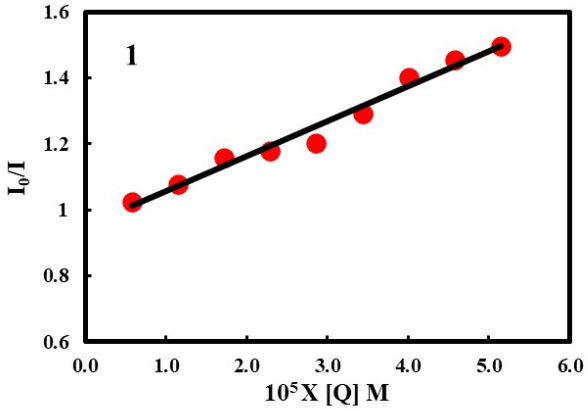
1
I_0/I
10^5X [Q] M

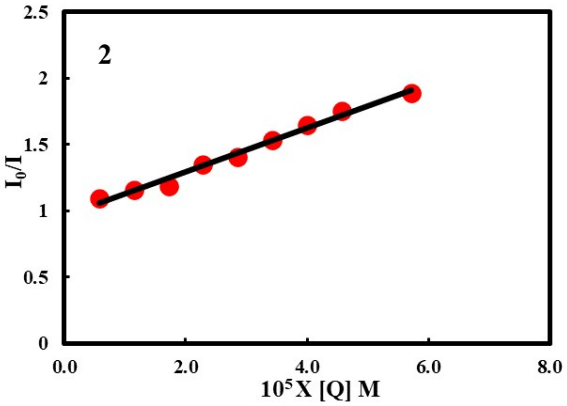
2
I_0/I
10^5X [Q] M

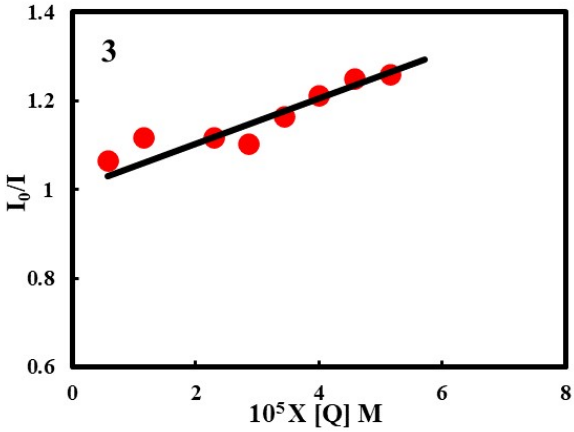
3
I_0/I
10^5X [Q] M

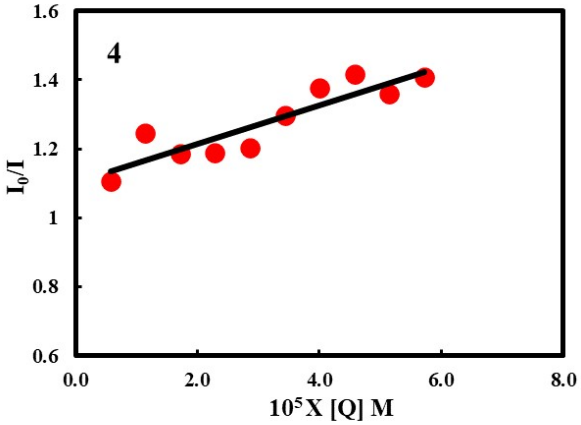
4
I_0/I
10^5X [Q] M

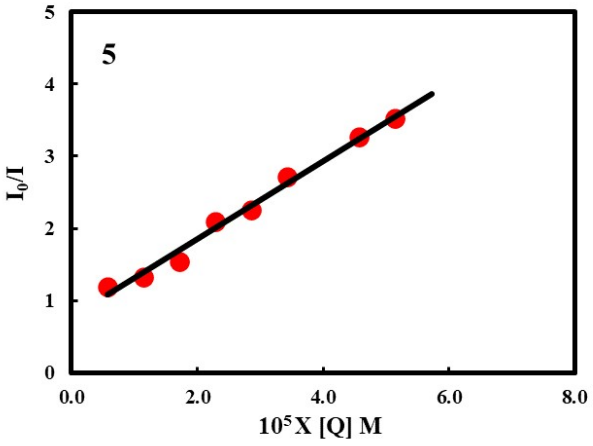
5
I_0/I
10^5X [Q] M

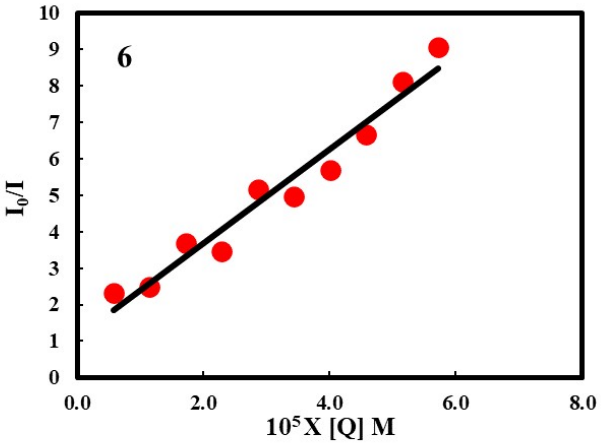
6
I_0/I
10^5X [Q] M

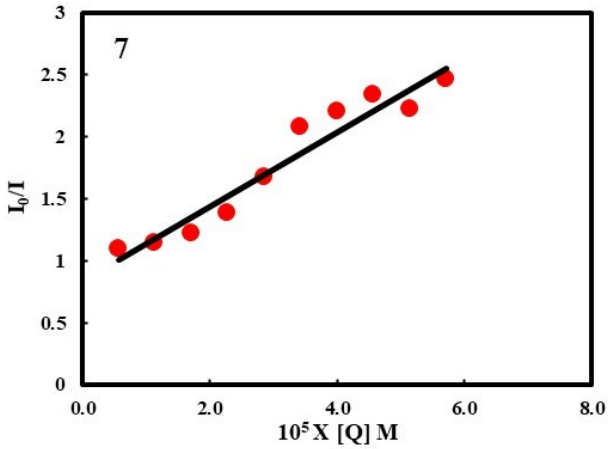

Fig. S27. Stern-Volmer quenching plot of EB-DNA for complexes **1**–**7**.

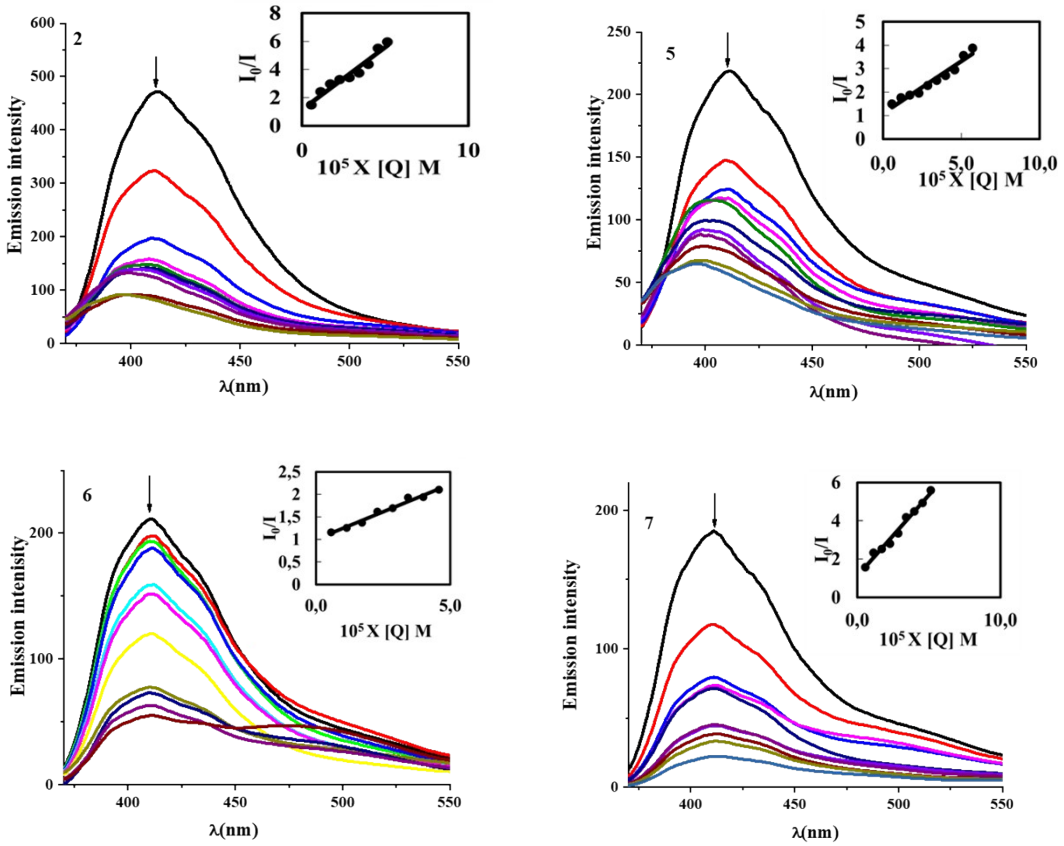

Fig. S28. Fluorescence spectra of Hoechst-CT DNA in the presence of varying amounts of complexes **2**, **5**, **6** and **7** in 10 mM PBS. Arrow shows the changes in fluorescence intensity upon increasing the concentration of complexes **2, 5, 6** and **7**. Insert graph: Stern-Volmer plots of Hoechst-CT DNA for complexes **2**, **5, 6** and **7**.

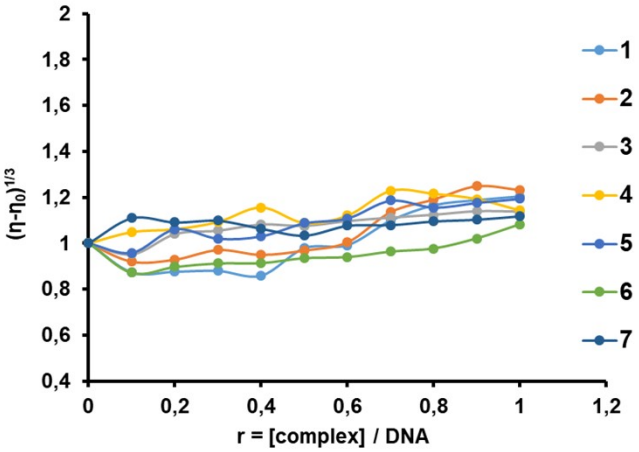

Fig. S29. Relative viscosity $(\eta/\eta_0)^{1/3}$ of CT DNA (0.01 mM) in 10 mM PBS in the presence of the increasing amounts of complexes **1**–**7** (*r*).

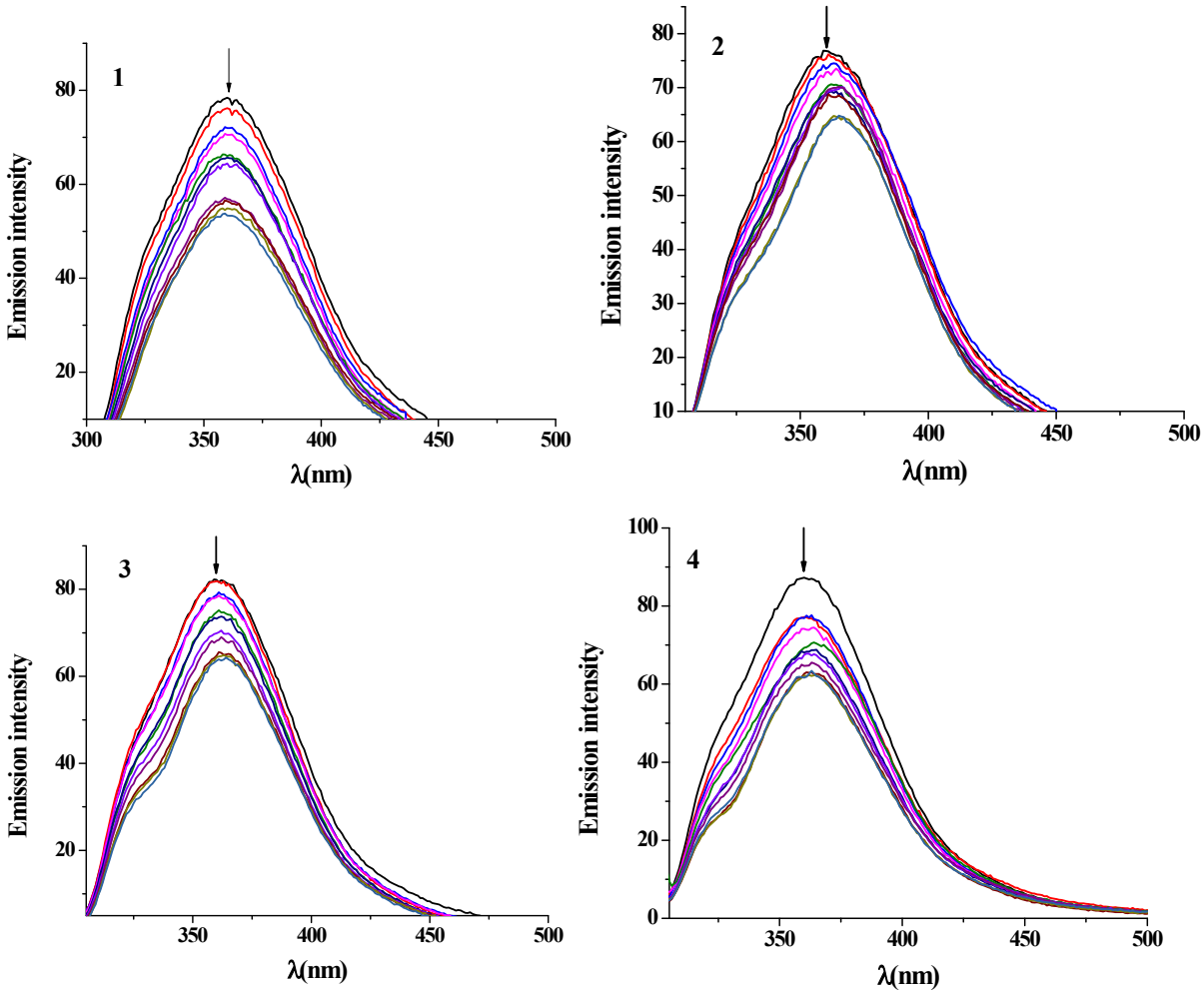

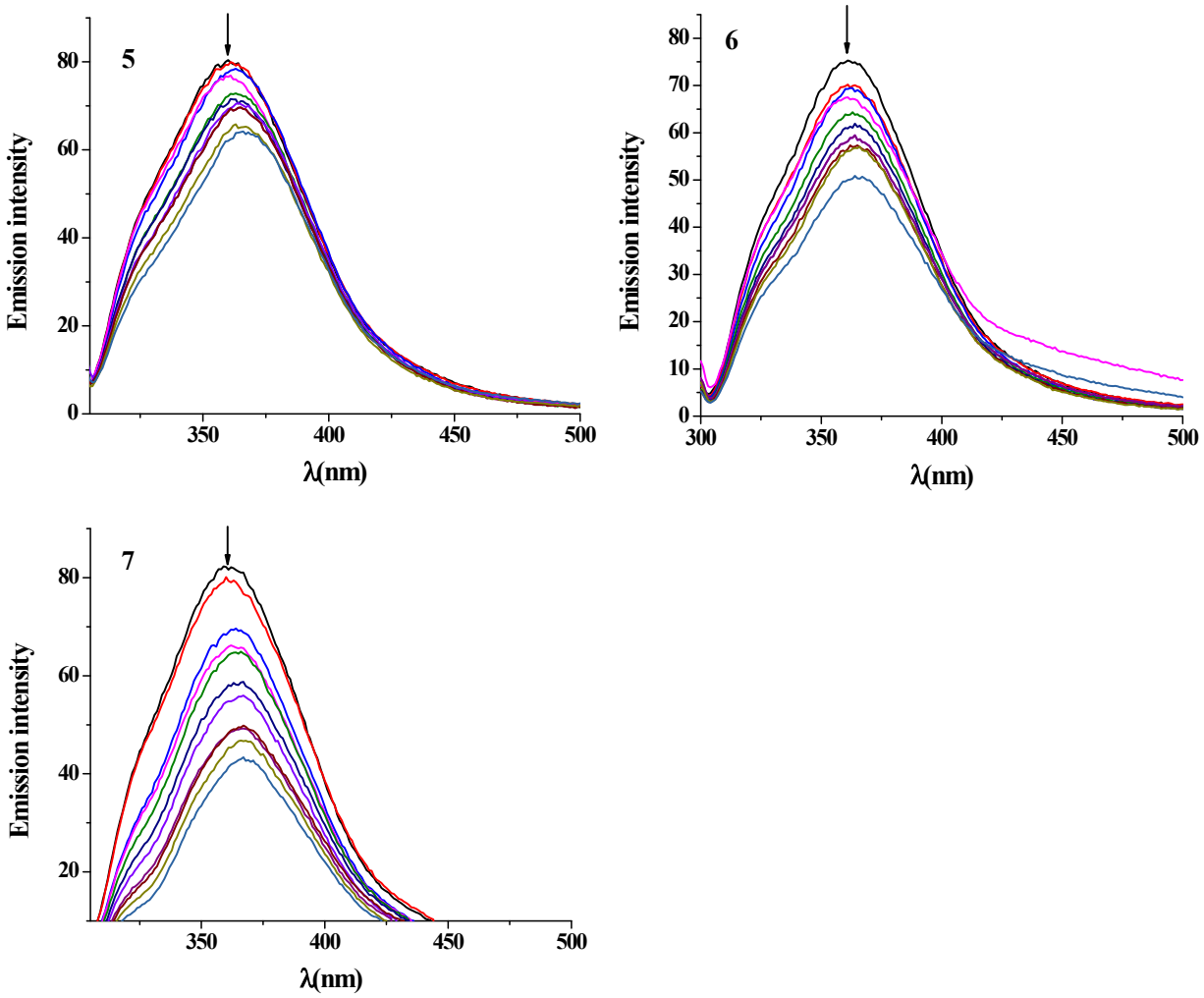

Fig. S30. Emission spectra of HSA in the presence of complexes **1–7**. [HSA] = 2 μM, [Ru] = 0–20 μM; λ_{ex} = 295 nm. Arrow shows the changes in intensity upon increasing the concentration of complexes.

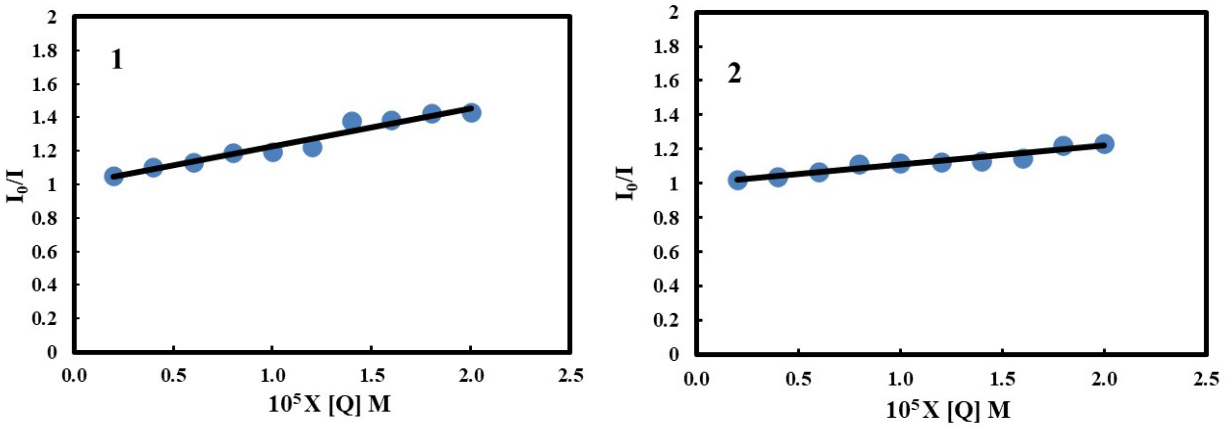

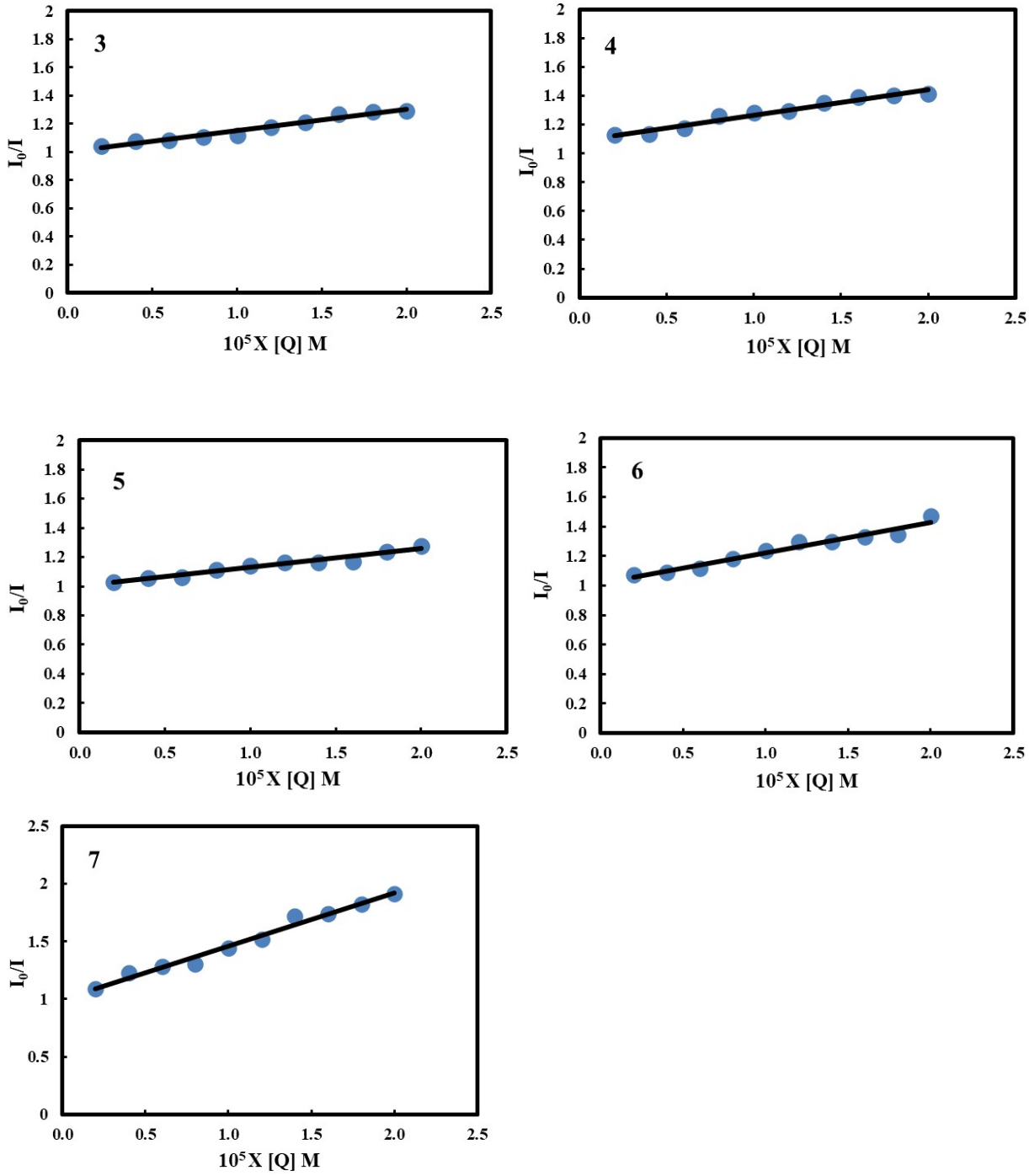

Fig. S31. Stern-Volmer quenching plots of HSA for complexes **1–7**.

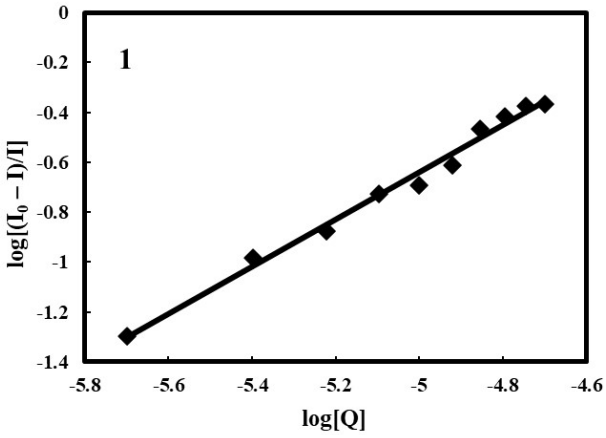
1
log[(I0 – I)/I]
log[Q]
0
-0.2
-0.4
-0.6
-0.8
-1
-1.2
-1.4
-5.8
-5.6
-5.4
-5.2
-5
-4.8
-4.6

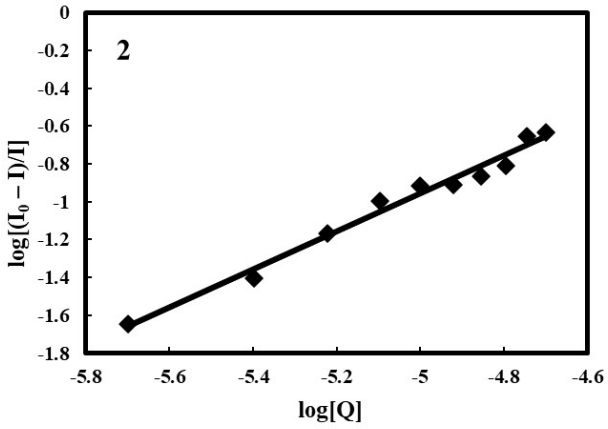
2
log[(I0 – I)/I]
log[Q]
0
-0.2
-0.4
-0.6
-0.8
-1
-1.2
-1.4
-1.6
-1.8
-5.8
-5.6
-5.4
-5.2
-5
-4.8
-4.6

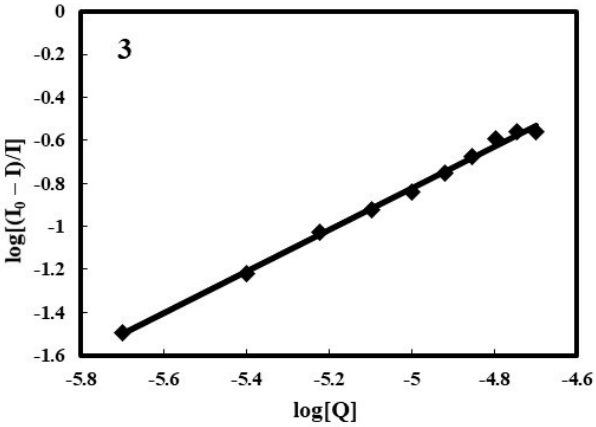
3
log[(I0 – I)/I]
log[Q]
0
-0.2
-0.4
-0.6
-0.8
-1
-1.2
-1.4
-1.6
-5.8
-5.6
-5.4
-5.2
-5
-4.8
-4.6

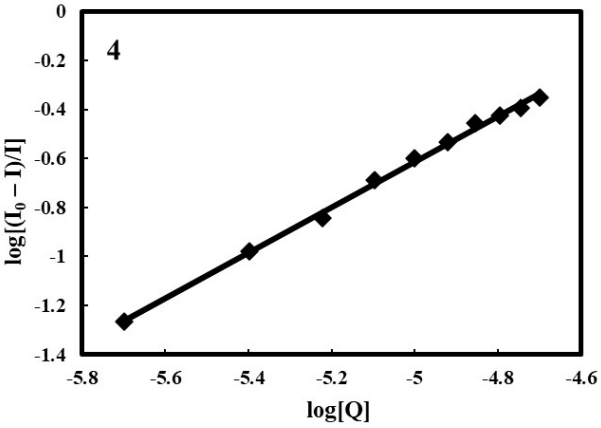
4
log[(I0 – I)/I]
log[Q]
0
-0.2
-0.4
-0.6
-0.8
-1
-1.2
-1.4
-5.8
-5.6
-5.4
-5.2
-5
-4.8
-4.6

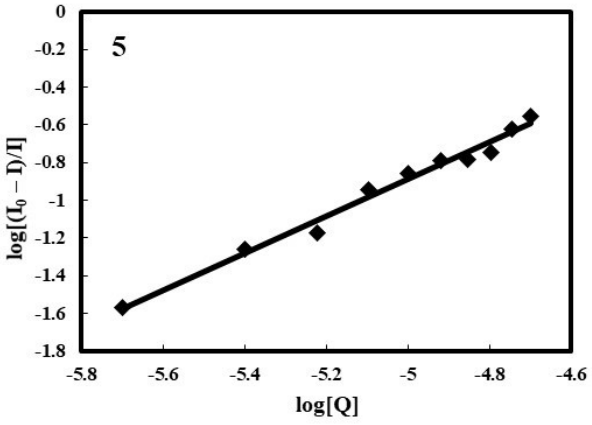
5
log[(I0 – I)/I]
log[Q]
0
-0.2
-0.4
-0.6
-0.8
-1
-1.2
-1.4
-1.6
-1.8
-5.8
-5.6
-5.4
-5.2
-5
-4.8
-4.6

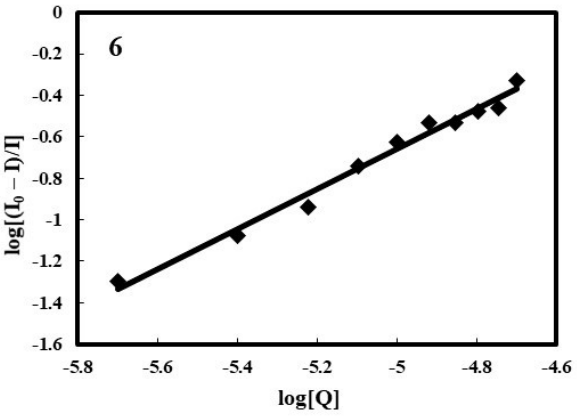
6
log[(I0 – I)/I]
log[Q]
0
-0.2
-0.4
-0.6
-0.8
-1
-1.2
-1.4
-1.6
-5.8
-5.6
-5.4
-5.2
-5
-4.8
-4.6

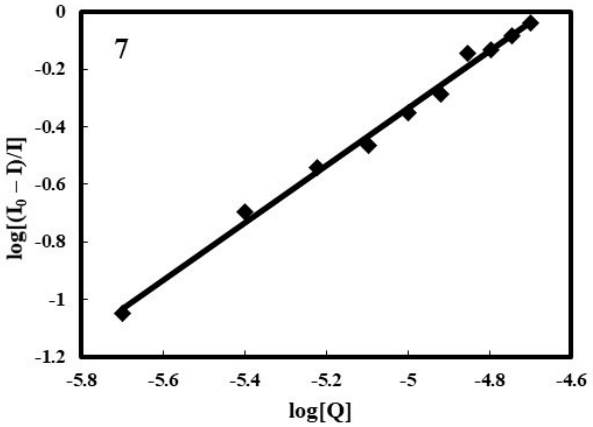

Fig. S32. Dependency of log [(I_0-I)/I] *vs*. log [Q] for the interactions of **1–7** with HSA.

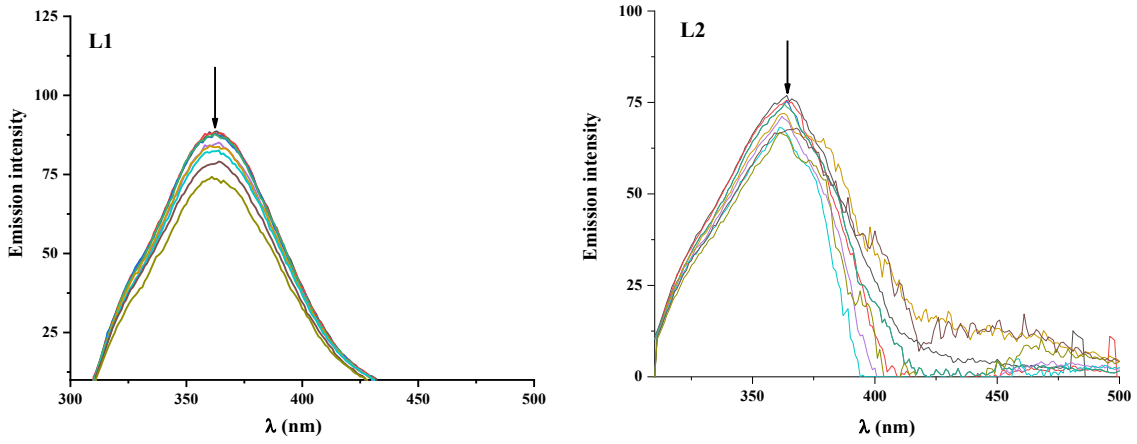

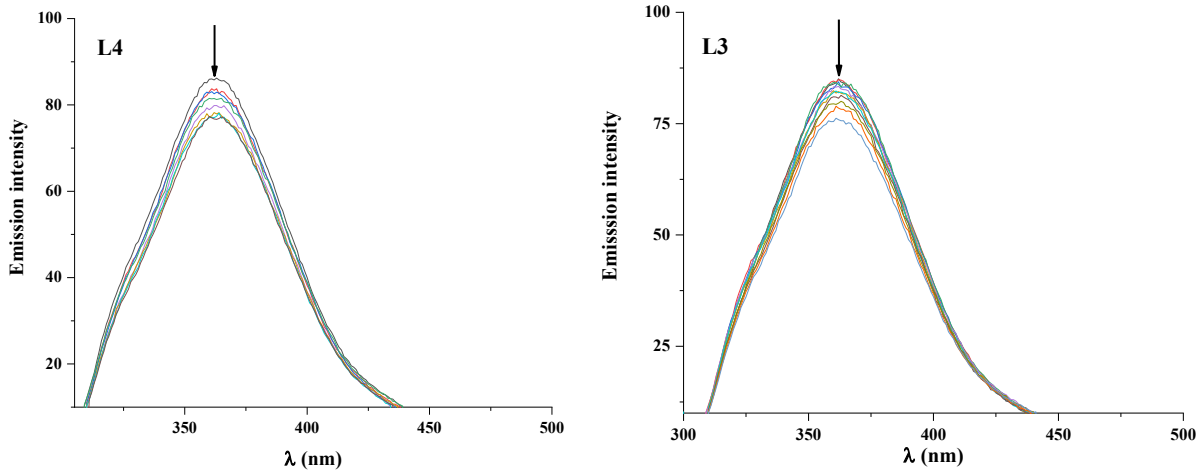

Fig. S33. Emission spectra of HSA in the presence of ligands **L1 – L4**. [HSA] = 2 μM, [L] = 0–20 μM; λ_{ex} = 295 nm. Arrow shows the changes in intensity upon increasing the concentration of ligands.

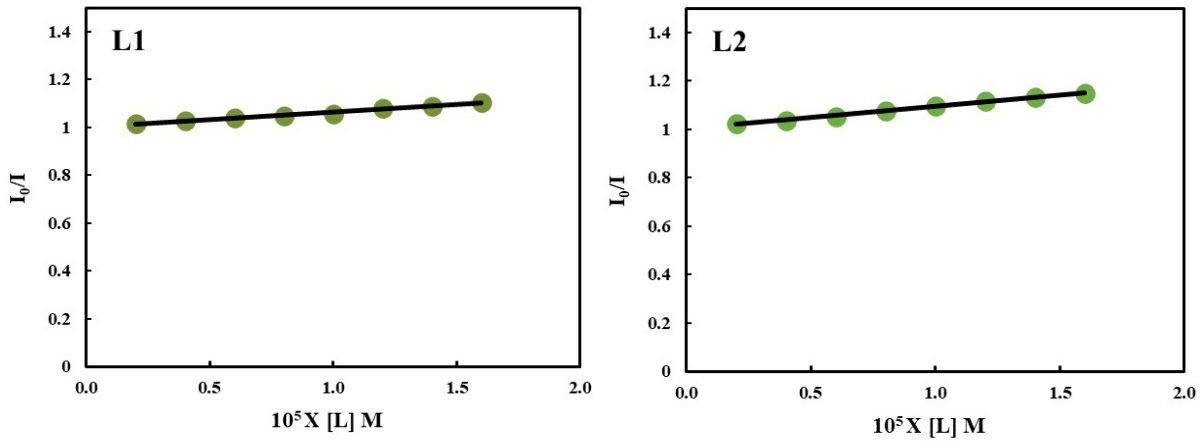

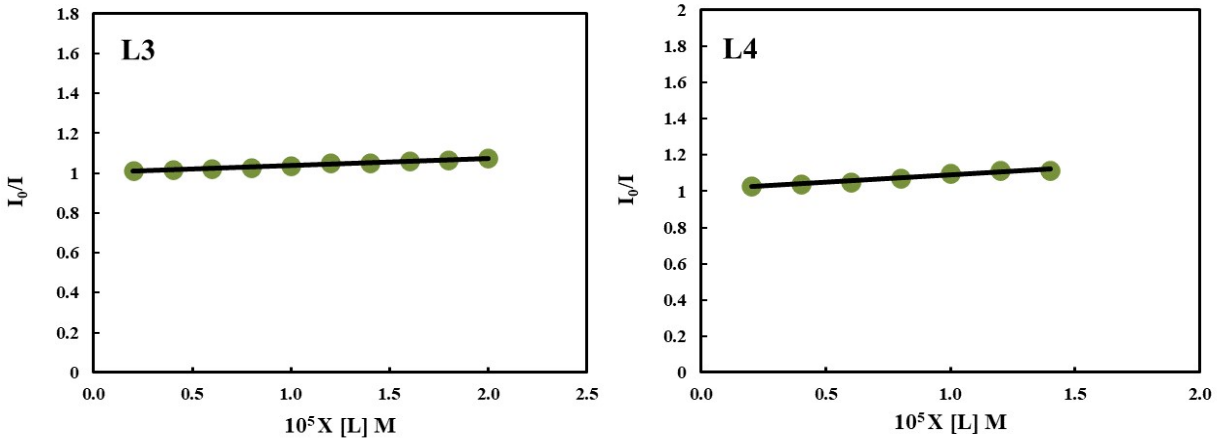

Fig. S34. Stern-Volmer quenching plots of HSA for ligands **L1 – L4**.

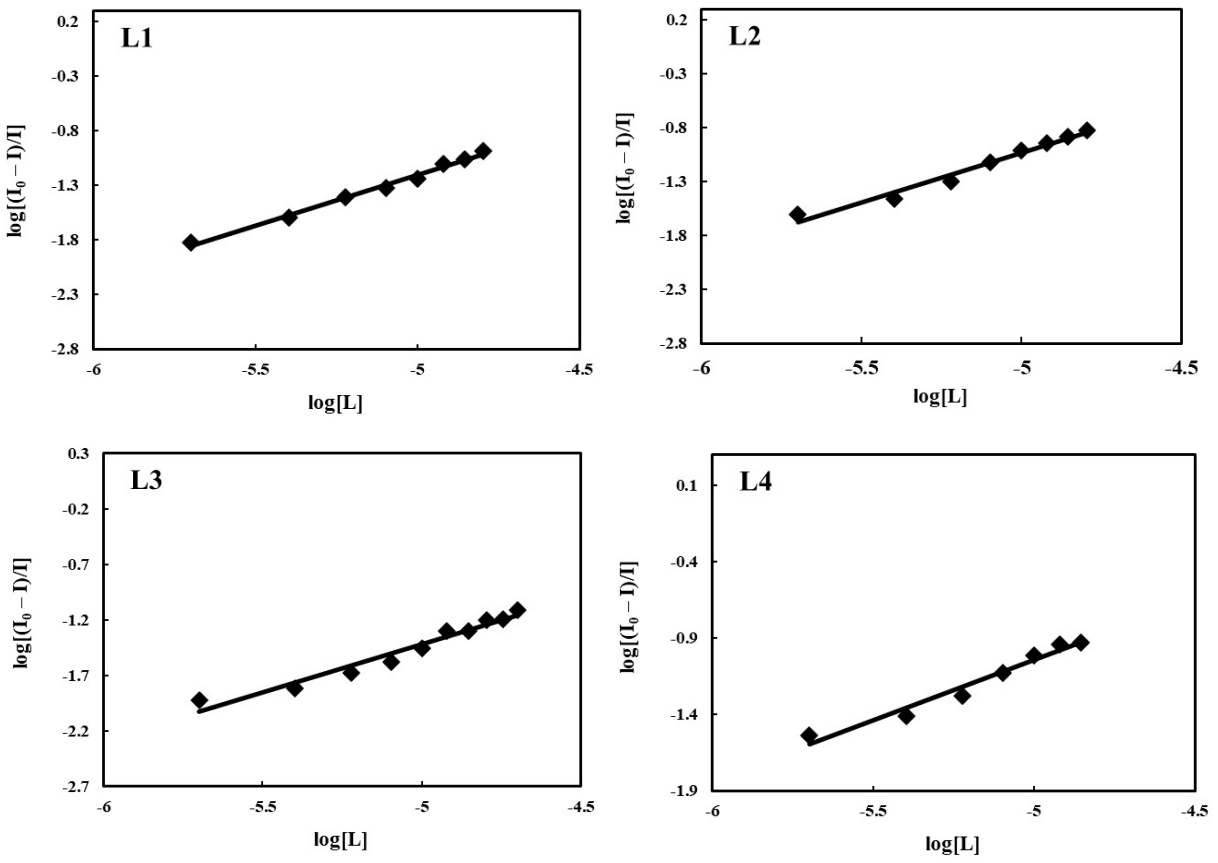

Fig. S35. Dependency of log [(I0-I)/I] vs. log [L] for the interactions of **L1 – L4** with HSA.

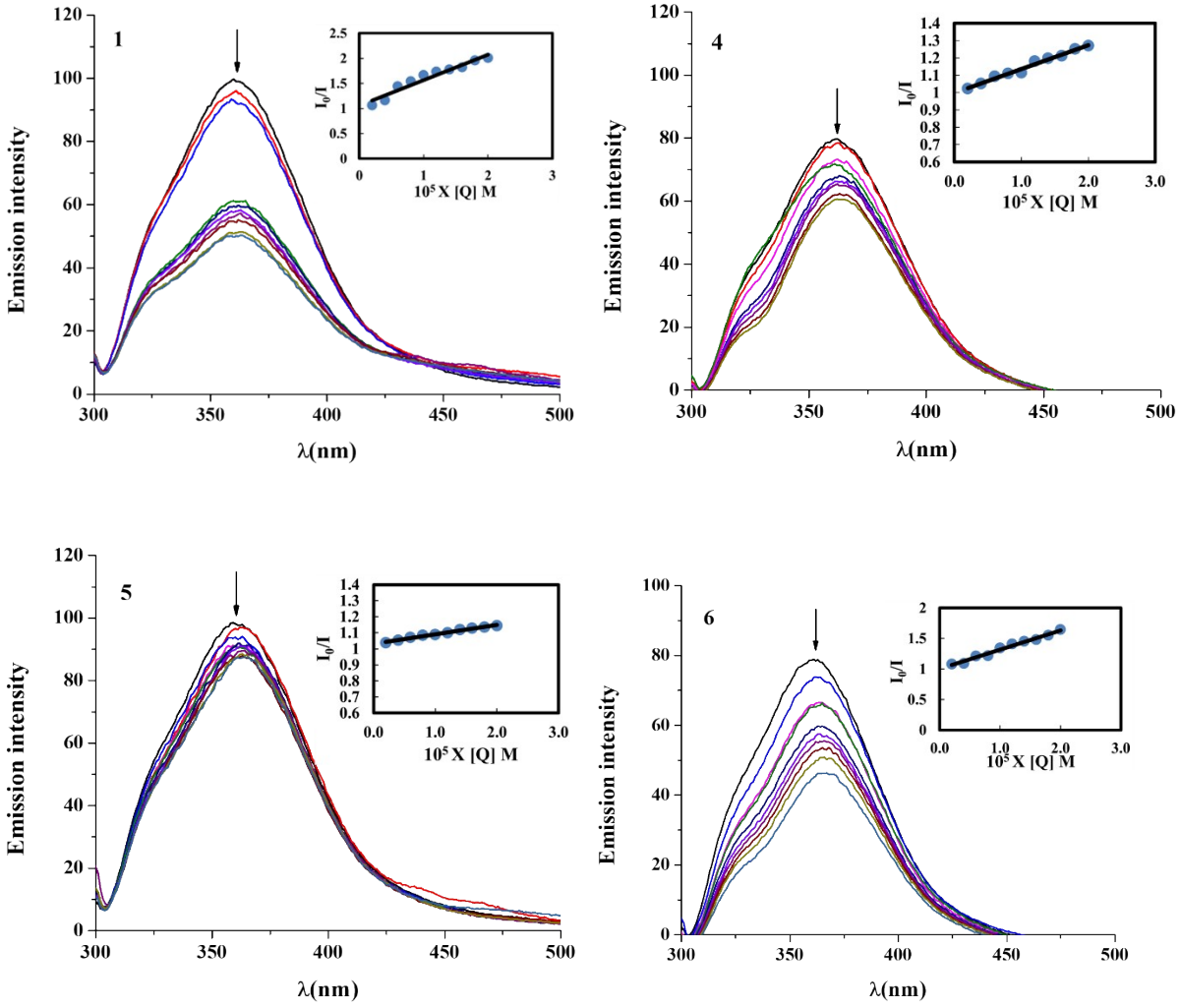

Fig. S36. Emission spectra of HSA-Ibuprofen in the presence of complexes **1, 4, 5** and **6**. [HSA] = 2 μM [Ibuprofen] = 2 μM, [Ru] = 0–20 μM; λ_{ex} = 295 nm. Arrow shows the changes in the fluorescence intensity upon increasing the concentration of complexes. Insert graph: Stern-Volmer quenching plot of HSA-Ibuprofen for complexes **1–7**.

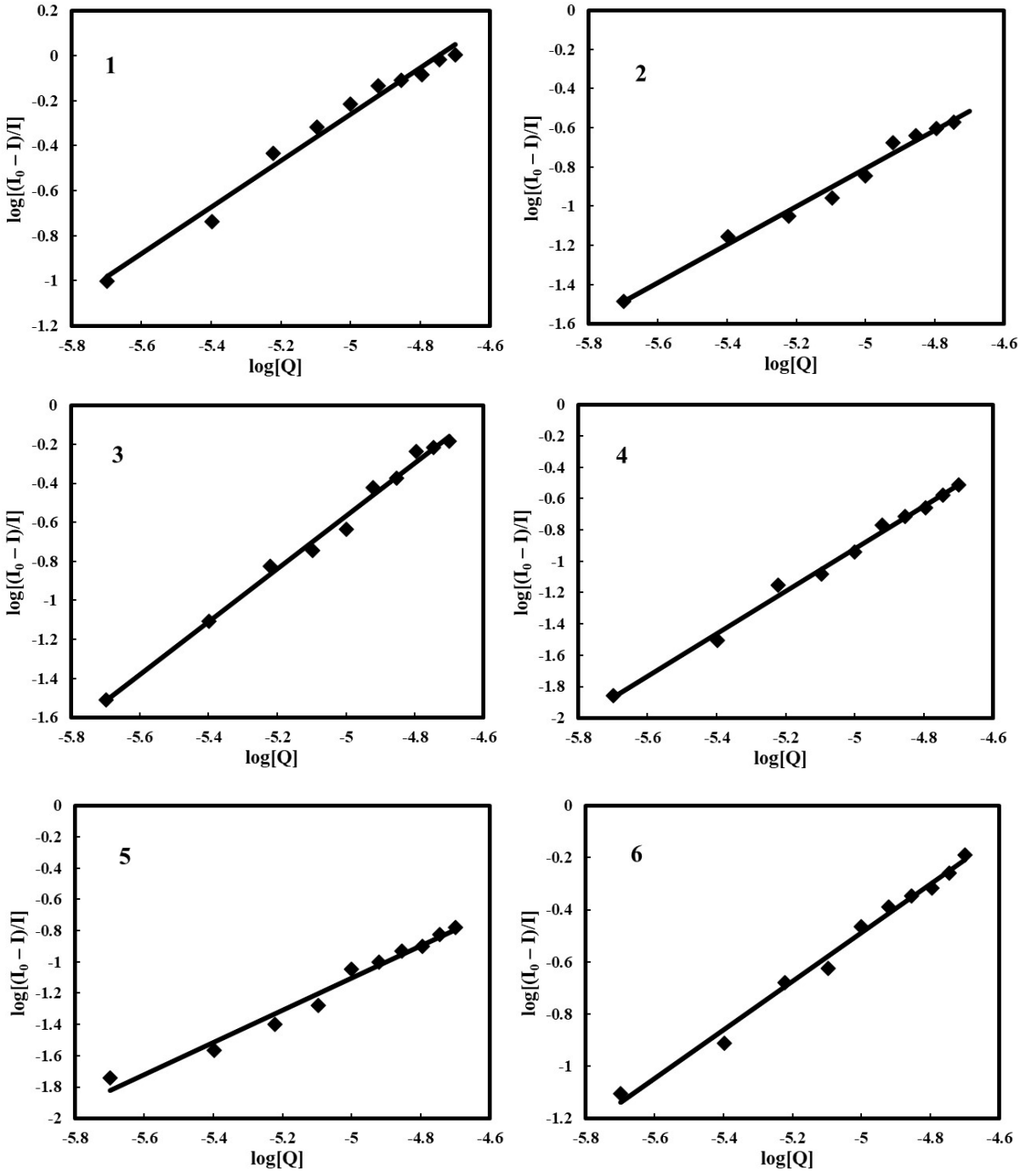
1
2
3
4
5
6
log[(I0 – I)/I]
log[Q]

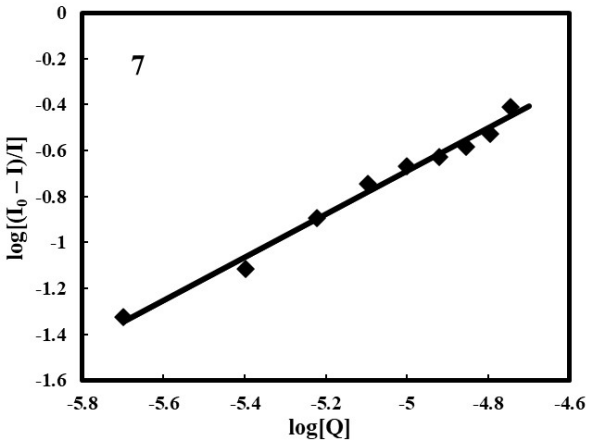

Fig. S37. Dependency of log [(I_0-I)/I] *vs*. log [Q] for the interactions of **1–7** with HSA-Ibuprofen

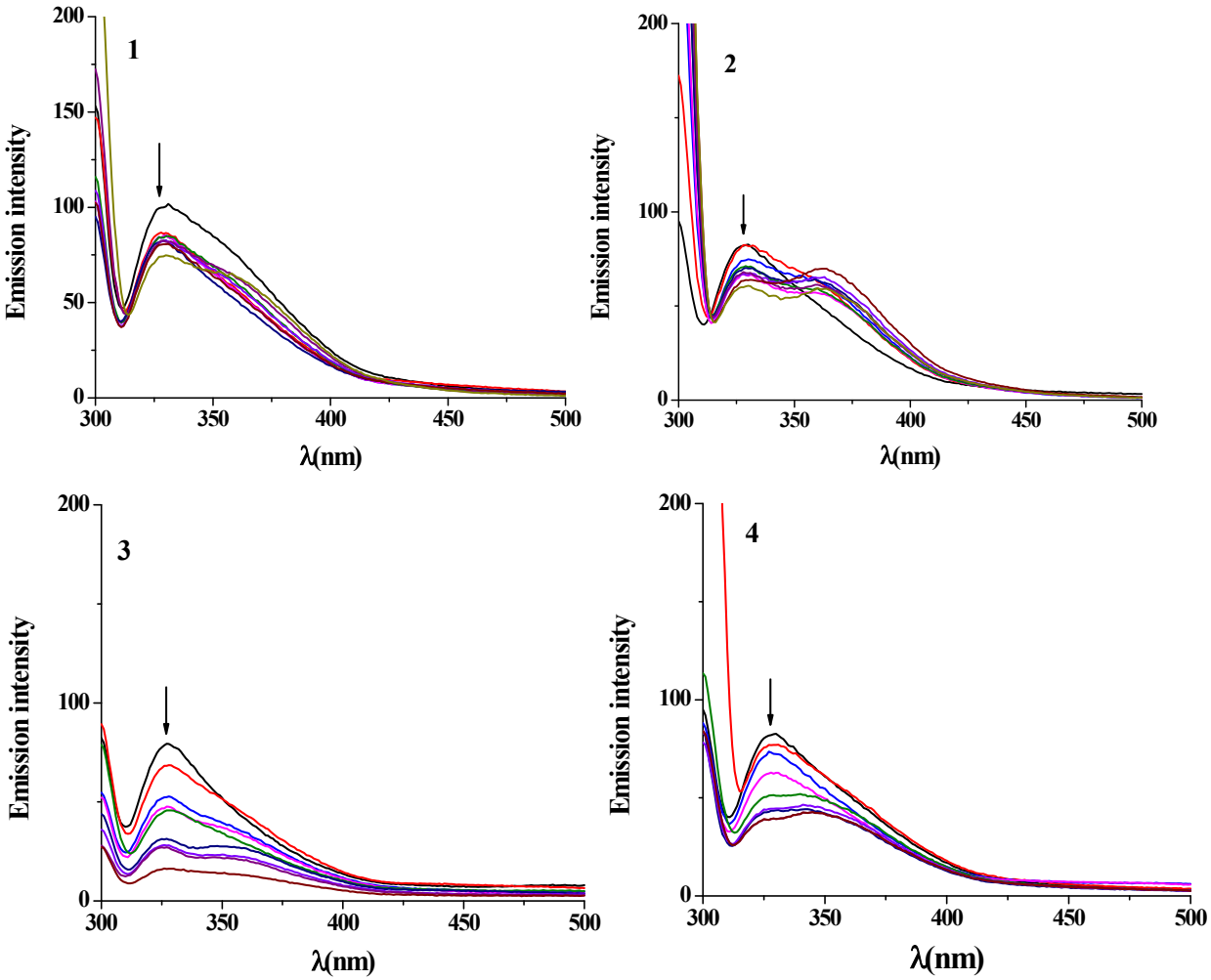

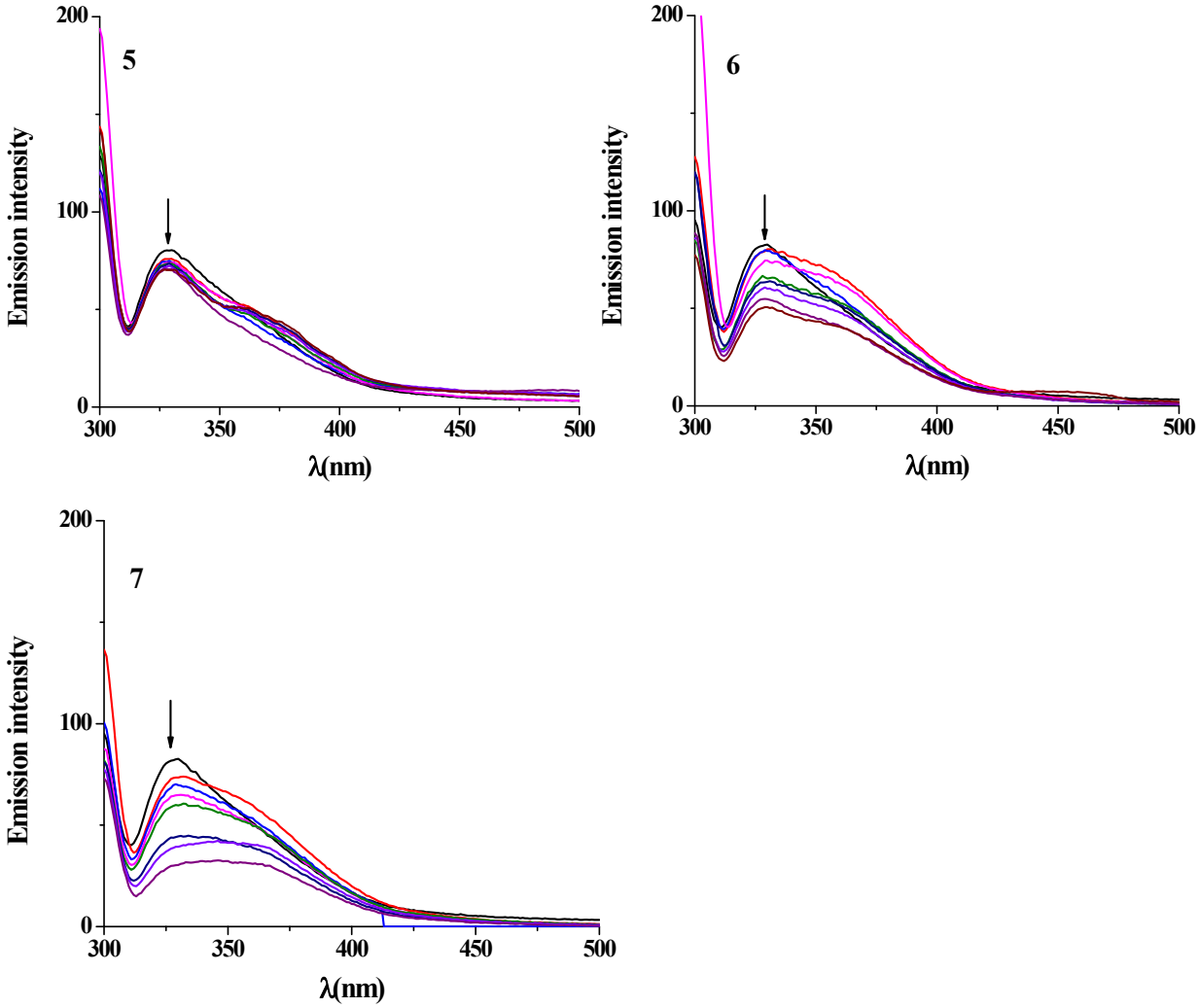

Fig. S38. Emission spectra of HSA-Eozin Y in the presence of complexes **1–7**. [HSA] = 2 Mm, [Eozin Y] = 2 μM, [Ru] = 0–20 μM; λ_{ex} = 295 nm. Arrow shows the changes in intensity upon increasing the concentration of complexes.

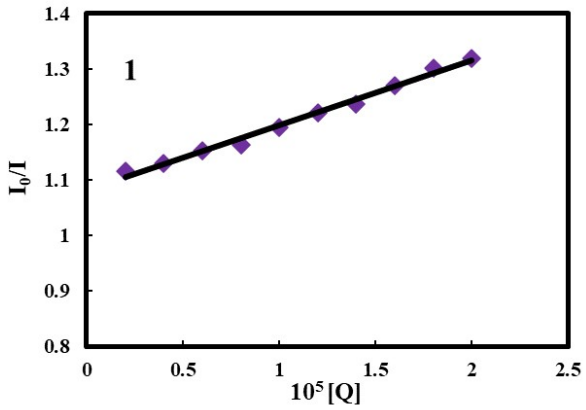
1
I_0/I
10^5 [Q]

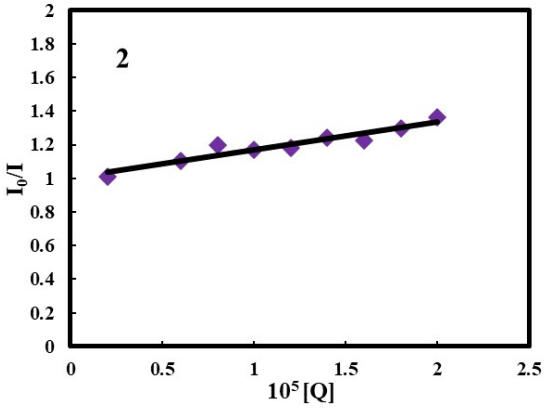
2
I_0/I
10^5 [Q]

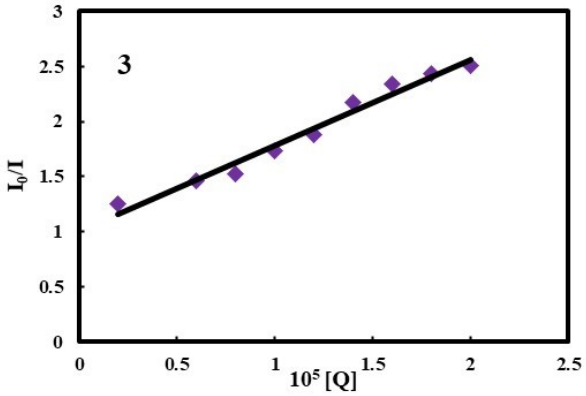
3
I_0/I
10^5 [Q]

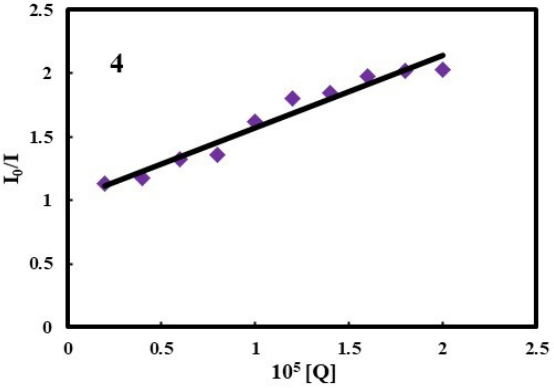
4
I_0/I
10^5 [Q]

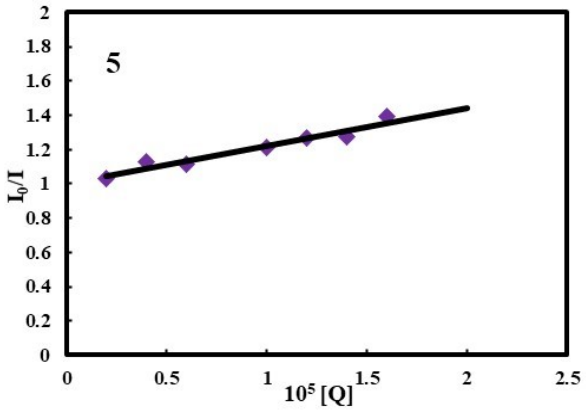
5
I_0/I
10^5 [Q]

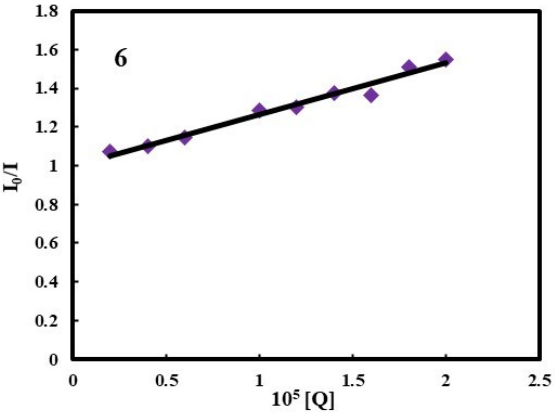
6
I_0/I
10^5 [Q]

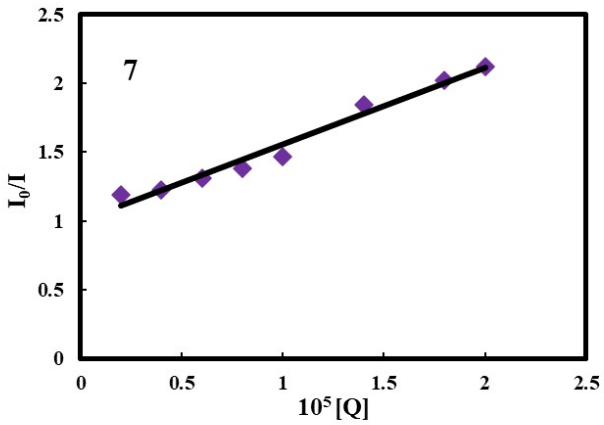

Fig. S39. Stern-Volmer quenching plot of HSA-Eozin Y for complexes **1–7**.

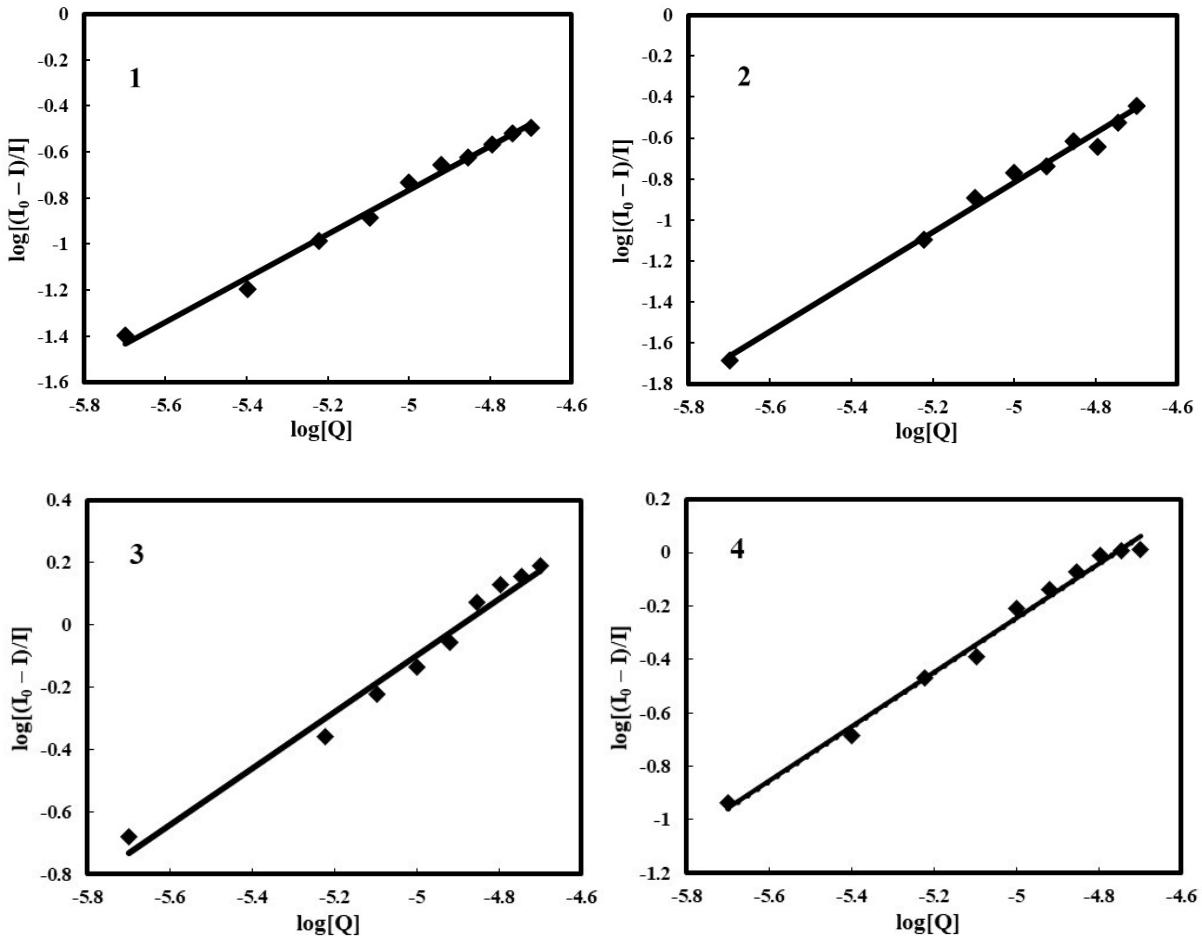

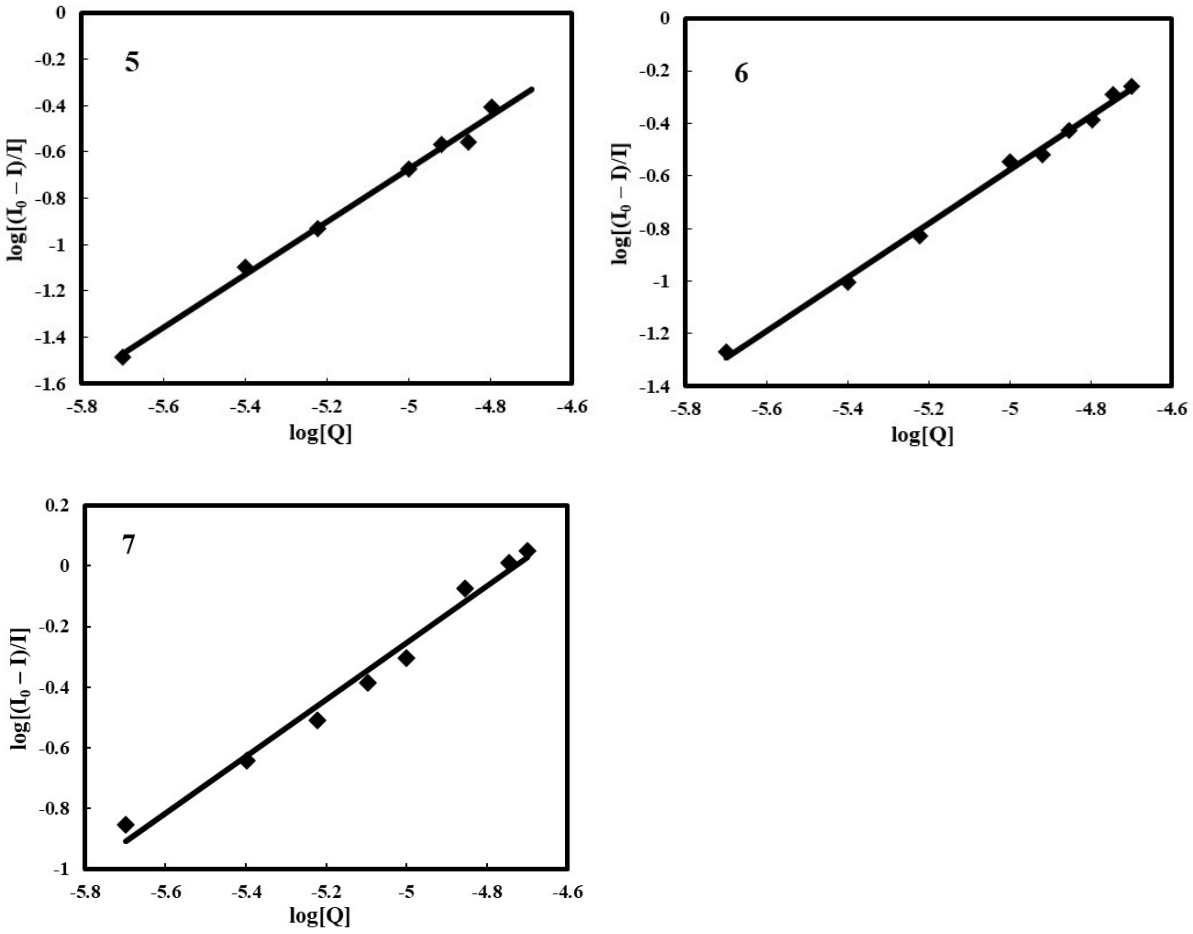

Fig. S40. Dependency of log [(I_0-I)/I] *vs*. log [Q] for the interactions of **1–7** with HSA-Eozin Y.

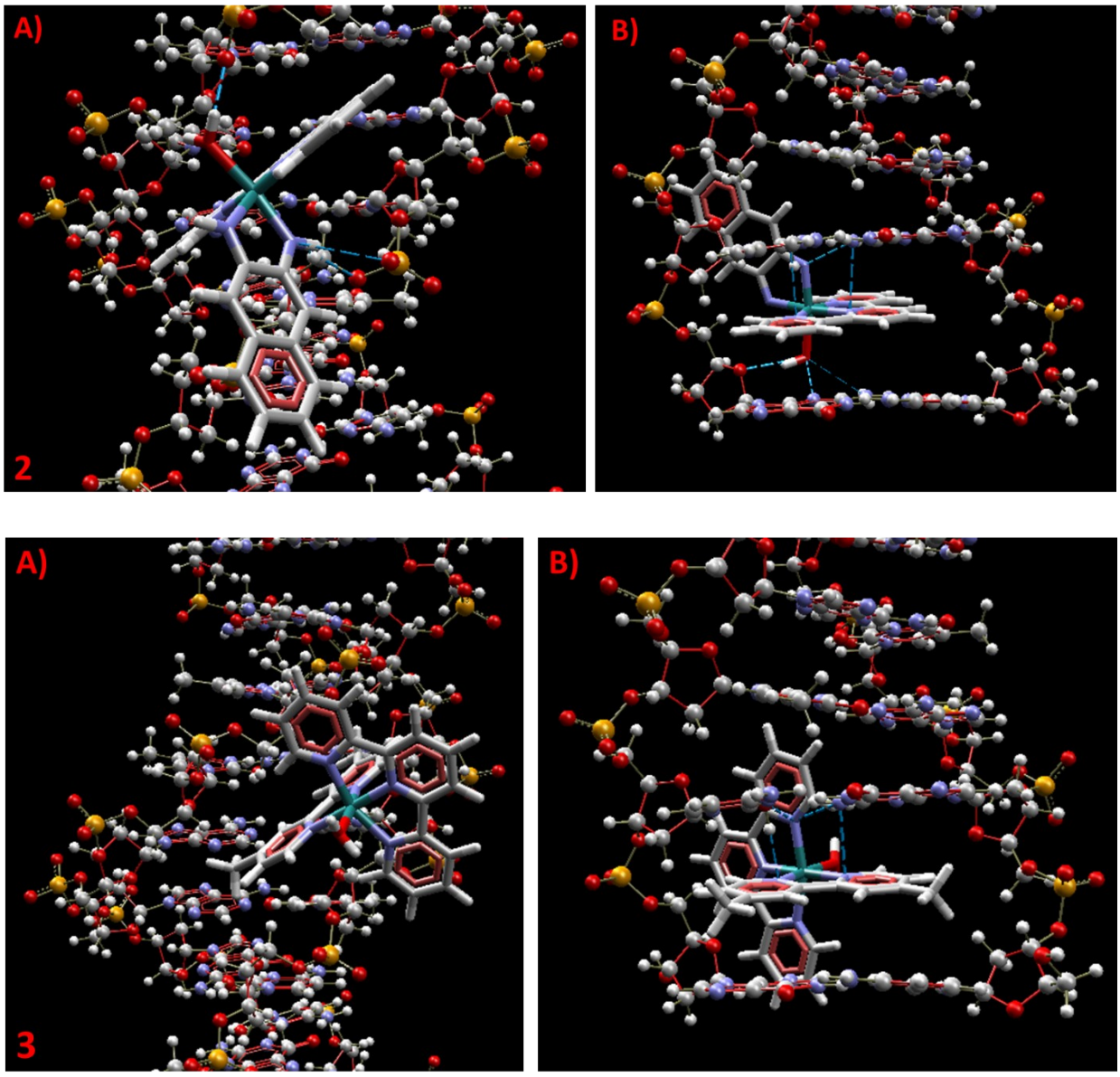
A)
2
B)
A)
3
B)

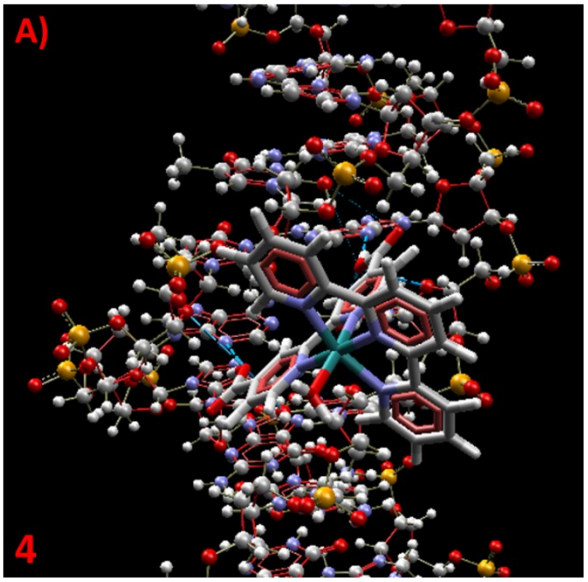
A)
4

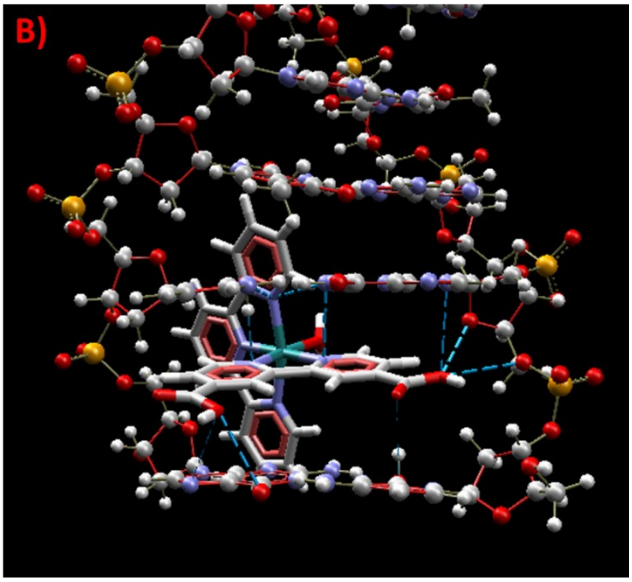
B)

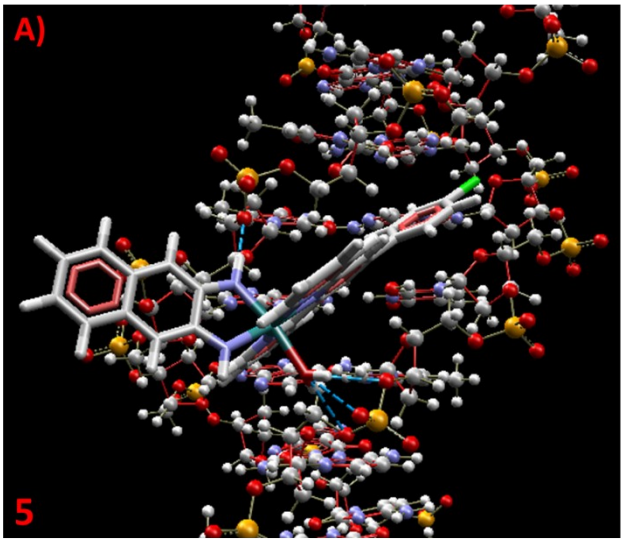
A)
5

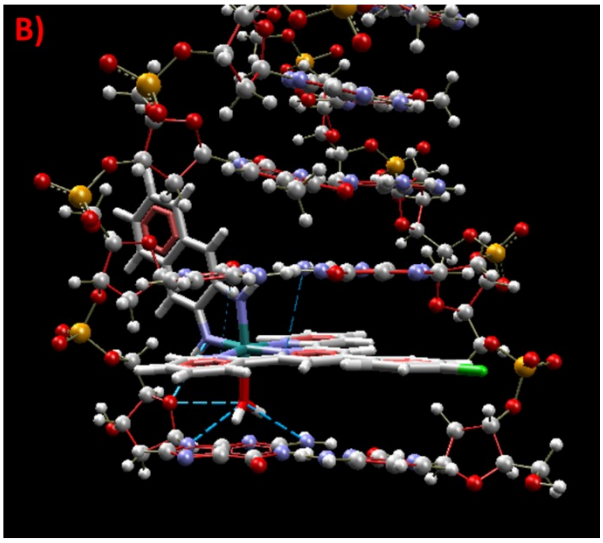
B)

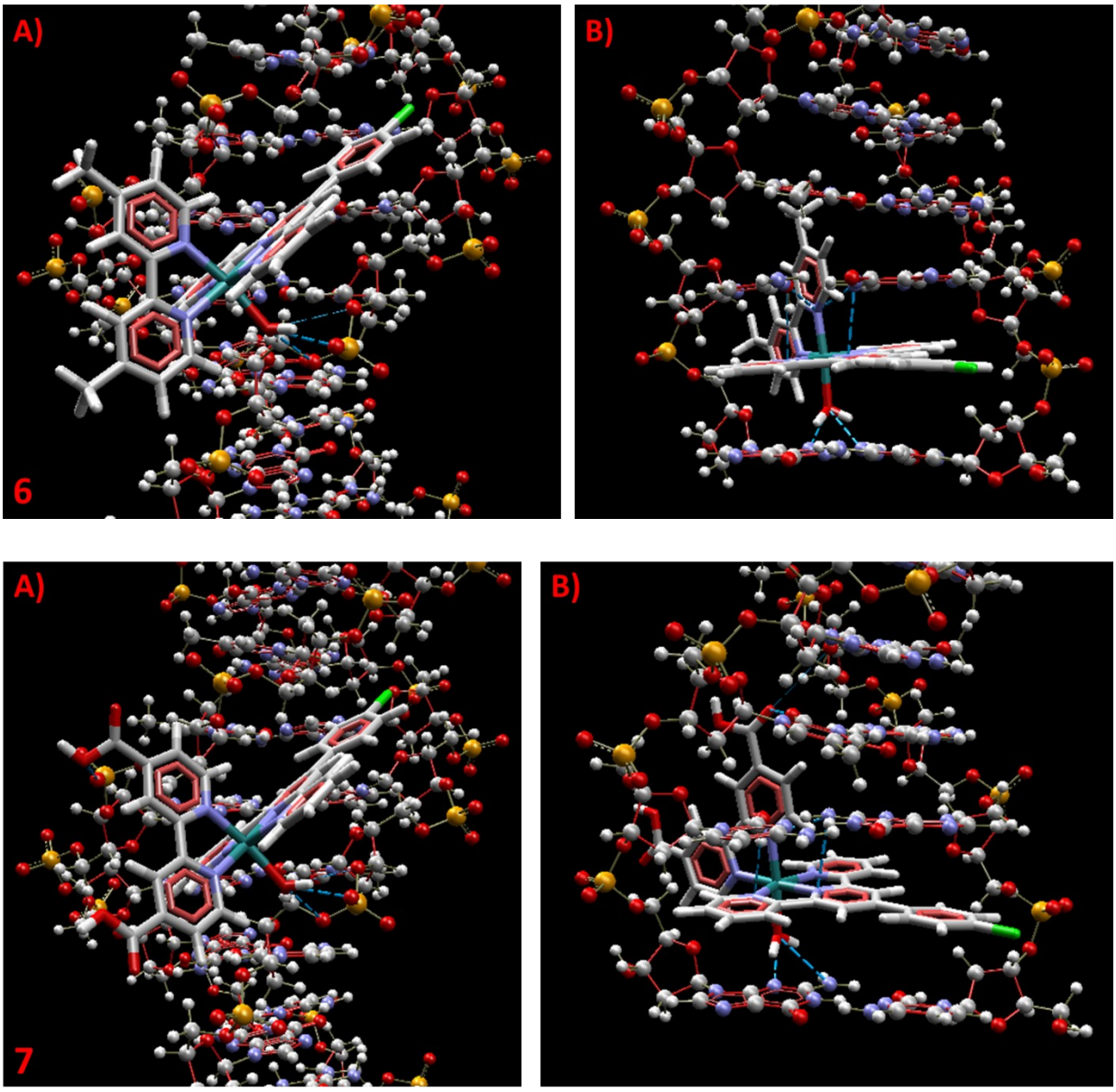

Fig. S41. Computational docking model illustrating interactions between complexes **2**, **3**, **4**, **5**, **6**, **7** and DNA with the A) minor groove and B) intercalation gap. Hydrogen bonds are shown in blue dotted lines.

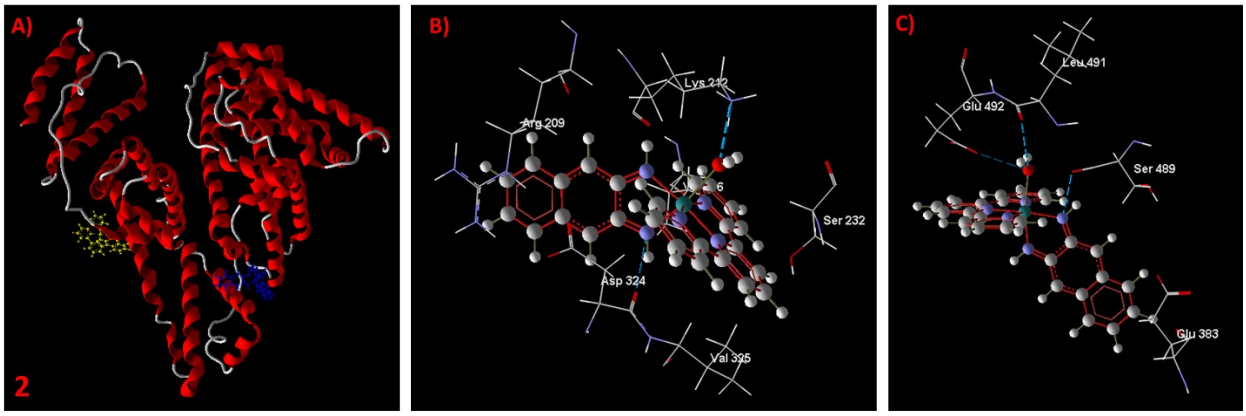
A)
2
B)
Lys 212
Arg 209
Ser 232
Asp 324
Val 325
C)
Leu 491
Glu 492
Ser 489
Glu 383

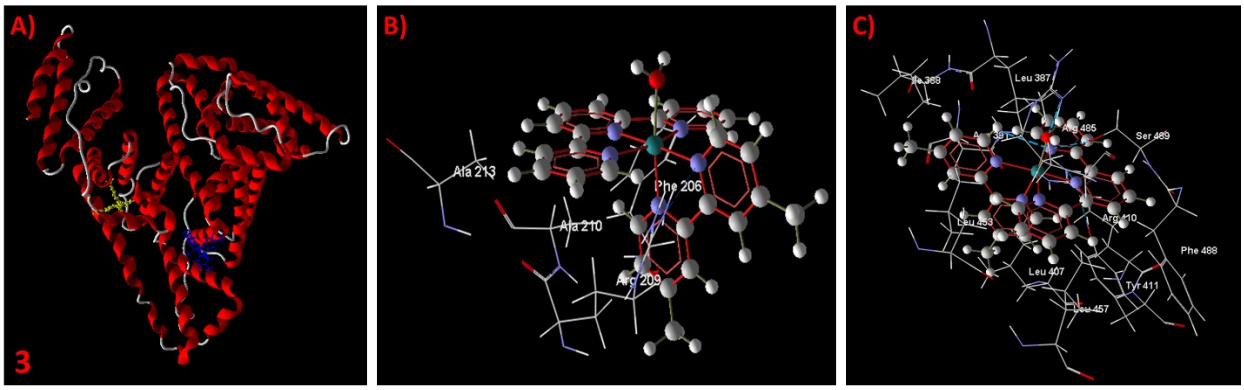
A)
3
B)
Ala 213
Phe 206
Ala 210
Arg 209
C)
Leu 387
Arg 485
Ser 489
Arg 410
Phe 488
Leu 407
Tyr 411
Leu 457

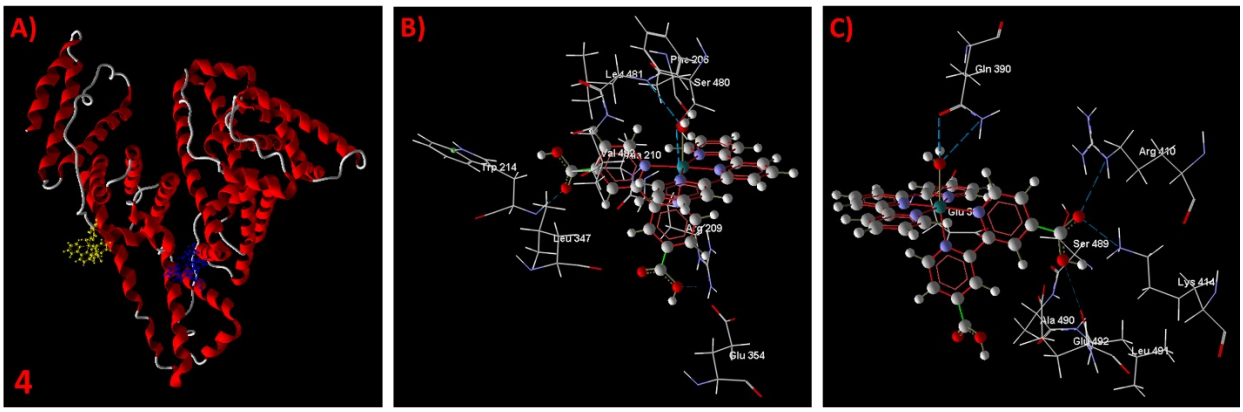
A)
4
B)
Phe 206
Leu 481
Ser 480
Trp 214
Ala 210
Leu 347
Arg 209
Glu 354
C)
Gln 390
Arg 410
Ser 489
Lys 414
Ala 490
Glu 492
Leu 491

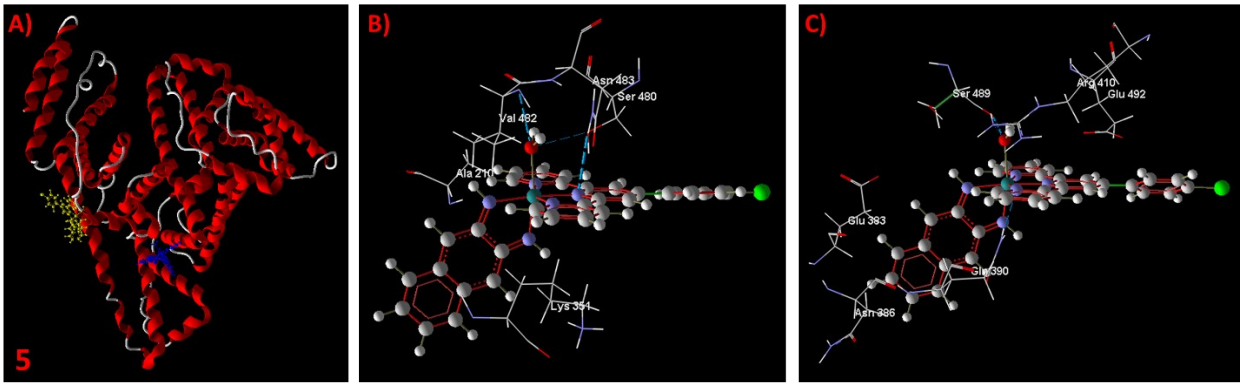
A)
5
B)
Asn 483
Ser 480
Val 482
Ala 210
Lys 351
C)
Ser 489
Arg 410
Glu 492
Glu 383
Glu 390
Asn 386

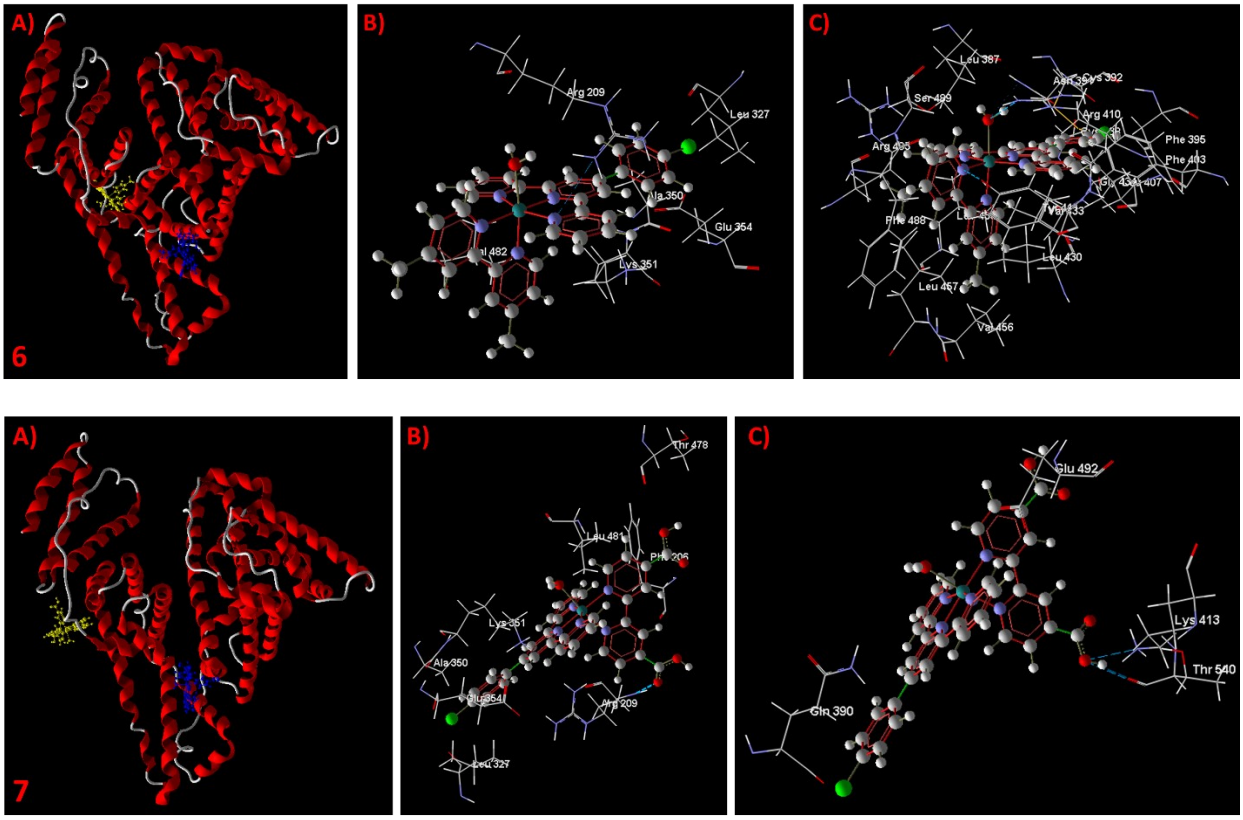

Fig. S42. A)Molecular docking of HSA with docking poses of complexes **2**, **3**, **4**, **5**, **6** and **7** illustrated on protein's backbone (blue binding into the binding site I and yellow binding into the binding site II), binding site of investigated complexes on HSA protein and selected amino acid residues represented by stick models B) binding into site I and C) site II. Hydrogen bonds are shown in blue dotted lines.

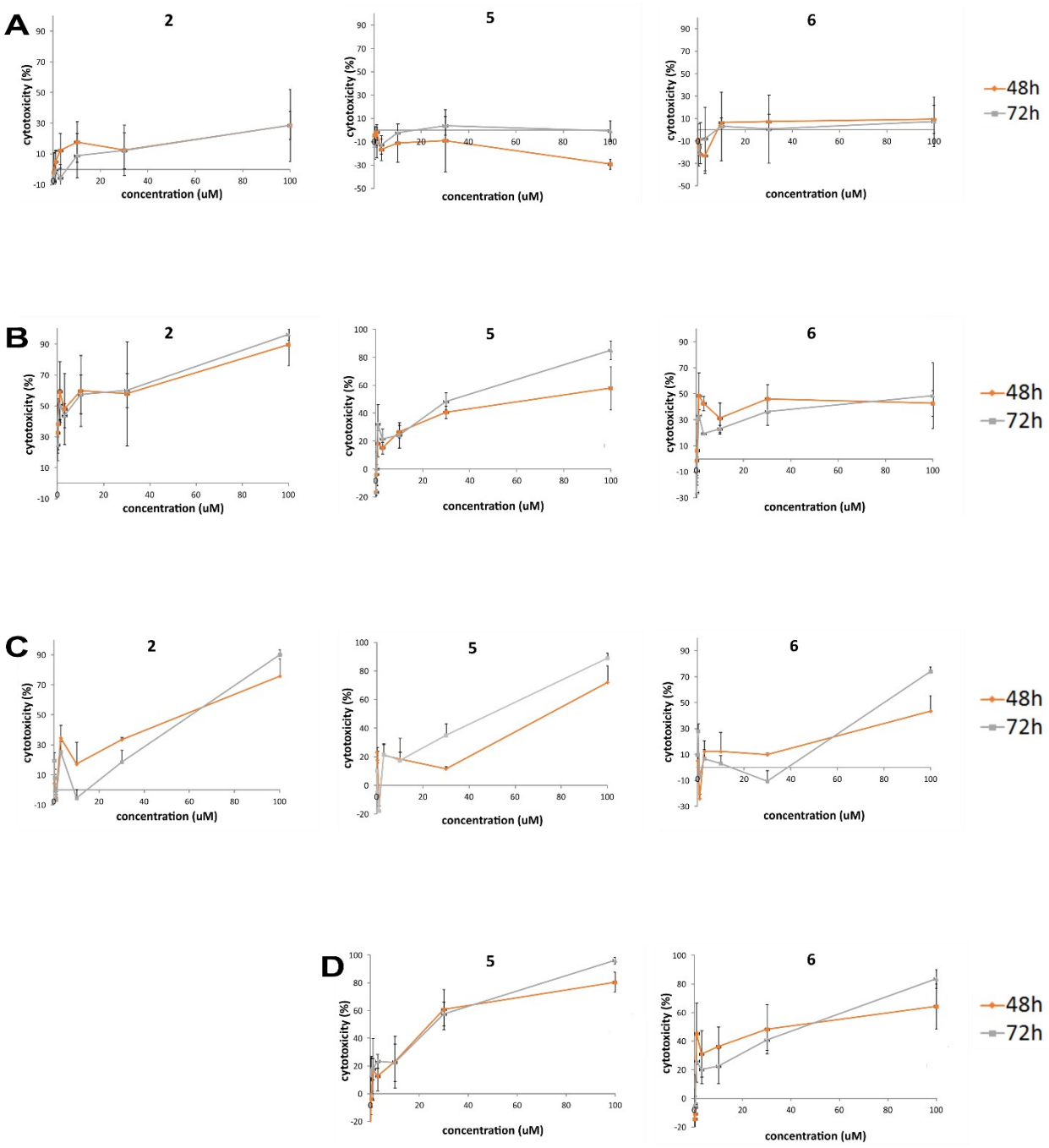

Fig. 43. Dose-response curves of cytotoxic effect of various concentrations of complexes **2**, **5**, and **6** against MRC-5 (A), MDA-MB 231 (B), HCT116 (C), and HeLa cells (D) after 48 h and 72 h treatment. The results are presented as mean ± SD of three separate experiments.

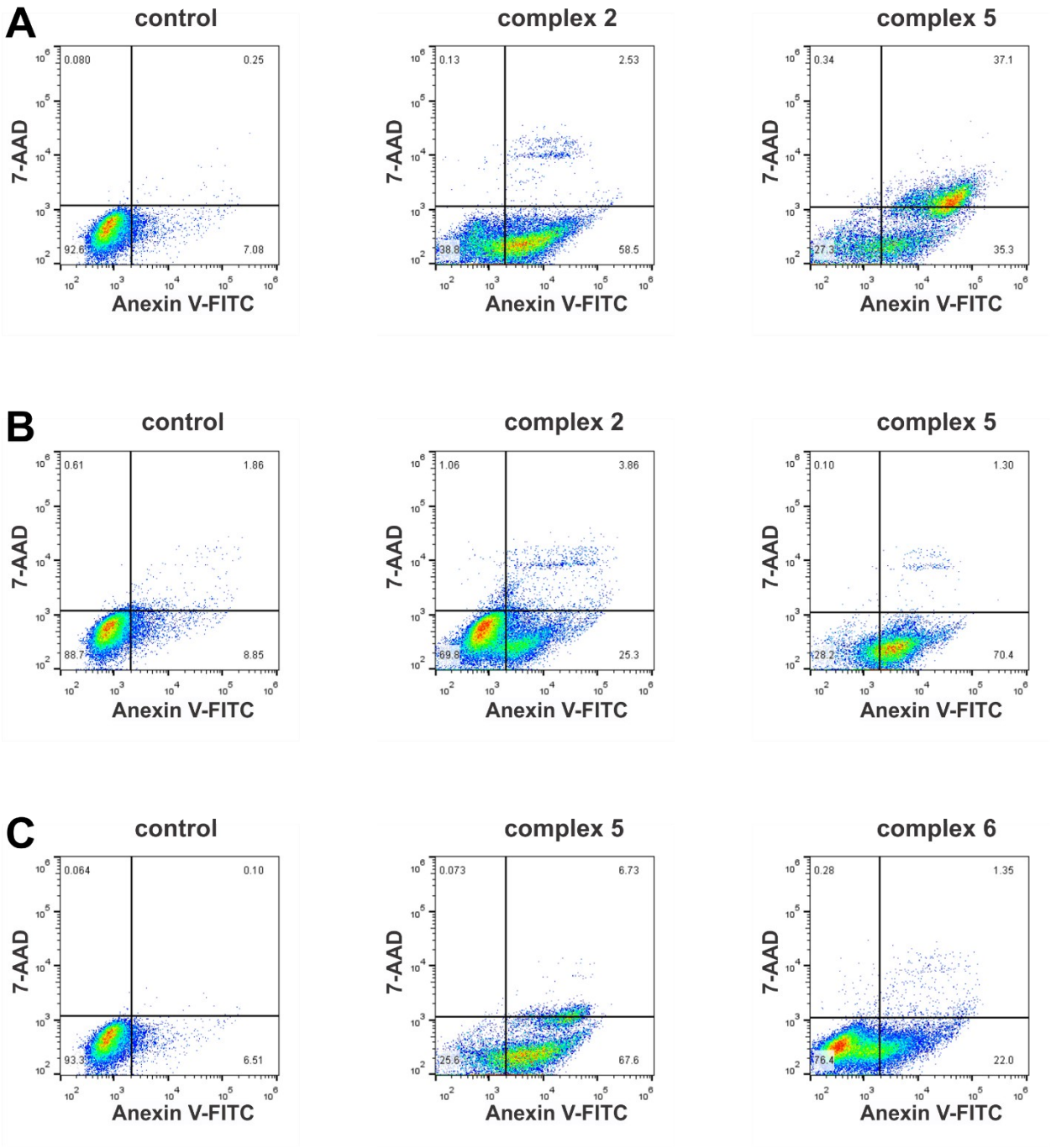

Fig. S44. Representative dot plots presenting percentages of viable (Annexin V-7-AAD-), early apoptotic (Annexin V+7-AAD-), late apoptotic (Annexin V+7-AAD+) and necrotic cells (Annexin V-7-AAD+) in MDA-MB 231 (A), HCT116 (B), and HeLa cells (C) treated with complexes **2, 5**, and **6**.

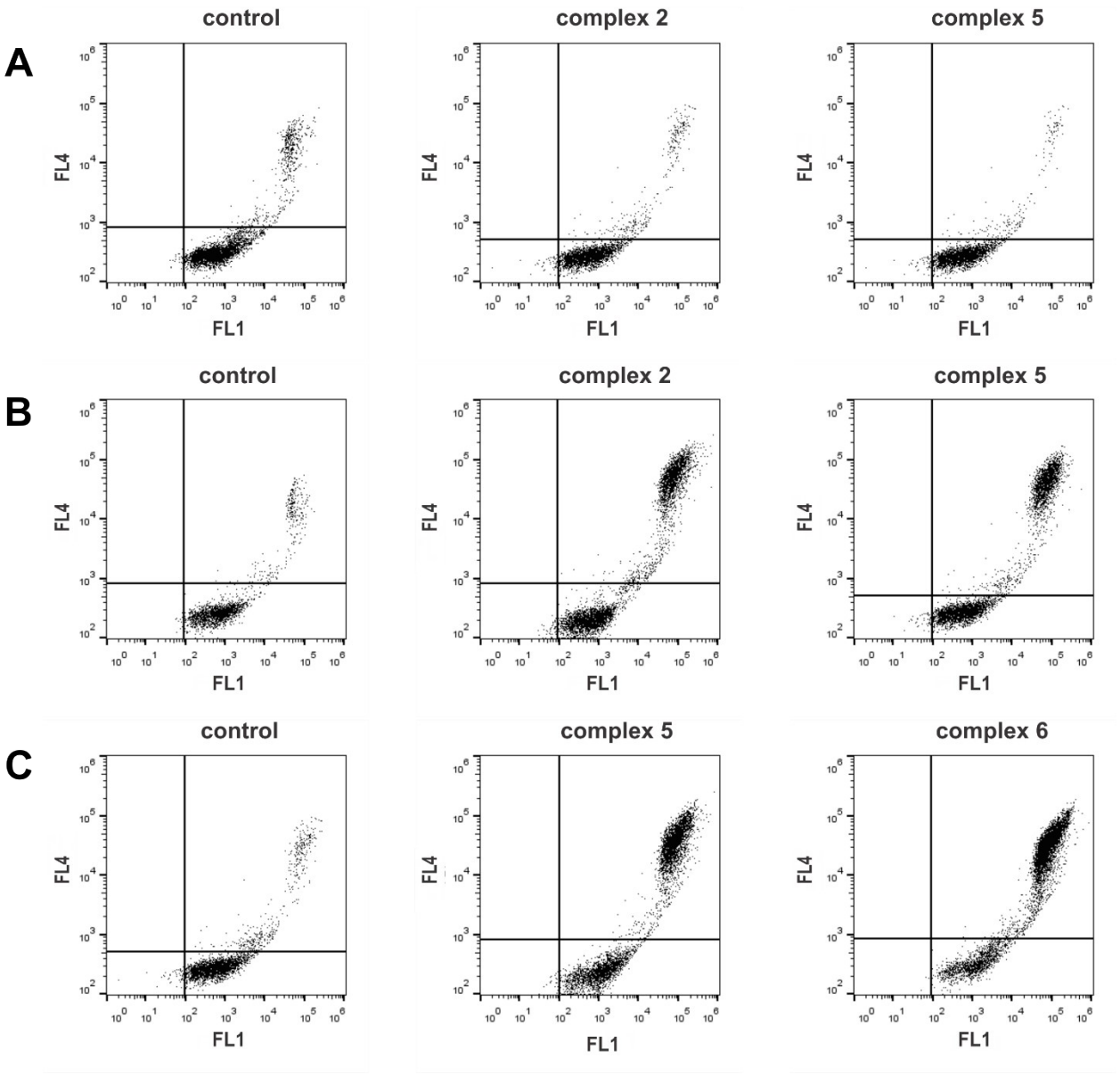

Fig. S45. Representative dot plots presenting acridin orange stained MDA-MB 231 (A), HCT116 (B), and HeLa cells (C) treated with complexes **2, 5**, and **6**.

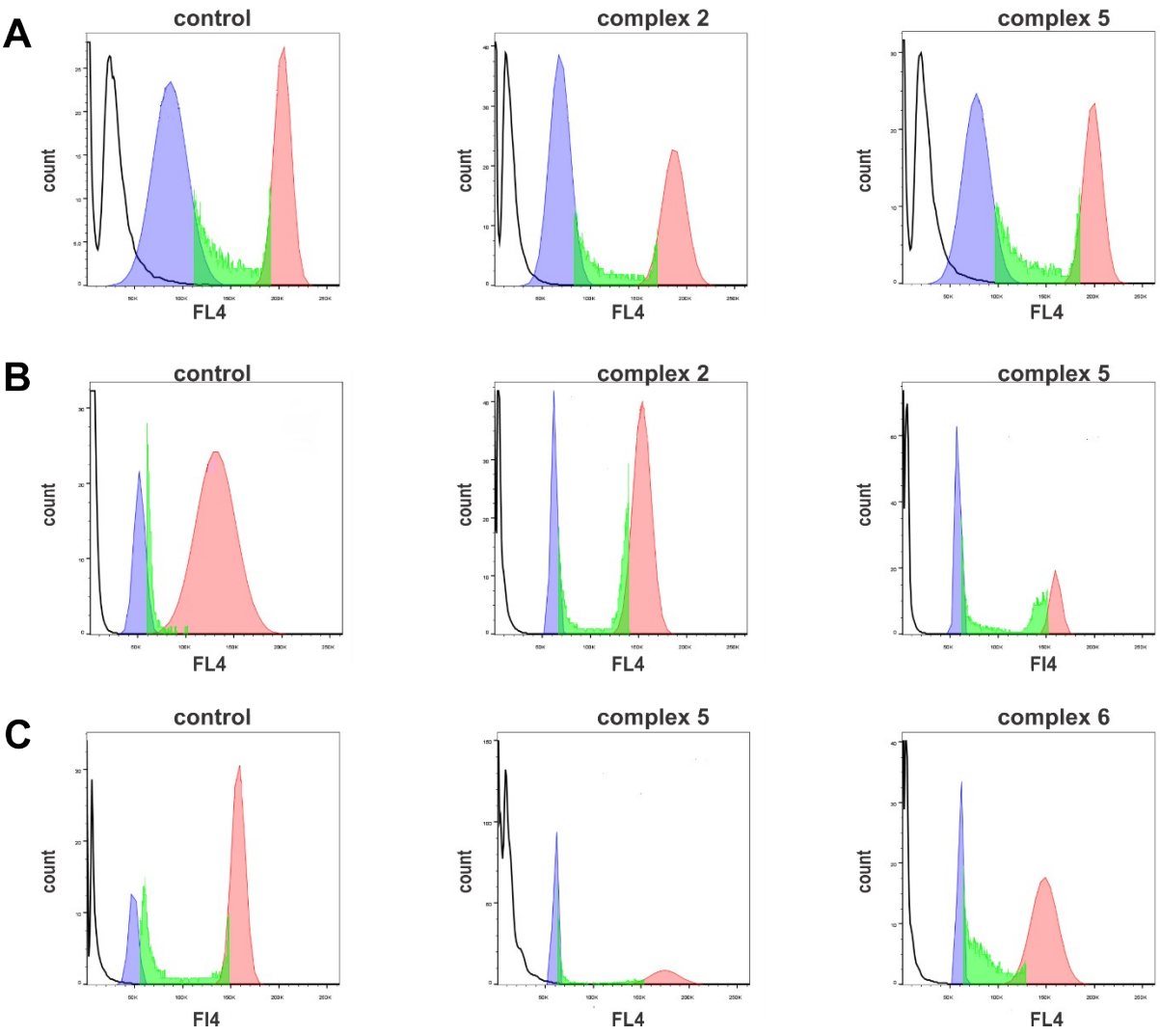

Fig. S46. Representative histograms presenting cell cycle distribution in MDA-MB 231 (A), HCT116 (B), and HeLa cells (C) in untreated (control) and cells treated with complexes **2**, **5**, and **6.**

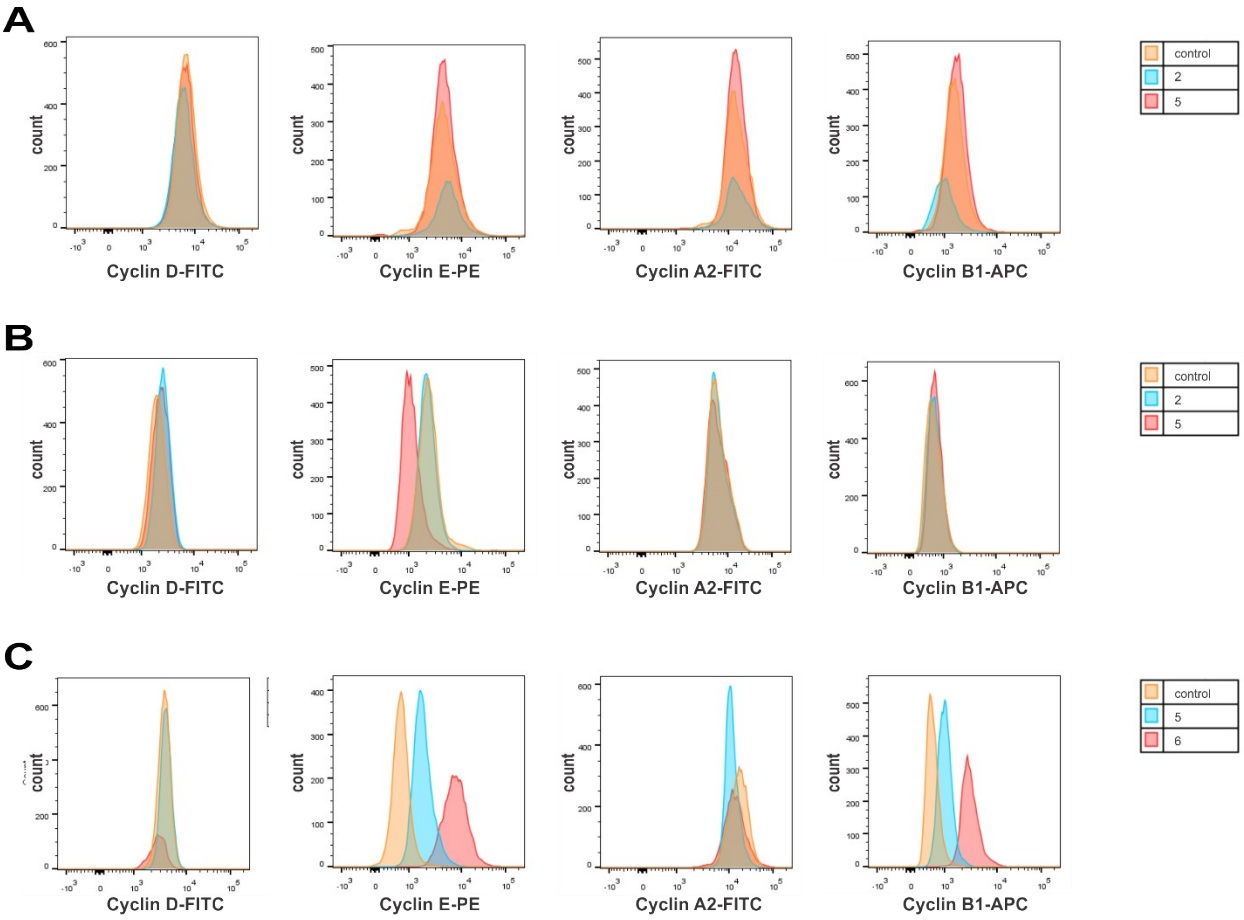

Fig. S47. Overlaid histograms presenting the expression of cyclins D, E, A2, and B1 in untreated and treated MDA-MB 231 (A), HCT116 (B), and HeLa (C) cells.

Table S1. Observed *pseudo*-first order rate constants as a function of complex concentration and temperature for the reaction of complex **1** with 5'-GMP (**L**) in water.

λ_{max} (nm)	t (ºC)	$C_{\mathbf{L}}$ [10^{-3} M]	k_{obsd} [10^{-4} s^{-1}]
506	15.0	5.00	3.62(2)
		4.00	2.75(3)
		3.00	2.13(2)
		2.00	1.62(3)
		1.00	0.66(3)
	25.0	5.00	6.99(3)
		4.00	6.19(2)
		3.00	4.13(3)
		2.00	2.85(3)
		1.00	1.49(3)
	37.0	5.00	20.80(3)
		4.00	15.50(2)
		3.00	11.21(3)
		2.00	9.05(2)
		1.00	4.10(2)

Table S2. Observed *pseudo*-first order rate constants as a function of complex concentration and temperature for the reaction of complex **1** with L-Cys (**L**) in water.

λ_{max} (nm)	t (ºC)	$C_{\mathbf{L}}$ [10^{-3} M]	k_{obsd} [10^{-4} s^{-1}]
522	15.0	5.00	0.70(3)
		4.00	0.55(3)
		3.00	0.38(3)
		2.00	0.30(2)
		1.00	0.14(3)
	25.0	5.00	2.20(2)
		4.00	1.70(2)
		3.00	1.25(3)
		2.00	0.77(3)
		1.00	0.52(3)
	37.0	5.00	3.80(3)
		4.00	2.57(3)
		3.00	1.79(2)
		2.00	1.12(2)
		1.00	0.85(2)

Table S3. Observed *pseudo*-first order rate constants as a function of complex concentration and temperature for the reaction of complex **1** with L-Met (**L**) in water.

λ_{max} (nm)	t (ºC)	$C_{\mathbf{L}}$ [10^{-3} M]	k_{obsd} [10^{-4} s^{-1}]
502	15.0	5.00	0.70(3)
		4.00	0.52(3)
		3.00	0.42(3)
		2.00	0.30(2)
		1.00	0.13(3)
	25.0	5.00	1.84(3)
		4.00	1.37(2)
		3.00	0.97(3)
		2.00	0.65(2)
		1.00	0.47(3)
	37.0	5.00	2.58(2)
		4.00	2.19(3)
		3.00	1.47(3)
		2.00	1.03(3)
		1.00	0.60(2)

Table S4. Observed *pseudo*-first order rate constants as a function of complex concentration for the reaction of complex **2** with 5'-GMP, L-Cys and L-Met (**L**) in water.

Ligand	λ_{max} (nm)	C_L [10^{-3} M]	k_{obsd} [10^{-4} s^{-1}]
5'-GMP	528	5.0	2.59(3)
		4.0	1.97(2)
		3.0	1.65(2)
		2.0	1.15(2)
		1.0	0.44(3)
L-Cys	526	5.0	1.49(3)
		4.0	1.26(3)
		3.0	0.90(2)
		2.0	0.51(3)
		1.0	0.36(2)
L-Met	533	5.0	1.30(3)
		4.0	1.13(2)
		3.0	0.80(2)
		2.0	0.46(2)
		1.0	0.32(3)

Table S5. Observed *pseudo*-first order rate constants as a function of complex concentration for the reaction of complex **3** with 5'-GMP, L-Cys and L-Met (**L**) in water.

Ligand	λ_{max} (nm)	C_L [10^{-3} M]	k_{obsd} [10^{-4} s^{-1}]
5'-GMP	506	5.0	0.80(3)
		4.0	0.62(2)
		3.0	0.51(3)
		2.0	0.29(3)
		1.0	0.18(3)
L-Cys	508	5.0	0.50(2)
		4.0	0.40(2)
		3.0	0.35(2)
		2.0	0.20(3)
		1.0	0.09(2)
L-Met	482	5.0	0.44(3)
		4.0	0.35(2)
		3.0	0.25(3)
		2.0	0.17(2)
		1.0	0.01(3)

Table S6. Observed *pseudo*-first order rate constants as a function of complex concentration for the reaction of complex **4** with 5'-GMP, L-Cys and L-Met (**L**) in water.

Ligand	λ_{max} (nm)	C_L [10^{-3} M]	k_{obsd} [10^{-4} s^{-1}]
5'-GMP	506	5.0	3.20(3)
		4.0	2.70(3)
		3.0	2.07(3)
		2.0	1.43(2)
		1.0	0.52(2)
L-Cys	500	5.0	2.22(2)
		4.0	1.80(3)
		3.0	1.25(2)
		2.0	0.95(3)
		1.0	0.44(2)
L-Met	509	5.0	1.72(3)
		4.0	1.35(3)
		3.0	0.99(3)
		2.0	0.68(3)
		1.0	0.36(2)

Table S7. Observed *pseudo*-first order rate constants as a function of complex concentration for the reaction of complex **5** with 5'-GMP, L-Cys and L-Met (**L**) in water.

Ligand	λ_{max} (nm)	C_L [10^{-3} M]	k_{obsd} [10^{-4} s^{-1}]
5'-GMP	526	5.0	70.00(3)
		4.0	58.00(2)
		3.0	40.00(2)
		2.0	25.00(2)
		1.0	16.70(3)
L-Cys	529	5.0	18.20(2)
		4.0	15.00(3)
		3.0	13.30(2)
		2.0	7.96(3)
		1.0	2.68(2)
L-Met	527	5.0	8.52(3)
		4.0	6.00(3)
		3.0	4.00(3)
		2.0	3.63(3)
		1.0	1.76(2)

Table S8. Observed *pseudo*-first order rate constants as a function of complex concentration for the reaction of complex **6** with 5'-GMP, L-Cys and L-Met (**L**) in water.

Ligand	λ_{max} (nm)	C_L [10^{-3} M]	k_{obsd} [10^{-4} s^{-1}]
5'-GMP	498	5.0	48.00(2)
		4.0	39.00(3)
		3.0	26.50(2)
		2.0	17.50(3)
		1.0	11.40(2)
L-Cys	494	5.0	13.60(3)
		4.0	11.00(3)
		3.0	7.30(2)
		2.0	6.23(2)
		1.0	2.46(2)
L-Met	529	5.0	3.33(3)
		4.0	2.64(2)
		3.0	1.66(2)
		2.0	1.10(3)
		1.0	0.90(3)

Table S9. Observed *pseudo*-first order rate constants as a function of complex concentration for the reaction of complex **7** with 5'-GMP, L-Cys and L-Met (**L**) in water.

Ligand	λ_{max} (nm)	C_L [10^{-3} M]	k_{obsd} [10^{-4} s^{-1}]
5'-GMP	539	5.0	57.60(2)
		4.0	45.00(2)
		3.0	30.80(3)
		2.0	20.00(2)
		1.0	14.30(2)
L-Cys	526	5.0	15.20(2)
		4.0	11.00(2)
		3.0	8.46(3)
		2.0	6.34(3)
		1.0	2.98(2)
L-Met	525	5.0	4.72(3)
		4.0	3.54(3)
		3.0	2.54(3)
		2.0	2.02(3)
		1.0	0.91(3)

Table S10. List of amino acids exhibiting most pronounced interactions with the investigated complexes

Serum albumin docking PDB ID of SA	Complex	Steric interactions	Hydrogen bonds
1AO6 – humane serum albumin	**1**[a]	Asn-483, Lys-351, Ser-480, Val-482, Trp-214	Leu-481, Ser-480, Val-482
	1[b]	Leu-407, Leu-453, Leu-457, Ser-489, Arg-485, Leu-387, Ile-388, Asn-391, Arg-410, Val-433	Ser-489, Asn-391, Arg-410
	2[a]	Asp-324, Arg-209, Val-216, Ser-323, Lys-212, Trp-214, Val-325	Asp-324, Lys-212
	2[b]	Glu-383, Glu-492, Leu-491, Ser-489	Ser-489, Glu-492, Leu-491
	3[a]	Arg-209, Ala-210, Ala-213, Trp-214, Phe-206	Arg209
	3[b]	Leu-407, Asn-391, Ser-489, Leu-387, Phe-488, Arg-410, Tyr-411, Leu-457, Leu-453, Ile-388	Tyr-411, Arg-410, Ser-489, Arg-485, Asn-391
	4[a]	Val-482, Ser-480, Leu-481, Ala-210, Leu-347, Trp-214, Arg-209, Glu-354, Phe-206	Leu-481, Ser-480, Trp-214, Arg-209
	4[b]	Glu-383, Gln-390, Lys-414, Leu-491, Ser-489, Glu-492, Arg-410, Ala-490	Leu-491, Gln-390, Lys-414, Arg-410
	5[a]	Ser-480, Asn-483, Lys-351, Ala-210, Trp-214	Ser-480, Val-482
	5[b]	Ser-489, Arg-410, Gln-390, Asn-386, Glu-383, Slu-492	Arg-410, Ser-489, Sln-390
	6[a]	Ala-350, Lys-351, Arg-209, Trp-214, Val-482, Glu-354	Arg-209
	6[b]	Phe-403, Val-433, Cys-392, Leu-407, Asn-391, Tyr-411, Ser-489, Leu-457, Val-456, Arg-485	Asn-391, Arg-410, Tyr-411
	7[a]	Leu-481, Thr-478, Phe-206, Arg-209, Trp-214, Lys-351, Ala-350, Leu-327, Glu-354	Arg-209
	7[b]	Gln-390, Glu-492, Thr-540, Lys-413	Lys-413, Thr-540

[a]Binding into the subdomain IIA (site I)
[b]Binding into the subdomain IIIA (site II)

Table S11. Percent of cytotoxicity induced by 48 h treatment of MRC-5, MDA-MB 231, HCT116 and HeLa cells with 100 μM complexes. Result are expressed as mean±SD.

	MRC-5	HCT116	SS	HeLa	SS	MDA-MB 231	SS
1	29.8±5.9	54.7±0.6	**1.8**	32.2±4.1	**1.1**	48.3±4.4	**1.6**
2	28.6±7.3	84.0±1.9	**2.9**	34.4±7.5	**1.2**	91.4±6.0	**3.2**
3	49.0±7.8	39.9±1.5	**0.8**	56.2±4.1	**1.2**	51.8±7.1	**1.1**
4	21.4±7.0	26.7±1.3	**1.3**	28.9±3.1	**1.4**	18.0±7.5	**0.8**
5	-8.2±5.7	83.1±5.3	**>100**	45.3±6.8	**>100**	50.5±5.9	**>100**
6	2.9±6.3	65.7±6.7	**22.5**	86.2±5.5	**29.5**	65.7±8.3	**22.5**
7	24.1±4.8	24.3±3.9	**1.0**	33.4±3.8	**1.4**	23.3±4.1	**1.0**